GPCR Signal Attenuation:
Biochemical and Spectroscopic Analysis of Interaction with Affiliate Proteins

By

Abhinav Sinha

A DISSERTATION

Presented to the Department of Biochemistry and Molecular Biology
and
The Oregon Health and Science University
School of Medicine

In partial fulfillment of the requirements for the degree of

Doctor of Philosophy

May 2012

School of Medicine

Oregon Health & Science University

CERTIFICATE OF APPROVAL

This is to certify that the PhD dissertation of

Abhinav Sinha

has been approved

_____
Dr. David L. Farrens, Thesis Advisor

_____
Dr. Ujwal Shinde, Committee Chair

_____
Dr. Kim Neve, Committee Member

_____
Dr. Francis Valiyaveetil, Committee Member

_____
Dr. James R. Lundblad, Committee Member

Table of contents

List of Figures

List of Abbreviations

α	alpha
A (amino acid)	alanine
Å	angstrom
ABS	absorption
Ala	alanine
AP-1	oxidative sensitive transcription factor
AP-2	adaptor protein 2 of the cellular endocytosis machinery
Arg	arginine
Arr	arrestin
Asn	asparagine
Asp	aspartic acid
ATP	adenosine triphosphate
ATR	all-*trans* retinal
A.U.	arbitrary units
B	beta
χ^2	chi-squared, which describes the deviance of the residuals to a fit
C (atom)	carbon
C (amino acid)	cysteine
C-	carboxyl-
°C	degrees Celsius
Ca	calcium
cal	calorie
cAMP	3’-5-cyclic adenosine monophosphate

CD	circular dichroism
cDNA	complementary DNA synthesized from a mature mRNA
cGMP	cyclic guanosine monophosphate
Cl	chlorine
cm	centimeter
Cys	cysteine
Δ	delta, or the difference between two values
D (amino acid)	aspartic acid
Da	Dalton, unit of atomic mass
DM	*n*-dodecyl-β-D-maltopyranoside
DNA	deoxyribonucleic acid
DOPS	1,2-dioleoyl-*sn*-glycero-3-phospho-L-serine (sodium salt)
DTT	dithiothreitol
ε	extinction coefficient
E (amino acid)	glutamic acid
E-2	second extracellular loop of rhodopsin
E_a	energy of activation
EDTA	ethylenediamine-tetraacetic acid
EPR	electron paramagnetic resonance
et al.	*et alii* (Latin), “and others”
F (amino acid)	phenylalanine
F	flluorescence intensity

F_0	fluorescence intensity in the absence of quencher, or the fluorescence intensity before light-activation of the sample
FRET	fluorescence resonance energy transfer
γ	gamma
g	acceleration due to gravity
G	G-factor that corrects for monochromator bias in transmitting parallel *versus* perpendicularly polarized light
G (amino acid)	glycine
G_α	alpha subunit of heterotrimeric G-protein
$G_{\beta\gamma}$	beta and gamma subunits of heterotrimeric G-protein
GC	guanylate cyclases
GDP	guanosine diphosphate
Gln	glutamine
Glu	glutamic acid
Gly	glycine
GMP	guanosine monophosphate
GPCR	G-protein coupled receptor
G protein	guanine nucleotide-binding regulatory protein
G_t	transducin (photoreceptor G-protein)
$G_t\alpha$	alpha subunit of transducin
GTP	guanosine triphosphate
h	hour
H (atom)	hydrogen

H (amino acid)	histidine
HEPES	*N*-2-hydroxyethylpiperazine-*N*'-2-ethanesulfonic acid
His	histidine
hν	light
I (atom)	iodine
I (amino acid)	isoleucine
Ile	isoleucine
k	rate constant
K (atom)	potassium
K (amino acid)	lysine
K (temperature)	degrees Kelvin
Kcal	kilocalories
K_D	equilibrium dissociation constant
kDa	kilodalton
k_q	bimolecular quenching constant
L (amino acid)	leucine
Leu	leucine
Lys	lysine
λ_{em}	wavelength of emission
λ_{ex}	wavelength of excitation
λ_{max}	wavelength of maximum absorption or emission
M	molar
M (amino acid)	methionine

mB	bimane label
MES	4-morpholineethanesulfonic acid
Met	methionine
Meta I (MI)	Metarhodopsin I
Meta II (MII)	Metarhodopsin II
Meta III (MIII)	Metarhodopsin III
max	maximum or maximal
µg	microgram
mg	milligram
min	minute
µl	microliter
ml	milliliter
µM	micromolar
mM	millimolar
mol	mole
µs	microsecond
mRNA	messenger RNA
MW	molecular weight
N	normal
N (atom)	nitrogen
N (amino acid)	asparagine
N-	amino-
Na	sodium

ng	nanogram
NH_2OH	hydroxylamine
nm	nanometer
nM	nanomolar
ns	nanosecond
O (atom)	oxygen
O.D.	optical density
P (atom)	phosphate
P (amino acid)	proline
PCR	polymerase chain reaction
PDE	phosphodiesterase
pH	potential of hydrogen
Phe	pheylalanine
PMSF	phenylmethylsulfonyl fluoride
POPC	1-palmitoyl-2-oleoyl-*sn*-glycero-3-phosphocholine
POPG	1-palmitoyl-2-oleoyl-*sn*-glycero-3-phospho-(1'-rac-glycerol)
Pro	proline
Q (amino acid)	glutamine
R (amino acid)	arginine
Rho	rhodopsin
Rho*	light-activated rhodopsin
Rho-P	phosphorylated rhodopsin
RK	rhodopsin kinase

RNA	ribonucleic acid
ROS	rod outer segment, or wild-type rhodopsin in native membranes
ROS*	light-activated rhodopsin in native membranes
ROS-P	phosphorylated rhodopsin in native membranes
s	second
S (amino acid)	serine
SDS	sodium dodecyl sulfate
SDS PAGE	SDS polyacrylamide gel electrophoresis
sec	second
Ser	serine
T	temperature
T (amino acid)	threonine
τ	fluorescence decay lifetime
$\langle\tau\rangle$	amplitude-weighted average fluorescence lifetime
$t_{1/2}$	half-life
TCA	trichloroacetic acid
TCEP	tris(2-carboxyethyl) phosphine
Thr	threonine
Tricine	*N*-[2-hydroxy-1,1-bis(hydroxymethyl)ethyl]glycine
Tris	2-amino-2-hydxymethyl-1-3-proanediol
Trp	tryptophan
Tyr	tyrosine
UV	ultraviolet

V (amino acid)	valine
vs.	*versus*
Val	valine
W (amino acid)	tryptophan
WT	wild-type
Y (amino acid)	tyrosine

Acknowledgements

This dissertation is a result of many years of sweat and toil with many highs and lows. I could not have completed this journey in isolation. Many people have helped me along the way in manner big and small and I am sincerely thankful to all who have contributed to the successful completion of the dissertation.

Professionally, I thank my advisor, Dr. David Farrens for taking me under his wings and teaching me the intricacies of biochemistry. More importantly, Dr. Farrens helped inculcate in me a scientific temper and the ability to think critically about science. The Farrens lab has been a place full of wonderful individuals, who, over the years, have been great friends and helpful colleagues, and have provided a fun and stimulating atmosphere in the lab. I thank the current and past members of the lab - Jonathan Fay, Amber Jones-Hackathorne, Dr. Steve Mansoor, Dr. Eva Ramon, Dr. Martha Sommer, Dr. Hisao Tsukamoto, Chistopher Schafer, Emily Lorenzen and Mark DeWitt. I also thank my thesis advisory committee – Dr. James Lundblad, Dr. Ujwal Shinde, Dr. Kim Neve, Dr. Francis Valiyaveetil and Dr. Svetlana Lutsenko – for their support and guidance over the years. Especially, I would like to thank Dr. Shinde, who has been a patient guide and mentor through the years, and Dr. Lundblad, who has always been extremely supportive and encouraging in all my research endeavors.

I would be failing in my duty if I do not recognize the helpful role of my friends at OHSU and beyond. My classmates have been with me through thick and thin and have made the graduate school experience fun and rewarding. Also, I owe a lot to all my friends from India, who have, over the years, provided a great support system and a social life beyond the lab. Especially, Merryl, Aravind, Sangeet, Hrebesh, Feroz and Sheeja have been with me at every step over the past few years, which were extremely testing for me.

Last, but certainly not the least, I owe a lot to my family that has provided unflinching support and love, without which this dissertation would not have been possible. Didi, Jijaji, Bhai and Bhabhi have been a huge part of my support system and have been my punching bags at every turn. My wife, Parvathy, has been a source of love and constant support and has shown tremendous patience, given the long duration of graduate school, and I thank her for everything. Finally, I cannot sufficiently express my gratitude to my parents, who have taught me how to be a good human being. They have taken everything that I have thrown at them with patience and showered me with unconditional love and support, which has enabled the successful completion of this dissertation. I dedicate this dissertation to my family.

Abstract

G Protein-Coupled Receptors (GPCRs) are critical mediators of transmembrane signaling. Signaling via G proteins, in response to a cue from a ligand, is central to transduction of extracellular signals to the interior of a cell to trigger a cellular response. Equally important is the attenuation of GPCR signal by cytosolic modulators that limit the tone and duration of the response to any stimulus. This dissertation is aimed at understanding better the interactions, with the receptor, of different proteins involved in attenuating GPCR signals. Some of the key findings are outlined below.

We report that both visual arrestin and β-arrestin 1 can bind monomeric rhodopsin in nanodiscs, which are discoidal membranes structures, encapsulated by a belt of amphipathic lipid carrying proteins. In fact, arrestin bound monomeric rhodopsin in nanodiscs better than rhodopsin oligomers in nanodiscs or liposomes. Using a fast and simple one-step purification method, we purified rhodopsin kinase (RK) expressed in mammalian cells. We found that the kinase, too, could make a functional interaction with monomeric rhodopsin and phosphorylate the receptor. Next, our studies also suggest that both arrestin and RK bind the same region of rhodopsin as the G protein, transducin. These results point to conserved mode of interaction between rhodopsin and its various modulating proteins. Further, fluorescence studies employing tryptophan induced quenching (TrIQ) showed two distinct sites on arrestin interact with the base of TM6 of rhodopsin. Finally, initial characterization of a novel protein (CRIP1a) involved in the attenuation of the constitutive signaling of CB1 receptor, shows that protein is stable and as high β-sheet content, with no disulfide bonds. Crystal screens of CRIP1a have provided some conditions, which might require some more fine-tuning to get crystals of CRIP1s for structure determination.

Chapter 1

Introduction

G Protein-Coupled Receptors (GPCRs) are the largest family of cell surface receptors that detect extracellular cues and modulate various intracellular signaling pathways leading to a specific phenotypic response. These receptors control a wide array of sensory and physiological systems and are the largest class of pharmaceutical targets (Overington et al., 2006; Rosenbaum et al., 2009). Studying the regulation of these receptors in terms of both their activation and deactivation is critical to understanding the molecular basis of their action, and hence for the development of more effective therapeutics. This dissertation is focused on the investigation of three different proteins involved in the attenuation of GPCR mediated signaling. This chapter provides an introduction to GPCR systems, a review of literature relevant to the present study and a brief description of the spectroscopic approaches used in the dissertation, apart from an overview of the dissertation.

1.1. G Protein-Coupled Receptors

Introduction to GPCR family

GPCRs are transmembrane proteins that form the largest family of cell-surface receptors and are found in all eukaryotes. These receptors are critical mediators of extracellular information to the intracellular milieu. More than 800 distinct GPCRs are present in the human genome (~4% of the protein coding human genome), and individual receptor subtypes respond to photons, hormones, neurotransmitters, chemokines, odorants, and peptides, among others (Lagerstrom and Schioth, 2008). As such, they regulate a wide array or physiological systems – from the sense of vision, smell and taste to immune system, endocrine system, etc. Malfunctions associated with receptor function or regulation have been linked to diseases such as hypertension, obesity, heart abnormalities and blindness (Hopkins and Groom, 2002). Their

crucial role in regulation of cellular functions makes them a target of about 30-40% of drugs currently available in market (Lagerstrom and Schioth, 2008; Overington et al., 2006).

The GPCR superfamily is classified into six main families or classes determined by protein sequence similarity (Horn et al., 2003). These include family 1 or class A rhodopsin like, family 2 or class B secretin like, family 3 or class C metabotropic glutamate, family 4 or class D pheromone, family 5 or class E cAMP, and family 6 or class F frizzled/smoothened receptors. Family 1 is the largest and most studied of the classes, accounting for ~80% of the entire GPCR superfamily. The present work is focused on two members of class A GPCRs – rhodopsin and cannabinoid receptor CB1.

As the name suggests, GPCRs interact with heterotrimeric G protein (guanine nucleotide binding protein) for signaling (Holinstat et al., 2006). All GPCRs also share a common seven α-helical transmembrane structural core (Rosenbaum et al., 2009). While the overall topology and the broad signaling paradigm is the same, these receptors do exhibit significant variability in their amino acid sequence, which is responsible for structural and functional differences in their ligand binding and signaling capabilities. Further diversity in their functional profile is provided by the presence of a large pool of G protein subunits (21α, 6β and 12γ subunits), with different G proteins coupling to different effectors like adenylyl cyclase, ion channels, phosphodiesterases and phospholipases [Oldham and Hamm, 2008]. Significant diversity at these three levels, apart from their tissue-specific expression profile provides the basis for the ability of GPCRs to bind to a wide array of ligands and cause different physiological responses.

Because drugs that target GPCRs often engage receptor regulatory mechanisms that limit drug effectiveness, particularly in chronic treatment, there is great interest in understanding how GPCRs are regulated, as a basis for designing therapeutic drugs that evade this regulation (Kelly

et al., 2008). The major GPCR regulatory pathway involves phosphorylation of activated receptors by G protein–coupled receptor kinases (GRKs), followed by binding of arrestin proteins, which prevent receptors from activating downstream heterotrimeric G protein pathways while allowing activation of arrestin-dependent signaling pathways (Premont and Gainetdinov, 2007). Apart from these two, there are other GPCR Interacting Proteins (GIPs) that modulate receptor activity, including Homer, calmodulin, JAK2 and CRIP1a, among others (Maurice et al., 2011). The last of these, CRIP1a, has been shown to inhibit the constitutive activity of CB1 (Niehaus et al., 2007).

GPCR signaling: Activation

GPCRs transduce extracellular signals into cells by interacting with intracellular G proteins (Fig. 1.1). As mentioned earlier, G proteins are a diverse class of heterotrimeric proteins comprised of three subunits: α, β and γ. The alpha subunits bind guanine nucleotides and are divided into several families: α_s (stimulates adenylyl cyclase (AC)), $\alpha_{i/o}$ (inhibits AC), α_q (stimulates phospholipase C (PLC)), and $\alpha_{12/13}$ (stimulates guanine nucleotide exchange factors, GEFs) (Oldham and Hamm, 2006; Tesmer, 2010). Further, there are specialized alpha subunits: α_t, the alpha subunit of transducin (G_t) which is activated by the dim light photoreceptor, rhodopsin, and α_{olf} which interacts with olfactory receptors. The β and γ subunits are obligate dimers and can also interact with downstream effectors, such as phospholipase A or the G protein-coupled inwardly-rectifying potassium channel (GIRK). G proteins are also lipid-modified, via α and γ subunits, which keeps them associated with the plasma membrane and facilitates their interactions with receptors. In their basal state, G proteins are bound to guanosine diphosphate (GDP). When an agonist binds and activates a receptor, this induces a conformational change in the receptor, which in turn induces conformational changes in a

coupled, G protein (Oldham and Hamm, 2006). This conformational change activates the G protein by stimulating the release of GDP and allowing guanosine triphosphate (GTP) to bind, a process driven by the high millimolar concentration of intracellular GTP. An active G protein functionally dissociates into its constituent α and βγ subunits allowing each subunit to activate downstream effectors, which in turn lead to the production of various second messengers like 3'-5'-cyclic adenosine monophosphate (cAMP), diacylglycerol, inositol (1,4,5)-trisphosphate (IP3) and nitric oxide (NO) among others. G protein signaling is eventually terminated by the hydrolysis of GTP to GDP. Hydrolysis is achieved through the intrinsic GTPase activity of the α subunit and may be accelerated through an interaction with accessory proteins like the RGS proteins (Regulators of G protein Signaling) (Kaur et al., 2011). α, β and γ subunits then re-associate and the GDP-bound G protein can then rebind a receptor to complete the cycle.

The interaction of the receptor with its G protein and the production of second messengers by the downstream effector molecules are two critical stages in the receptor signaling scheme in that these steps provide avenues for the amplification of the original activation signal, and improve the efficiency of the response to the stimulus.

GPCR signaling: Deactivation/attenuation

Once the receptor has been activated by an agonist and has transduced the signal via G proteins, the duration of the signal has to be regulated at the level of the receptor, which is achieved by three processes: desensitization, internalization and resensitization (Holinstat et al., 2006; Kobilka, 2007; Kohout and Lefkowitz, 2003). Desensitization is a cellular adaptive process to wane the signal at the cell surface by uncoupling the G protein, while internalization refers to the endocytosis of the receptor to reduce the amount of agonist-responsive receptors at the cell surface. The internalized receptors can either be recycled back to the cell surface or

targeted for degradation to either maintain the cellular response or terminate the receptor mediated signal.

The canonical pathway of receptor desensitization involves the phosphorylation of the receptor by G protein-coupled receptor kinases (GRKs), which phosphorylate a cluster of serine or threonine residues in the C-terminal tail of the receptor or in the intracellular loops of the agonist-activated receptor (Kelly et al., 2008). The phosphorylated, activated receptor is then recognized by cytosolic adapter protein called arrestin, which competitively inhibits G protein and terminates G protein mediated signaling. In case of non-visual receptor systems, arrestin family member β-arrestin 1 or 2 can recruit the endocytic machinery to help internalize the receptor. In many receptor systems, β-arrestins can initiate a second wave of intracellular signaling, independent of the G protein signal transduction pathway. In the visual system, however, there is no evidence of a second wave of signaling, initiated by arrestin.

1.2. Structure and Function of Rhodopsin

Signaling mechanism

Rhodopsin is the photoreceptor in the rod cells of retina and is responsible for dim light, or scotopic, vision (Palczewski, 2006; Wald, 1951). Rhodopsin is present at extremely high density in flat, disc-like phospholipid sacks near the tip of the rod cells, in a region known as the rod outer segment (ROS).

The protein rhodopsin is comprised of the apoprotein opsin, and its covalently linked chromophore, retinal, which is formed by the oxidation of vitamin A (Palczewski, 2006; Palczewski et al., 2006; Ridge et al., 2003). Retinal is composed of a β-ionone ring and an 11-carbon polyene chain. In the dark, inactive state, retinal is in its 11-cis conformation, and is

linked to opsin via a Schiff base at K296. Light activation results in the photoisomerization of 11-cis-retinal to all trans-retinal. This photoisomerization event causes conformational changes in the receptor leading to the activation of the retina-specific G protein, transducin (G_t) (Fig. 1.2). Upon receptor mediated activation, G_t exchanges GDP for GTP and the transducin heterotrimer dissociates into α and βγ subunits. The activated α subunit binds to and activates its effector protein, a phosphodiesterase (PDE6), which cleaves cGMP to form GMP. The reduction in the cellular level of cGMP causes the closing of cyclic nucleotide gated channels, which, in turn, inhibits Na+ channels, and leads to hyperpolarization of the cell, which is eventually perceived as a visual signal.

Central to the entire phototransduction cycle is the sequence of events that occur at or around the covalent ligand, retinal. The various intermediate states of the receptor have been delineated because of the ability to follow spectrophotometrically the absorbance properties of retinal (Ernst and Bartl, 2002) (Fig. 1.3). In the dark, inactive state, 11-cis-retinal is covalently attached to K296 by a Schiff base. The positive charge created by protonation of the Schiff's base increases electron delocalization along the conjugated retinylidene chain and shifts the absorption band from the short wavelength range to the middle of the visible spectrum and its spectral properties are tuned by its interactions with the amino acid residues lining the ligand binding pocket, with the maximum absorbance at 500nm. The process of vision is started upon the absorption of a photon by 11-cis-retinal. Photon absorption leads to photoisomerization of 11-cis-retinal within femtoseconds to a highly distorted 11-trans conformation. Progressive release of the strain in the chromophore leads through batho- and lumirhodopsin to Metarhodopsin I (Meta I, λ_{max} ~ 480nm), as seen by the different absorption maxima that arise from changes in chromophore/protein interaction. Meta I formation is accompanied by the

switch of the Schiff base counterion from E113 of TM3 to E141 on the extracellular loop E-II of rhodopsin. After Meta I, the active G protein-binding intermediate Meta II is formed (λ_{max}: 380nm), in which the retinal Schiff base is still intact but deprotonated. Dissociation of the proton from the Schiff base breaks a major constraint in the protein and enables further activating steps, including an outward tilt of TM6 and formation of a large cytoplasmic crevice for uptake of the interacting C terminus of the G_t subunit. MI and MII are in an equilibrium, which can be altered by pH, temperature or the binding of other proteins like transducin or arrestin. The MII state can either then go into a long term storage form MIII which absorbs at ~465nm or can dissociate into opsin and free all-trans-retinal. All-trans-retinal is reduced to retinol by retinol dehydrogenase and transported out of the photoreceptor cell to adjacent retinal pigment epithelial cells, where 11-cis-retinal is regenerated to be used for the formation of functional rhodopsin.

Once the receptor has initiated the perception of the visual signal, the signal has to be terminated. This process of receptor desensitization is initiated by the phosphorylation of rhodopsin kinase (Palczewski, 2006; Palczewski et al., 1991; Palczewski et al., 2006; Ridge et al., 2003). The major site of receptor phosphorylation is the C-terminal tail, which has a cluster of serines and threonines that get phosphorylated. However, the sequence and extent of receptor phosphorylation required for the reproducible deactivation of rod cell signaling isn't clear yet. The phosphorylated, activated rhodopsin, Rho*, is recognized by another cytosolic protein, arrestin, which uncouples the G protein by competitive inhibition and causes the termination of rhodopsin mediated transducin signaling.

Rhodopsin structure: Inactive or dark State

Rhodopsin was the first GPCR to be crystallized, initially in an inactive state with the bound inverse agonist 11-cis-retinal [Palczewski, et al, 2000]. The structure shows a seven-transmembrane helix architecture (TM1-7) with a cytoplasmic Helix8 (Fig. 1.4). The transmembrane helices are connected by three extracellular loops and three intracellular loops. The protein has an extracellular or intradiskal N-terminus and a cytosolic or luminal C-terminus. The extracellular side of rhodopsin, consisting of the N terminus and three extracellular loops (E-I, E-II and E-III), is folded into a well-organized structure. The N-terminus is composed of two strands and is glycosylated at N2 and N15 residues. Extracellular loop E-II forms a highly ordered lid over the retinal binding site and contains two short beta strands that are constrained by a highly conserved disulfide between C110 and C187 and a salt bridge between D177 and D190. The seven transmembrane helices form a compact bundle that contains the binding site for the retinal chromophore. The cytoplasmic face of rhodopsin consists of three intracellular loops, a membrane anchored cationic amphipathic Helix8 and the C-terminal tail. Helix8 is membrane anchored via two palmitoyl groups at C322 and C323, which are added post-translationally. In contrast to the structured extracellular surface of rhodopsin, the C-terminus and the three intracellular loops are more mobile. In the crystal structure, the C-terminal tail interacts with Helix8 and in the region of three phosphorylatable serines (S334, S338 and S343) (Sokal et al., 2002), which may block their exposure to rhodopsin kinase. Rhodopsin activation may change the conformation of the tail and facilitate phosphorylation and the subsequent arrestin binding.

The inactive state of the rhodopsin is stabilized by a few critical interactions, including the salt bridge between the protonated retinal Schiff base and its counter ion, E113 (Palczewski, 2006). Also, the E(D)RY motif, a highly conserved motif in GPCRs, in TM3 is involved in

stabilizing ionic interactions with TM6. R135 of this motif makes interactions with D134 one residue above itself, as well as with E247 and T251 on TM6. There is evidence to suggest that these two sets of interactions - the E113-Schiff base and R135-E247 - could be two protonation switches that control rhodopsin activation. The NPxxY motif, another well conserved sequence in GPCRs, makes stabilizing interactions with TM6 and Helix8. Within the NPxxY motif, an electrostatic interaction between Y306 and F313 side chains constrains TM7 and Helix8. As part of a hydrogen-bonding network, N302 of the NPxxY motif is linked to the most conserved residues in TM1 and TM2, N55 and D83, respectively. A test for the role of these interactions in stabilizing the receptor comes from the fact that mutations affecting these critical regions yield receptors that are constitutively active, and are seen in human retinal diseases like congenital night blindness and Autosomal Dominant Retinitis Pigmentosa (ADRP). G90D and A296E introduce charges that replace E113 as the counterion, while charge neutralization at R135 by a mutation like R135L disrupts the ionic lock. M257 side chain is situated in the interface between TM6 and 7, and is tightly packed among side chains of N302, I305, and Y306 in TM7. Mutation of M257 to a residue other than a leucine (which has similar molecular dimension as methionine) disrupts this set of interactions and yields a constitutively active receptor. These results clearly indicate the role of these stabilizing interactions in maintaining the inactive structure of the receptor in the dark state.

In this dissertation, I have used the M257Y constitutively active mutant of opsin to study arrestin binding. The M257Y mutation was introduced in a N2C/D282C disulfide-stabilized cysteine-less construct of opsin. The disulfide stabilization allowed the study of the receptor in its unliganded opsin form, which enabled clear fluorescence spectroscopic study arrestin-

receptor interaction without the added complication of energy transfer to the retinal chromophore in either its 11-cis- form or the all-trans- conformation.

While the classical model of GPCR activation considers the receptor as a monomer, there is a growing body of evidence to show that GPCRs do exist as dimers and/or higher order oligomers. In native membranes, rhodopsin has been shown to exist in arrays of dimers by electron microscopy and by atomic force microscopy. Lanthanide resonance energy transfer (LRET) and fluorescence resonance energy transfer (FRET) analysis has shown that rhodopsin can self associate into dimers or higher order oligomers when reconstituted into lipid vesicles. Also, FRET analysis has showed that rhodopsin expressed in COS-1 cells forms dimers. Two sets of possible monomer-monomer interaction faces have been proposed for rhodopsin dimers: one where TM4 and 5 are present at the interface and a second where TM1 and 2, and TM8 form the interface. While the exact orientation of the monomers in forming a rhodopsin dimer is not yet clear, it is well established that rhodopsin does exist as a dimer or higher order oligomer. The functional implication of the rhodopsin dimer is not yet well understood. This dissertation addresses the ability of monomeric rhodopsin to bind arrestin in Appendix A1 and rhodopsin kinase in Chapter 3.

Rhodopsin structure: Active or meta II

The absorption of light by the chromophore 11-cis-retinal initiates a chain of events that alters the conformation of rhodopsin, leading to its activation, wherein it can interact with its G protein, transducin (G_t), and lead to the visual transduction cascade. The atomic level details of the activated state structure of rhodopsin have been elucidated by extensive biochemical and biophysical studies over the past two decades, apart from a slew of crystal structures over the last

five years, including those of opsin, opsin with transducin tail peptide and metarhodopsin II among others.

Light absorption by the chromophore 11-cis-retinal leads to its photoisomerization to its all-trans form. This photon-induced cis-trans isomerization in the retinal leads to a sterically strained excited-state rhodopsin that thermally decays through a series of photointermediates to form the active-state Meta II. This strain gradually relaxes through all the photointermediates until the fully relaxed conformation seen in the Meta II crystals is reached. It is only in the lumirhodospin state that the protein responds to the elongation of the retinal and the energy stored in the retinal strain is transmitted to the protein, causing conformational changes in the receptor, leading to its activation. During the thermal relaxation, the protein moiety of rhodopsin undergoes a series of conformational changes that lead to the formation of a G protein binding site on the cytoplasmic side of the helical bundle in the Meta II state. Two major conformation changes are observed during rhodopsin activation. The first such change to be discovered was an outward movement and rotation of TM6. This movement separates the cytoplasmic ends of TM3 and 6 by about 7Å apart, which leads to disruption of the stabilizing ionic lock between R135 (on TM3) and E247 (on TM6). The side chains of the ionic lock residues are now stabilized by Y223 and K231 (both on TM5), respectively. Thus in the active structure, the new Y223-R135 and K231-E247 interactions link TM5 with TM3 and 6, respectively. This rearrangement of the ionic lock residue interactions is made possible by an elongation of TM5 and a 2-3 Å tilt of TM5 towards TM6. These structural changes also lead to the rearrangement of Y306 and F313 NPxxY motif. The interaction between the side chains of these two residues, which stabilizes the inactive rhodopsin state by tethering TM7 and 8, is broken in Meta II. Y306 swivels towards TM6 where it is linked via water molecules in a potential hydrogen-bonding network to M257 and Y223. As

a result of TM5 and 6 motion, the cytoplasmic domain of opsin shows an open conformation and exposes a hydrophobic patch required for G protein coupling. In fact, individual mutation of hydrophobic residues L226, T229 and V230 to alanines lowers the binding affinity of a peptide corresponding to the C-terminus of G_t by over two orders of magnitude. Once G_t binds the activated receptor, it can then exchange GDP for GTP and lead to downstream signaling, culminating in the perception of vision.

1.3. Phosphorylation and Rhodopsin Kinase

Rhodopsin kinase family

Any good switch must have an ON and an OFF state. While light activation activates rhodopsin and turns it ON, there must be a way to turn it OFF, too. One of the first steps in this process, known as desensitization, is the phosphorylation of rhodopsin by rhodopsin kinase (RK). The phenomenon of rhodopsin phosphorylation upon light activation was discovered in the 1970s and RK was purified from ROS subsequently (Kuhn and Wilden, 1982). RK is a member of a family of serine-threonine kinases that phosphorylate GPCRs called G Protein Coupled Receptor Kinase (GRK). Since it was the first member of the GRK family, it is also known as GRK1. There are seven members of the GRK family, named GRK1-7, which are grouped into three families based on sequence homology. The different GRKs have different tissue distributions, with GRK1 being expressed in the retina and the pineal gland.

C-tail and number of phosphates

Rhodopsin kinase phosphorylates the cytoplasmic tail of Rho* (light activated rhodopsin). *In vivo*, it has been shown that incorporation of one phosphate per Rho* leads to ~50 % reduction in G_t activation (Kuhn and Wilden, 1982; Maeda et al., 2003). However, there are

seven potential phosphorylation sites in the rhodopsin C-tail. The principal sites of phosphorylation are S338 and S343, with S334 being a minor site. Threonines at positions 335, 336, 340 and 342 have also been detected to be phosphorylated. Multiple phosphorylation of rhodopsin is required for efficient arrestin binding and is required for the efficient and reproducible deactivation of rod cell signaling.

While rhodopsin kinase by itself can decrease Meta II activity by ~50%, the binding of arrestin completely quenches Meta II activity (Kuhn and Wilden, 1987). Arrestin affinity increases with increase in the number of phosphates, but the exact number of phosphates and the sites of their attachment is not known with certainty. However, most studies agree that three phosphates are necessary and sufficient for complete arrestin binding.

Rhodopsin kinase structure

Rhodopsin kinase, like other GRKs, is a member of the AGC protein kinase family. Each GRK consists of an N-terminal helical element of ~20 amino acids, followed by an RH (Regulator of G Protein Signaling Homology) domain (Fig. 1.5). A protein kinase domain is inserted into a loop of the RH domain. Following the RH domain is a variable C-terminal region that is typically involved in membrane targeting. The kinase domain of RK closely resembles that of Protein Kinase A (PKA) and consists of small and large lobes, followed by the “C-tail,” an extension of the protein kinase fold that spans both lobes and contributes residues to the active-site cavity. The post translational modifications of rho kinase include α-carboxymethylation, farnesylation and phosphorylation.

Rhodopsin kinase interaction

Light activated rhodopsin is both a substrate and an allosteric activator of RK, and Rho* is a far better substrate for RK than peptide substrates, with 2–3 orders of magnitude

improvement in K_m and V_{max} (Palczewski et al., 2006). Even though the sites of RK phosphorylation on the C-tail of rhodopsin are freely accessible even in the dark state, they are not phosphorylated by the kinase. But a single Rho* can activate RK and lead to RK-mediated trans-phosphorylation of hundreds on rhodopsin molecules, a phenomenon termed high gain phosphorylation. Moreover, the phosphorylation of a peptide substrate is enhanced by ~160 fold in the presence of Rho* lacking its C-terminal tail. All the RK crystal structures exhibit an open kinase domain which is not conducive for catalyzing phosphorylation. All these lines of evidence indicate that there is an allosteric receptor-docking site distinct from the active site that helps stabilize the kinase in an active state. The second and third cytoplasmic loops of rhodopsin appear most important for binding RK, and site-directed mutants of residues in these loops inhibit GRK1 activation. Functional studies have identified residues in the N terminus, the small lobe, and the C-tail of the kinase domain as being important for the phosphorylation of activated GPCRs.

Rhodopsin kinase stoichiometry

As discussed earlier, rhodopsin can form dimers or higher order oligomers (Kota et al., 2006; Liang et al., 2003; Mansoor et al., 2006). The structural and functional implication of such an organization is not well elucidated yet. One implication for the interaction with its cytosolic partners could be trans-activation or trans-desensitization of the nearby receptors, leading to increase in the sensitivity and efficiency of response. In the case of RK, the higher order organization and high density in the ROS membranes might be responsible for the phenomenon of high-gain phosphorylation, as discussed earlier. However, despite the tendency of rhodopsin to form oligomerize, the basic question remains: how RK-mediated phosphorylation is affected by the oligomeric state of the receptor? Specifically, what is the minimal functional unit of

rhodopsin that can be phosphorylated by RK? In other words, can RK phosphorylate monomeric receptor? In Chapter 3, I have addressed this question by using monomeric rhodopsin in "nanodiscs", which are flat discoidal phospholipid bilayers, surrounded by a belt of an amphipathic alpha helical membrane scaffold protein (MSP), which is modeled on apolipoprotein A (Bayburt et al., 2007; Bayburt and Sligar, 2010).

1.4. Arrestin: Structure and Function

Arrestin family

Arrestins are a small family of cytosolic proteins with four members: rod arrestin (S-antigen or arrestin 1) in the rod and cone cells of the retina, cone arrestin (X-arrestin or arrestin 4) in cone cells and β-arrestin1 and 2 (arrestin 2 and 3, respectively), which are expressed ubiquitously in most tissues(Gurevich and Gurevich, 2006). Arrestin 1 was the first arrestin to be discovered as S-Antigen in the autoimmune disease uveitis, before being discovered as the 48kDa protein that binds phosphorylated rhodopsin and "arrests" or shuts down rhodopsin signaling – hence the name arrestin. β-arrestin1 was the first non-visual arrestin to be discovered as the arrestin for β-adrenergic receptor (Attramadal et al., 1992; Lohse et al., 1990). All arrestins share high sequence similarity to the tune of ~60%. They also share the common function of binding activated, phosphorylated GPCRs and uncoupling G proteins and terminating G protein-mediated signaling. In the non-visual system, β-arrestin1 and 2 are also involved in the internalization of the receptors by recruiting proteins like clathrin and AP-2. β-arrestins further initiate another round of signaling, independent of the G protein pathways, by acting as scaffolding proteins to recruit members of the MAP kinase pathway, thus acting as an important bridge between two major cellular pathways. While β-arrestin1 and 2 are very similar in

sequence, structure and function, different GPCRs exhibit preferential binding to one over the other (e.g., β-2-adrenergic receptor), while others do not seem to exhibit any discernible preference (e.g., angiotensin receptor 1). The molecular basis for these functional differences has not been well established yet.

Arrestin structure

The crystal structure of all the four arrestin subtypes has been solved (Granzin et al., 1998; Han et al., 2001; Sutton et al., 2005; Zhan et al., 2011). All the four arrestin family members show the same overall structural fold, exemplified by rod arrestin, which was the first arrestin to be crystallized. Arrestin is a highly beta stranded molecule with a bilobed structure with two distinct domains – The N- and the C-domain (Fig. 1.6). Each domain folds in two layers of anti-parallel beta sheet on top each other. The two domains are linked via a long loop, which forms the hinge region. The N-terminal domain also contains a short amphipathic alpha helix. There are a number of loops in arrestin which have been shown to have a context dependent structural change, with some showing a helical propensity upon receptor binding. Arrestin also has a long, C-tail, which has so far not been resolved in any crystal structure, indicating its flexibility. The C-tail originates within the C-domain and interacts with the N-domain at the N-terminal beta sheet and α-helix1. The C-terminal tail also makes interactions with the N-domain, and passes over a part of the domain interface, over a region of the protein, known as the polar core. Both the polar core, which is marked by the presence of a group of charged residues buried at the interface if the N- and C-domain, and the C-tail have been implicated in arrestin activation, as described in the next section.

The visual arrestin crystal structure shows two different conformers – α and β. The two conformers show the maximum variability in three loops regions: (i) residues 67-79 that form the

"finger" loop, (ii) residues 155-165 (160 loop) and (iii) 337-347 (Fig. 1.6b). Region (i) or the "finger" loop is present in an open, extended conformation in the α conformer and a closed, folded-over conformation in β. Region (ii), on the other hand, forms a short α helix in the conformer, while in the β conformer, it forms a strand-turn-strand motif. These regions of conformational plasticity might have a functional role in interaction with the receptor or other binding partners. Studies investigating their role in receptor interaction have been reviewed in the next section. Also, their role in receptor binding is investigated in Chapter 2.

Structural basis of arrestin-rhodopsin interaction

Visual arrestin shows high selectivity for binding to light activated, phosphorylated rhodopsin (Rho*-P) (Gurevich and Benovic, 1997; Gurevich and Gurevich, 2006). This implies that there are at least two regions of rhodopsin that are involved in arrestin binding: (a) a region of rhodopsin that is exposed upon light activation, and (b) rhodopsin C-terminal tail with its attached phosphates. In fact, based on the crystal structure of arrestin and extensive mutational analysis, a two-step binding mechanism has been proposed for arrestin binding to rhodopsin: The C-terminal phosphates first destabilize arrestin's basal, non-interacting structure, which would then cause a conformational change in arrestin which would properly align arrestin's high affinity binding sites for the activated receptor(Gurevich and Gurevich, 2006). A recent report detects at least two sequential conformational changes occur in arrestin upon binding Rho-P* (Kirchberg et al., 2011). In fact, high activation energy of ~140kJ/mol associated with arrestin-rhodopsin binding suggests the possibility of large conformational changes involved in the interaction (Schleicher et al., 1989). However, the nature and extent of these conformational changes are yet to be elucidated in detail.

A detailed model of the conformational changes in arrestin that are involved in receptor binding has been proposed (Gurevich and Gurevich, 2006). This model proposes a two-step mechanism of arrestin binding to the receptor, beginning with arrestin binding to the receptor phosphates. Arrestin residues K14, K15 and R175 have been proposed to have a role of phosphate sensors based on mutational analysis (Gray-Keller et al., 1997; Gurevich and Benovic, 1997; Gurevich and Gurevich, 2006). A recent report suggests that this proposed set of interaction might not be universal - the role of receptor phosphates and the K14-K15 "phosphate sensor" is dependent on the arrestin-receptor pair in question (Vishnivetskiy et al., 2011). Initial interaction with the phosphates "guides" the phosphates to the arrestin "polar core" and disrupts the salt bridge interaction involving R175 and D296. This then causes large conformational changes in arrestin, thus arriving at its final conformation. Proposed conformational changes include the disruption of a hydrophobic "three element" interaction involving the C-tail, and β-strand 1 and α-helix 1 of the N-domain and the recruitment of the amphipathic α-helix 1 to the membrane. Finally, the disruption of these stabilizing interactions has been proposed to cause an inter-domain movement in a manner similar to a clam-shell closing. However, various biophysical approaches have failed to detect large scale structural changes within arrestin, upon receptor binding (Carter and Hill, 2005; Palczewski et al., 1992b; Vishnivetskiy et al., 2010).

In the absence of clear evidence showing large scale conformational changes in arrestin activation, it is possible that the high activation energy for interaction is a result of multiple smaller conformational changes. Some of these changes might involve some of the loops of arrestin, which show conformational heterogeneity in the crystal structure. As discussed earlier, the arrestin "finger" loop shows two different conformations in the crystal structure. NMR studies have detected helix formation is induced in this loop upon receptor binding (Feuerstein et

al., 2009). Fluorescence and EPR studies have shown this loop to show a change in local environment and mobility upon receptor binding (Hanson et al., 2006; Sommer et al., 2007; Sommer et al., 2005). Similarly, arrestin loop 155-165 shows two different conformations in different crystal isoforms (Hirsch et al., 1999). The sequence of this loop falls into a class of polypeptides, termed “chameleons”, whose conformation is determined by the global environment, rather than the sequence, indicating a functional relevance for the loop (Hirsch et al., 1999; Minor and Kim, 1996). The role of these two loop regions of arrestin in binding the receptor has been studied in Chapter 2.

Sites of interaction

Studies using various approaches including mutagenesis, peptide inhibition and EPR, among others, have mapped the receptor binding interface of arrestin onto the concave face of both the N- and C-domain (Dinculescu et al., 2002; Hanson et al., 2006; Kieselbach et al., 1994; Ohguro et al., 1994; Pulvermuller et al., 2000; Smith et al., 2004; Smith et al., 1999; Vishnivetskiy et al., 2004). In fact, a few residues in the N- and C-domain have been proposed to be involved in determining the receptor specificity of arrestin (Vishnivetskiy et al., 2011). As discussed in the previous section, the arrestin loop regions might have a role in receptor interaction as well.

On the receptor side, the C-terminal phosphates bind arrestin at its phosphate sensor. These phosphates are generally clustered together, indicating the need for a concentrated negative charge density for arrestin binding (Gurevich and Benovic, 1993, 1995; Kuhn et al., 1984). In fact, spatially concentrated acidic amino acids like aspartates and glutamates, which can act as phosphate mimics, can also “trip” the arrestin phosphate sensor, and cause it to bind to the receptor. However, this does not work for the visual arrestin-rhodopsin interaction (Smith et

al., 2011). Apart from the receptor phosphates, all three cytosolic loops have been implicated in arrestin binding (Krupnick et al., 1994; Shi et al., 1998). The conserved E(D)RY sequence may also be important for arrestin binding (Shi et al., 1998). Since arrestin recognizes the activated state of the receptor and the active state of rhodopsin shows an outward movement of TM6 which exposes a hydrophobic cavity in the receptor, it is likely that arrestin makes use of this region of the receptor for its binding. In fact, the G_t tail peptide has been shown to bind this region and make contacts with the exposed hydrophobic patch (Farrens et al., 1996; Janz and Farrens, 2004). Given the fact that arrestin competitively inhibits G_t, it is reasonable to hypothesize that arrestin binds in this same region of rhodopsin, and this model has been proposed by others (Gurevich and Gurevich, 2006; Huang et al., 2011).

While we know the individual regions of the two proteins involved in their interaction, we still do not have a residue-specific information regarding pairs of contact sites between arrestin and rhodopsin. Chapter 2 of this thesis tests some direct sites of interaction between arrestin and rhodopsin.

1.5. Spectroscopic Approaches

This dissertation makes use of various spectroscopic (absorbance and fluorescence) approaches to study the interaction of arrestin with rhodopsin. Some of these make use of the spectral properties of rhodopsin, resulting from the interaction of the apoprotein opsin with the retinal chromophore, while others use the spectral properties of a fluorescent label attached to specific cysteines in opsin.

Rhodopsin difference spectrum and extra-Meta-II assay

The 11-cis-retinal chromophore is attached to K296 of rhodopsin via a Schiff base. Its interaction with the amino acids lining the retinal binding pocket gives rhodopsin a characteristic 500nm absorbance in the dark state (Fig. 1.8). Upon light activation, the chromophore undergoes a cis-trans isomerization and forms all-trans-retinal. The receptor goes through a series of photointermediates to arrive at the active Meta-II (MII) species in equilibrium with Meta-I (MI) rhodopsin (478nm). Meta-II shows a characteristic absorbance at 380nm and lacks the 500nm absorbance peak of the dark state. Subtracting the dark state spectrum from the light activated spectrum gives rise to a difference spectrum, with a dip at 500nm, owing to the loss of 500nm absorbance upon light activation, and a peak at 380nm, indicative of the formation of the Meta-II species (Fig. 1.8).

The MI-MII equilibrium is pH and temperature dependent. Also, binding of proteins like transducin or arrestin stabilizes shifts the equilibrium towards Meta-II (Emeis and Hofmann, 1981; Hofmann et al., 1983). The large difference in the absorbance between MI and MII provides a spectroscopic monitor for the binding of these proteins, and is observed as an increase in absorbance at 380nm in the presence of the binding protein. We have used this assay as an indicator of arrestin binding to rhodopsin in Appendix A1.

Retinal trapping assay

Tryptophan residues in rhodopsin dark state are only weakly fluorescent, owing to energy transfer to the retinal chromophore. (Ebrey, 1971; Farrens and Khorana, 1995). Upon light activation, as the MII decays and retinal leaves the receptor, the quenching is relieved, and the intrinsic tryptophan fluorescence (measured at 330nm) of rhodopsin increases with time (Farrens

and Khorana, 1995) (Fig. 1.9). In the presence of arrestin, it has been shown that the release of arrestin and retinal are directly linked (Sommer et al., 2005). Also, in mixed micelles, arrestin traps about 50% of the retinal in rhodopsin (Sommer et al., 2006). This is reflected as a reduction in the increase in Trp fluorescence in the presence of arrestin (Fig. 1.9). Upon addition of hydroxylamine (HA), which cleaves the retinal Schiff base, there is a further increase in Trp fluorescence of rhodopsin samples in the presence of arrestin. This increase in fluorescence after HA addition is not seen in receptors without arrestin, indicating that all the retinal is already released from the receptors in the absence of arrestin. The amount of fluorescence increase after HA addition, expressed as a percent of the total final fluorescence, gives the percent of retinal that was trapped by arrestin, and can be used as an indicator of arrestin binding to the rhodopsin.

Tryptophan Induced Quenching (TrIQ)

Site-directed fluorescence labeling (SDFL) is a very useful way to study protein structure, dynamics and interactions. SDFL normally employs the introduction of cysteine residues at specific sites in a protein and labeling it with a cysteine-reactive fluorophore. The fluorescence spectrum of the fluorophore can provide insight into the local environment, secondary structure and solvent accessibility of the residue (Mansoor et al., 1999). One such fluorophore is monobromobimane (mBBr), which is a very useful probe for studying protein structure and dynamics, as it is small, non-polar, and has well-characterized spectral properties (Kosower, 1982; Mansoor et al., 1999). Trp residues have been shown to quench mBBr fluorescence, in a distance dependent manner by photo-induced electron transfer (PET) (Mansoor et al., 2010; Mansoor et al., 2002) (Fig. 1.10). This quenching phenomenon is termed Tryptophan-Induced Quenching or TrIQ. This can be used as a way to test the proximity of Trp and the mBBr labeled residue in a protein (Mansoor et al., 2002), and be used to study protein

dynamics (Islas and Zagotta, 2006). TrIQ occurs over when bimane and the quenching Trp are at or near van der Waal's distance (Cα-Cα distance between the site of label attachment and Trp is between 5-15Å) (Mansoor et al., 2010). Further, this quenching phenomenon can also be used to map interaction sites between proteins. For two interacting proteins, we can label one protein with mBBr at a specific cysteine residue and make Trp mutations at different sites on the second protein. Trp residues on the second protein that quench mBBr fluorescence of the first protein are predicted to be close to the labeled cysteine, thus enabling the mapping of binding sites within 5-15Å distance between the alpha carbons, as mentioned above.

TrIQ analysis to obtain distance-specific information

As mentioned above, TrIQ occurs when bimane and the quenching tryptophan are at or near van der Waal's contact distance from each other (5-15Å Cα-Cα distance) (Mansoor and Farrens, 2004; Mansoor et al., 2002). TrIQ can result from two types of quenching events: "dynamic" (or collisional) quenching and/or static quenching.

Mansoor, et al described a method to quantify the amount relative fractions of statically quenched, dynamically quenched and unquenched fluorophore populations (Mansoor et al., 2010). Their analysis is based on the effect of Trp-mBBr interaction on both the steady state integrated fluorescence intensity values (F_o and F_w in the absence and presence of the quenching Trp), as well as on the fluorescence lifetime of mBBr (τ_o and τ_w in the absence and presence of the quenching Trp) (Fig. 1.11).

In the presence of a quencher, a fluorophore can have three different fates: (a) it can stay unquenched, if the quencher is too far away in space, (b) it can get quenched by collision with a quencher, some time after photon absorption, while it is still in the excited state and (c) the

fluorophore can be complexed with the quencher, even before absorption of a photon, and not even get to the excited state (Fig. 1.12). If the fluorophore stays unquenched (with the Trp being too far away in space), both its fluorescence intensity and lifetime remain unchanged. If the fluorophore, after photon absorption, undergoes collision with a Trp residue during its excited state, it is said to undergo dynamic quenching. Dynamically quenched fluorophores exhibit both a reduced fluorescence intensity (F_w) as well as reduced fluorescence lifetime (τ_w) in the presence of the quenching Trp, compared to the corresponding values in its absence. As such, for dynamic quenching, (Fo/Fw) = (τ_o/τ_w). In the case of fluorophores that exhibit static quenching by forming a complex with Trp before light excitation, the fluorophores are non-fluorescent and do not contribute to the fluorescence intensity and do not affect the fluorescence lifetime. In this case, (Fo/Fw) $\neq$ (τ_o/τ_w) and (Fo/Fw) is greater than (τ_o/τ_w).

While comparing the ratios of (Fo/Fw) and (τ_o/τ_w) gives us a qualitative understanding of pure static or dynamic quenching processes, the quantitation of static and dynamically quenched componenets of fluorescence is based on the following equeations given below .

The relative fraction of Trp-fluorophore pairs not in a static complex was calculated using

Eq.1: $\gamma = (F_w/F_o).(\tau_o/\tau_w)$

The relative fraction of Trp-fluorophore pairs involved in a static complex is given by

Eq. 2: $\gamma_{SQ} = (1- \gamma)$

while those undergoing dynamic quenching is

Eq. 3: $\gamma_{DQ} = (1-(\tau_w/\tau_o)).\gamma$

The analysis showed that Trp residue causes static quenching of mBBr fluorescence at Cα-Cα distance less than 10Å, and dynamic quenching at distances less than 15Å. It should be reiterated that static quenching indicates direct physical interaction between the fluorophore and the Trp residue, keeping the fluorophore in the ground state, and that the complex is formed within the time scale of fluorescence excitation (sub-nanosecond). This analysis was used in Chapter 2 to determine the sites of direct interaction between arrestin and rhodopsin.

1.6. Cannabinoid Receptor System

The major psychoactive ingredient in marijuana belongs to a family of lipophilic molecules called cannabinoids. These compounds bind to and activate cannabinoid receptors, which are members of the GPCR superfamily. Two types of cannabinoid receptors have been identified so far: CB1, which is present in the central nervous system, and CB2, which is predominantly present in immune cells and tissues.

Signaling mechanism: Activation

CB1 receptor is one of the most abundant GPCRs in the central nervous system, with a high level of expression in cortex, amygdale, basal ganglia, and cerebellum (Herkenham et al., 1991). The CB1 receptor primarily transduces its physiological effects through inhibitory G proteins (G_i/G_o). These effects include inhibition of adenylyl cyclase, inhibition of calcium channels (N- and P/Q- types) and activation of inwardly rectifying potassium channels (Fig. 1.7) (Bouaboula et al., 1995; Mackie et al., 1995). Together, these effects can lead to the inhibition of neurotransmission. CB2 also couples to G_i in response to both endo- and synthetic cannabinoids, leading to inhibition of adenylyl cyclase-mediated cAMP accumulation (Gonsiorek et al., 2000). CB2 also couples with inwardly rectifying potassium channels (Ho et

al., 1999). A number of receptor specific ligands can be used to tease apart the roles played by the two receptors.

Signaling mechanism: Desensitization

Behavioral and physiological tolerance to cannabinoids develops rapidly and is primarily mediated by changes in the CB1 cannabinoid receptor (Paquette et al., 2007). Receptor desensitization or uncoupling has been consistently implicated as one of the molecular events underlying the onset of tolerance in many systems (Booker et al., 1998; Kovoor et al., 1997). Desensitization of GPCRs is associated with phosphorylation of the receptor by GRKs followed by binding of β-arrestin and a reduction in affinity for G proteins (Krupnick and Benovic, 1998; Zhang et al., 1997). This sequence of events effectively attenuates signaling by the GPCR and its ligand.

CB1 recycling and downregulation

GPCRs are either dephosphorylated and recycled back to the cell surface (resensitization) or targeted to lysosomes for degradation (down-regulation) (Drake et al., 2006). Rapid recycling of CB1 receptors heterologously expressed in AtT20 cells is observed after short (minutes) agonist exposure and requires dephosphorylation by phosphatase 1 or 2A (PP1 or PP2A) and endosomal acidification (Hsieh et al., 1999; Wu et al., 2008). Chronic (~1.5 hour) agonist exposure promotes down-regulation of CB1 receptors (Hsieh et al., 1999), as can briefer exposure to very high concentrations of agonists (Keren and Sarne, 2003; Martini et al., 2007). This downregulation is mediated by the interaction of CB1 with GPCR-associated sorting protein 1 (GASP1) which binds the receptor C-terminus and targets the receptor to lysosomes (Tappe-Theodor et al., 2007).

Constitutive activity and CRIP1a

Unlike rhodopsin, which acts as a strict ON-OFF switch, with almost no dark state signaling, many GPCRs, either wild-type or pathologically relevant mutants, show some level of constitutive activity in the absence of any ligand (Seifert and Wenzel-Seifert, 2002). In constitutively active receptors, the equilibrium between inactive and active receptor conformations is shifted towards the activated state(s) even in the absence of agonists, leading to measurable basal activation of intracellular signaling pathways (Milligan et al., 2003). While true "neutral" antagonists inhibit binding of both agonists and inverse agonists without favoring the equilibrium between active or inactive conformations (Kenakin, 2004), antagonists that inhibit the basal activation by stabilizing inactive receptor conformations are called inverse agonists (Milligan et al., 1997).

CB1 displays a high level of constitutive activity in the absence of any ligand either when heterologously expressed in non-neuronal cells or in neurons with endogenous receptors (Bouaboula et al., 1997; Landsman et al., 1997). The constitutive activity also leads to constitutive endocytosis of CB1, leading to a predominantly (~85%) endocytic localization of the receptor at steady state (Leterrier et al., 2004). Thus, by controlling the level of receptors on the cell surface, constitutive activity of CB1 plays a major role in modulating the function of the receptor.

Intracellular regulatory proteins can interact with the C-terminus of some GPCRs to regulate constitutive activity (Gavarini et al., 2004). Electrophysiological studies on heterologously expressed wild-type and truncated CB1 receptors in isolated superior cervical ganglion (SCG) cells from rats revealed that the truncation of the distal C-terminus of the CB1 receptor at amino acid 417 enhanced its constitutive activity (Nie and Lewis, 2001b). This

finding raised the possibility that a protein binds to the distal C-terminal tail that attenuates the constitutive activity of CB1.

A yeast two-hybrid screening of a human brain cDNA library, using the last 55 amino acids (418–472) of the CB1 receptor C-terminal tail as bait, led to the discovery of two novel proteins, termed cannabinoid receptor interacting proteins 1a and b (CRIP1a and CRIP1b) (Niehaus et al., 2007). CRIP1a and 1b turned out to be alternative splice variants of 164 and 128 amino acids, respectively. CRIP1a is expressed in the brain, and is also detected in heart, lung and intestine. It was also found to be expressed in the retina in the presynaptic terminals of cone photoreceptors, with the staining being very close to that of CB1 (Hu et al., 2010). While CRIP1a is found throughout vertebrates, CRIP1b seems to be unique to primates. CRIP1a co-immunoprecipitated with CB1 from rat brain and co-localized with CB1 when heterologously expressed in SCG neurons. Neither CRIP1a nor CRIP1b significantly altered the affinity of CB1 for the inverse agonist SR141716. However, CRIP1a, but not CRIP1b, significantly attenuated the constitutive inhibition of voltage-gated Ca^{2+} channels by CB1 receptors (Niehaus et al., 2007). This effect was blocked by the inverse agonist SR141716A. However, the inhibition of Ca^{2+} currents induced by the agonist WIN55,212-2 was not affected by either variant.

Comparative genomic analysis indicated that CRIP1a is conserved throughout the vertebrates. Hydropathy analysis revealed that CRIP1a contains no transmembrane domains, but contains a predicted palmitoylation site, which might help in association with the plasma membrane (Niehaus et al., 2007). The C-terminal tail of CRIP1a contains a predicted PSD-95/Disc-large-protein/ZO-1 (PDZ) class I ligand, which might be involved in interaction with PDZ domain-containing proteins. This finding suggests that CRIP1a, like many other proteins that interact with PDZ domains, may be important for regulating CB1 receptor signaling,

scaffolding or trafficking. Interestingly, many GPCRs are known to contain PDZ ligands and various GPCR-interacting proteins contain PDZ domains, suggesting that CRIP1a could indirectly link CB1 receptors to other GPCRs (Smith et al., 2010).

There are very few functional studies testing the effect of CRIP1a in the brain to date. One study found a decrease in the levels of CRIP1a mRNA along with the levels of CB1 mRNA in the hippocampi of patients with sclerotic epilepsy, compared those in a healthy cohort (Ludanyi et al., 2008). This might suggest a role for modulation of CB1 receptor function by CRIP1a in the pathogenesis of or in response to epilepsy. Cannabinoids have been shown to be neuroprotective in multiple systems (Abood et al., 2001; Hansen et al., 2002). However, both agonists and antagonists of the CB1 are neuroprotective, but the mechanisms responsible for these actions remain unclear. In an assay of glutamate neurotoxicity in primary neuronal cortical cultures, CRIP1a disrupted agonist-induced neuroprotection and conferred antagonist-induced neuroprotection, the mechanism of which is unclear, but hypothesized to be linked to the PDZ ligand in CRIP1a (Stauffer et al., 2011).

The above lines of evidence point to a growing body of knowledge regarding the potential role of CRIP1a in modulating CB1 receptor physiology. However, there is hardly any biochemical information regarding CRIP1a. In Appendix A2 of this thesis, I describe the expression and purification of tag-free CRIP1a. I have also studied the secondary structure and other physiochemical properties of the protein. Finally, I have performed some preliminary experiments to screen for conditions to crystallize CRIP1a and ultimately determine the structure of the protein.

1.7. Dissertation Overview

The main focus of this dissertation is to understand the structural interactions between GPCRs and their affiliate cytosolic proteins that attenuate receptor signaling. The studies have aimed at testing the stoichiometry of the interaction as well as the sites of interaction between the proteins, apart from the biochemical characterization of a novel protein involved in GPCR signal attenuation.

We studied the interaction of arrestin and rhodopsin to find direct sites of interaction between the two. In Chapter 2, I describe the use of a fluorescence spectroscopic approach to monitor protein-protein interaction and show that arrestin makes specific contacts with opsin at the cytosolic face of TM6. We labeled cysteine residues at positions 242 and 243 of opsin with the fluorophore monobromobimane (mBBr) and tested if Trp residues introduced at specific sites of arrestin can quench mBBr fluorescence (Tryptophan Induced Quenching or TrIQ (Mansoor et al., 2010)). By combining the steady state quenching data with lifetime measurements of the receptor-attached fluorophore in the absence or presence of arrestin, we show that two distinct sites on arrestin make contacts with the base of TM6. These results indicate two possible orientations of the arrestin molecule upon receptor binding.

In Chapter 3, we present results of an investigation into the interaction of rhodopsin kinase with rhodopsin. We describe a one-step purification strategy for rhodopsin kinase expressed in mammalian cells. We tested the functionality of the kinase on rhodopsin in native ROS membrane as well as purified rhodopsin in detergent micelles. Finally, we found that rhodopsin kinase does not need rhodopsin self-association for its function, as it can phosphorylate monomeric rhodopsin in nanodiscs. The implications of these studies are discussed in Chapter 4.

Appendix A1 describes the study of the interaction of arrestin with rhodopsin, from the point of view of the stoichiometry of interaction. We describe the reconstitution of rhodopsin into lipid-containing discoidal membranes, called nanodiscs. The samples were analyzed to show that the reconstituted rhodopsin retained its light sensitive spectral properties and was monomeric under these conditions. We found that both arrestin and β-arrestin 1 bound phosphorylated monomeric rhodopsin in nanodiscs upon light activation, as measured by their ability to stabilize the MII state of rhodopsin (extra MII assay) (Emeis et al., 1982). We also reconstituted phosphorylated rhodopsin into nanodiscs under conditions that would favour the formation of dimers or higher order oligomers. Surprisingly, the amount of extra MII formed upon arrestin binding was lower in the case of multimeric rhodopsin in nanodiscs or liposomes. We also confirmed that lipids with acidic head groups enhance arrestin binding to rhodopsin. These results confirmed that, like with rhodopsin kinase, arrestin binding, too, does not require rhodopsin to self-associate.

In Appendix A2, we have studied a novel protein, CRIP1a, which has been shown to inhibit the basal or constitutive activity of CB1 receptor (Niehaus et al., 2007). We determined conditions for the expression and purification of recombinant CRIP1a at high yields from *E. coli*. We have also carried out some preliminary biochemical and biophysical characterization of this protein. Circular dichroism study reveals that the protein is well folded and exhibits high β-sheet content. Urea melt studies indicate the protein is very stable. Also, size exclusion chromatography indicates that the protein is mostly monomeric in solution. The cysteines in the protein and quite labile and are likely not involved in intra- or intermolecular disulfide

formation. Finally, preliminary experiments have been carried out to find conditions to crystallize CRIP1a to determine its 3D structure.

Fig. 1.1. GPCR signaling pathway.

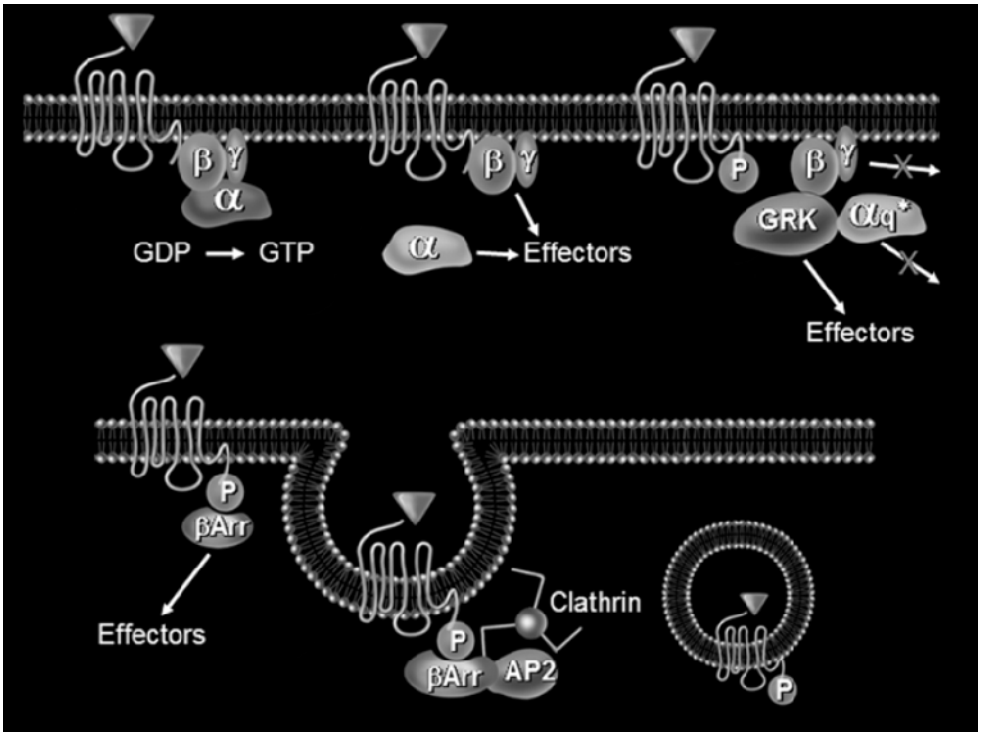

Fig. 1.1. GPCR signaling pathway.

Agonist binding activates the receptor, which, in turn, activates a heterotrimeric G protein. The α subunit exchanges GDP for GTP and dissociates from the βγ subunits and both the α and the βγ subunits go on to activate their respective effector molecules. The activated receptor is recognized by its kinase, GRK, which phosphorylates the receptor and starts the desensitization pathway. The phosphorylated receptor is bound by arrestin, which competitively inhibits G protein binding and terminates G protein mediated signaling. In the case of non-visual GPCRs, arrestin isoforms β-arrestin 1 and 2 can recruit members of the endocytic machinery, like AP-2 and clathrin, leading to receptor internalization. In some cases, β-arrestins can themselves start a second round of signaling. Figure is from (Gainetdinov et al., 2004)

Fig. 1.2. Rod cell phototransduction.

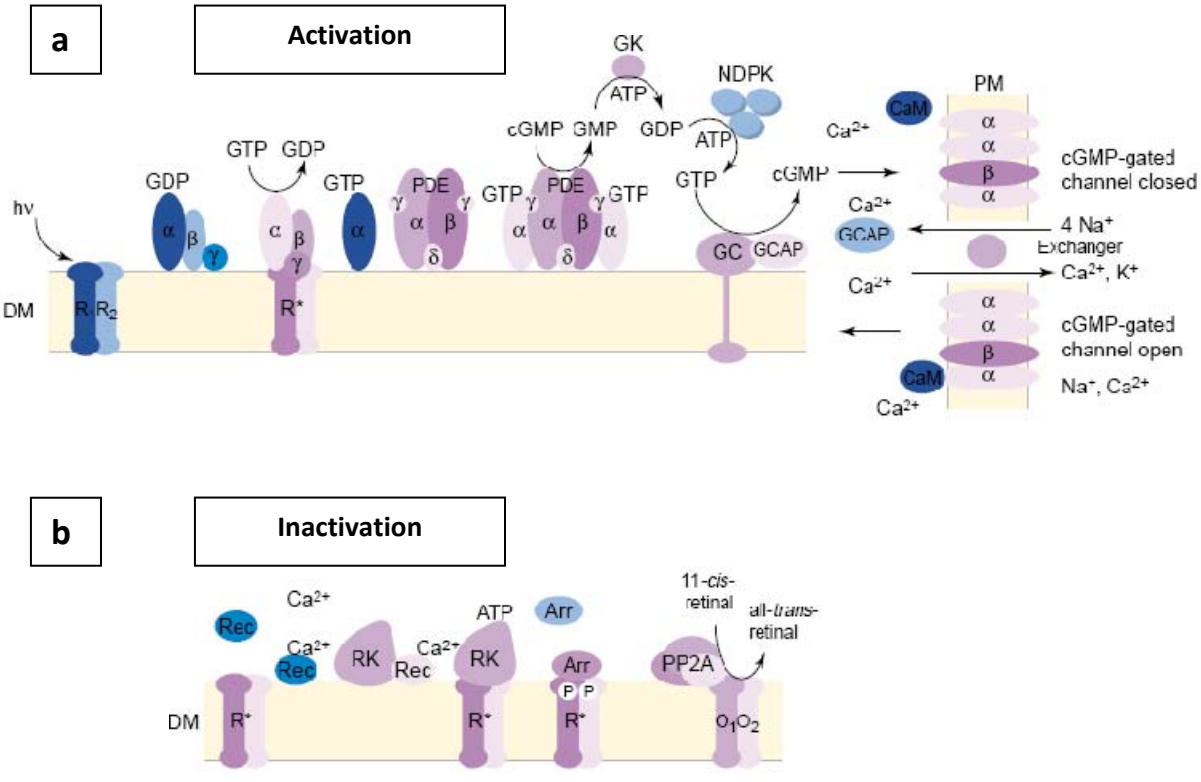

Fig. 1.2. Rod cell phototransduction.

A schematic representation of visual transduction in rod cells. (a) Signal propagation. Light activation leads to the isomerization of the chromophore 11-cis-retinal to all-trans-retinal, which activates rhodopsin. Active rhodopsin then activates its cognate G protein, transducin (G_t). Upon receptor mediated activation, G_t exchanges GDP for GTP and the transducin heterotrimer dissociates into α and βγ subunits. The activated α subunit binds to and activates its effector protein, a phosphodiesterase (PDE6), which cleaves cGMP to form GMP. The reduction in the cGMP levels causes the closing of cyclic nucleotide gated channels, which, in turn, inhibits Na+ channels, and leads to hyperpolarization of the cell, which is eventually perceived as a visual signal. (b) Inactivation pathway. As the Ca^{2+} level drops due to light activation, recoverin dissociates from RK and RK then phosphorylates rhodopsin, which is then bound by arrestin. Arrestin inhibits G_t binding and terminates the receptor signal. All-trans-retinal is released from the rhodopsin and the receptor gets dephosphorylated by PP2A, and the dephosphorylated opsin can undergo another round of regeneration. Figure is from (Ridge et al., 2003).

Fig. 1.3. Photointermediates of rhodopsin.

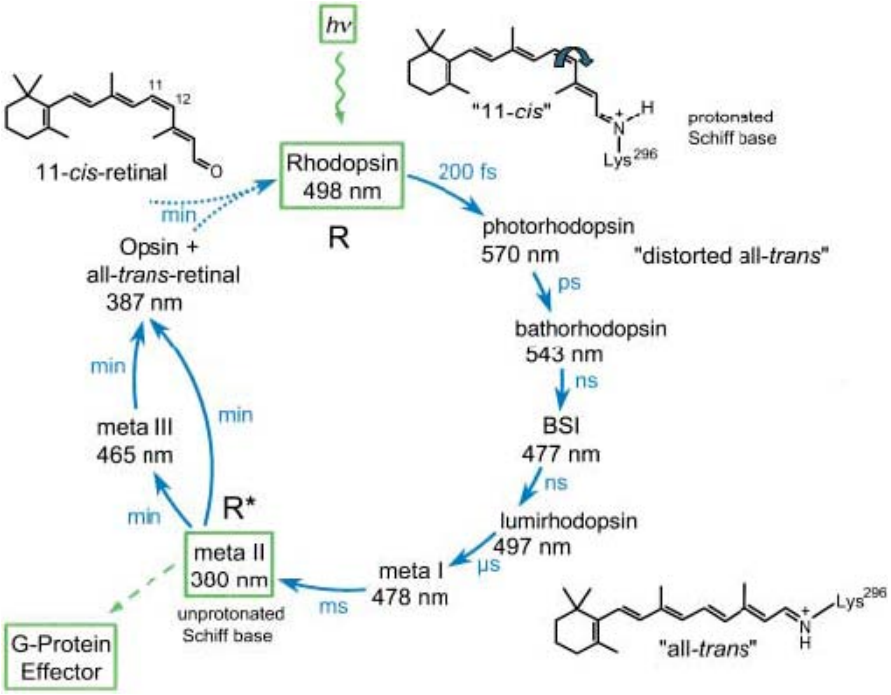

Fig. 1.3. Photointermediates of rhodopsin.

Rhodopsin activation by light causes the isomerization of its chromophore, 11-cis-retinal. Photoisomerization of the 11-cis double bond yields the photoproduct photorhodopsin which thermally relaxes through several intermediates which can be distinguished because of their distinct λ_{max} values. Progressive release of the strain in the chromophore leads through batho- and lumirhodopsin to Meta I (λ_{max} : 478nm), which is in equilibrium with the G protein interacting form, Meta II (λ_{max} : 380nm). Meta II decays either directly or through another photointermediate, Meta III (λ_{max} : 465nm), to opsin and all-trans-retina. The different spectral properties of the various photointermediates enable the structure-function studies of the photoreceptor. Figure is from (Ernst and Bartl, 2002).

Fig. 1.4. Structure of rhodopsin.

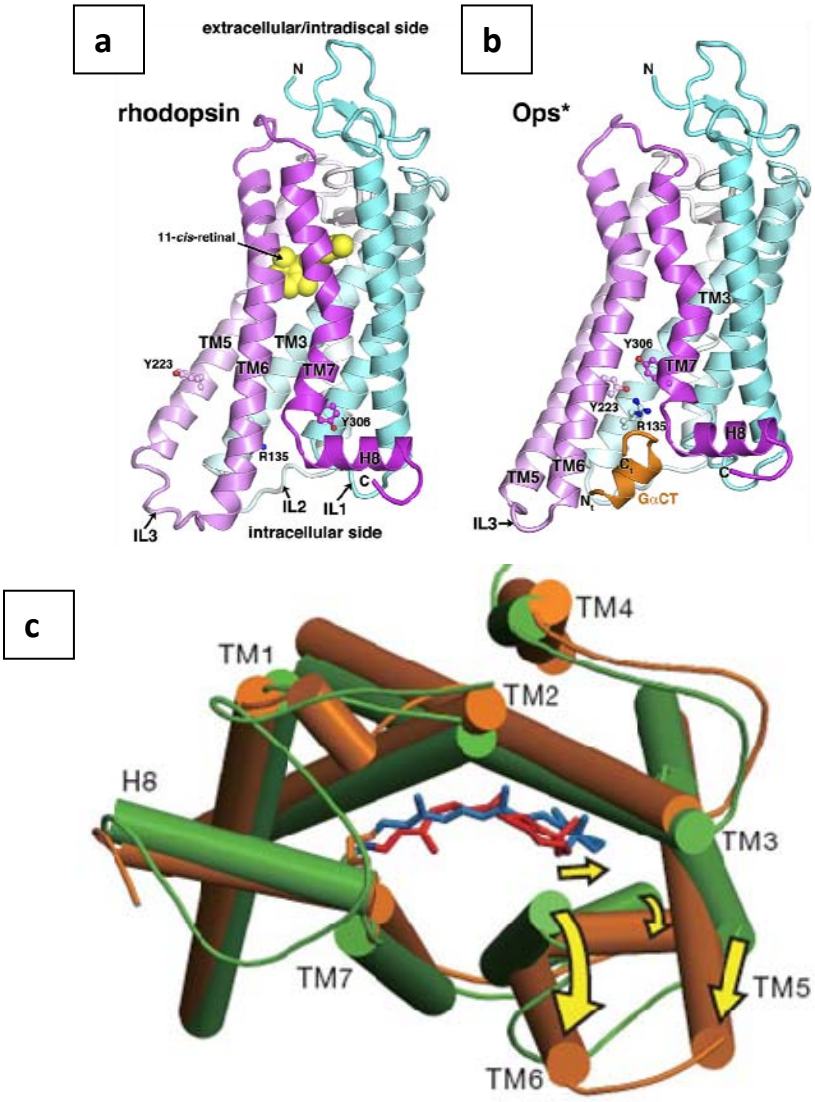

Fig. 1.4. Structure of rhodopsin.

Crystal structure of rhodopsin in (a) the dark state (1GZM), and (b) active-like Ops* state (3DQB), with the transducin C-terminal tail peptide bound. Both the structures are very similar overall, with a seven transmembrane architecture, and the retinal chromophore bound within the helical bundle. In the inactive structure, three highly conserved residues, R135 in TM3, Y233 in TM5, and Y306 in TM7, are well separated, and the chromophore is in the 11-cis conformation, while attached to K296 on the receptor, while in the Meta II structure, retinal is in the all-trans form. (c) In comparing dark state structure with the active, Meta II structure (3PQR), most of the difference is in the cytosolic end of the receptor, where the movement of TM5 and 6 upon receptor activation (shown by arrows), leads to transducin binding. The extracellular domain forms a four-stranded beta sheet which caps the retinal binding pocket. Figures adapted from (Choe et al., 2011; Huang and Tesmer, 2011).

Fig. 1.5. Structure of rhodopsin kinase.

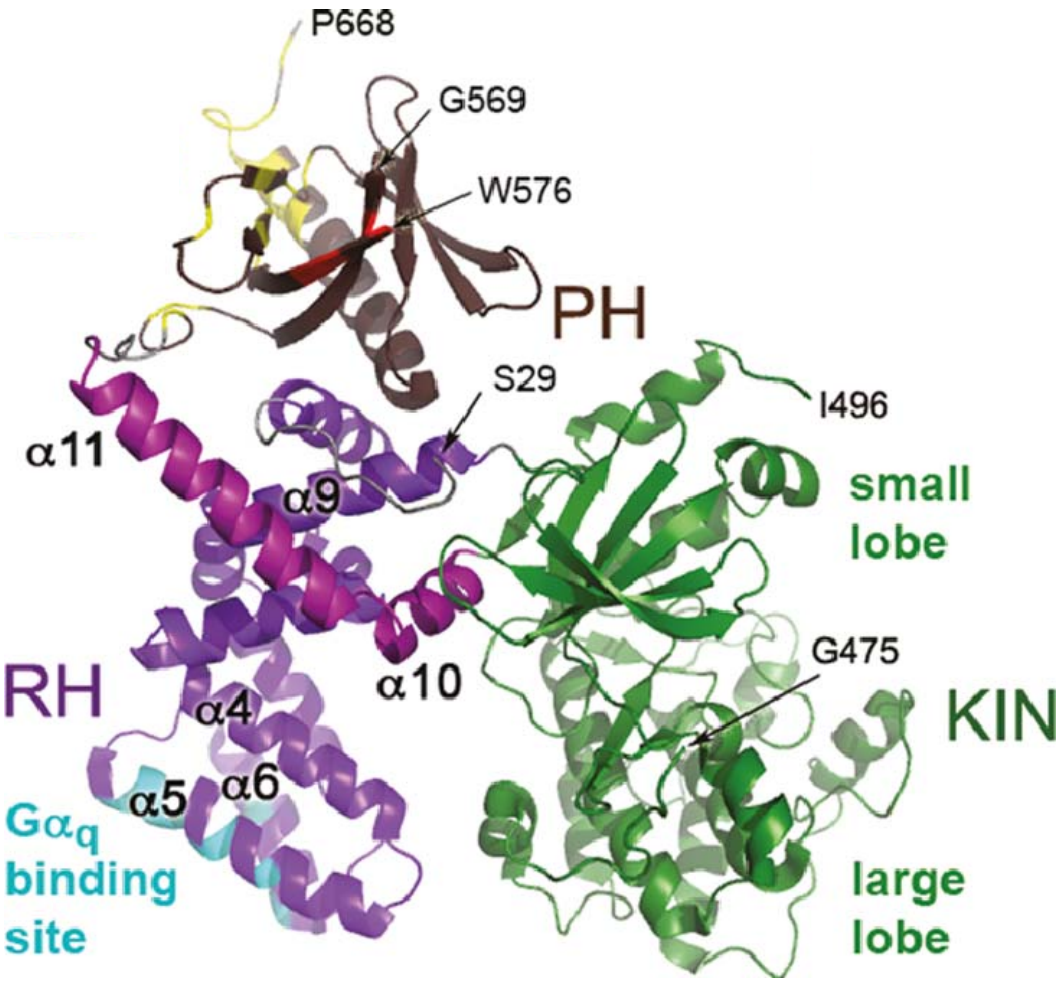

Fig. 1.5. Structure of rhodopsin kinase.

Crystal structure of a rhodopsin kinase shows it has an RGS homology domain (RH domain, in magenta), with the kinase domain (in green) inserted into a loop of the RH domain. The kinase domain itself has a small and a large domain, with the small domain composed of six β strands and two α helices, and the large domain being primarily alpha helical. The active site is at the interface of the large and the small kinase domains (Huang et al., 2009).

Fig. 1.6. Structure of arrestin.

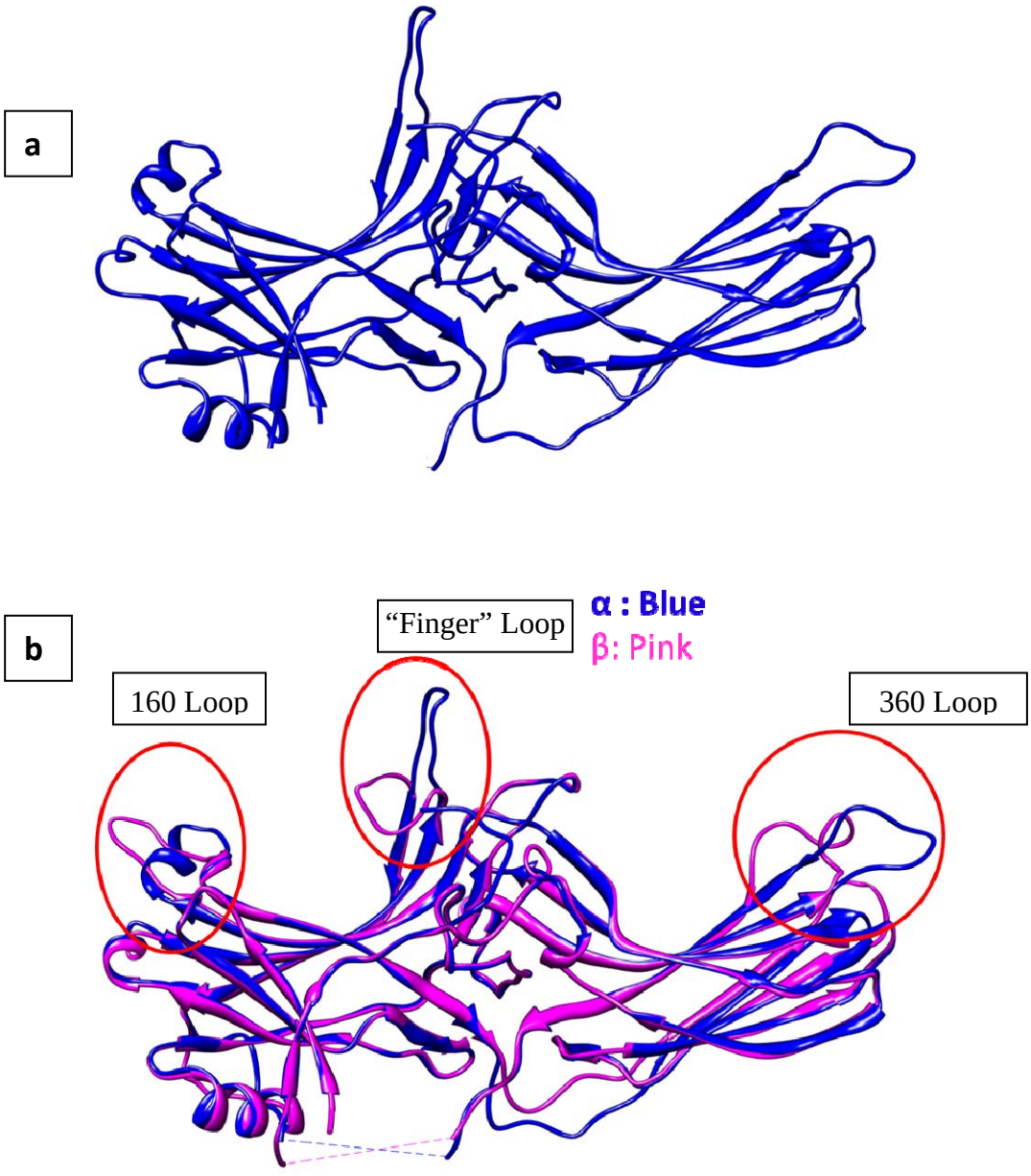

Fig. 1.6. Structure of arrestin.

(a) Crystal structure of visual arrestin (1CF1) shows that it is highly beta stranded protein. It is a bilobed protein with each lobe being comprised of a seven strand beta sandwich. The two lobes are joined by a flexible hinge region. (b) Alignment of two different crystal isoforms, α (in blue) and β (in pink) of arrestin show variability in the loop regions, especially, the “finger” loop the loop between residues 155-165 (160 loop) at the distal end of the N-domain, and the 360 loop at the distal C-domain. Models were made using UCSF Chimera.

Fig. 1.7. CB1 receptor signaling.

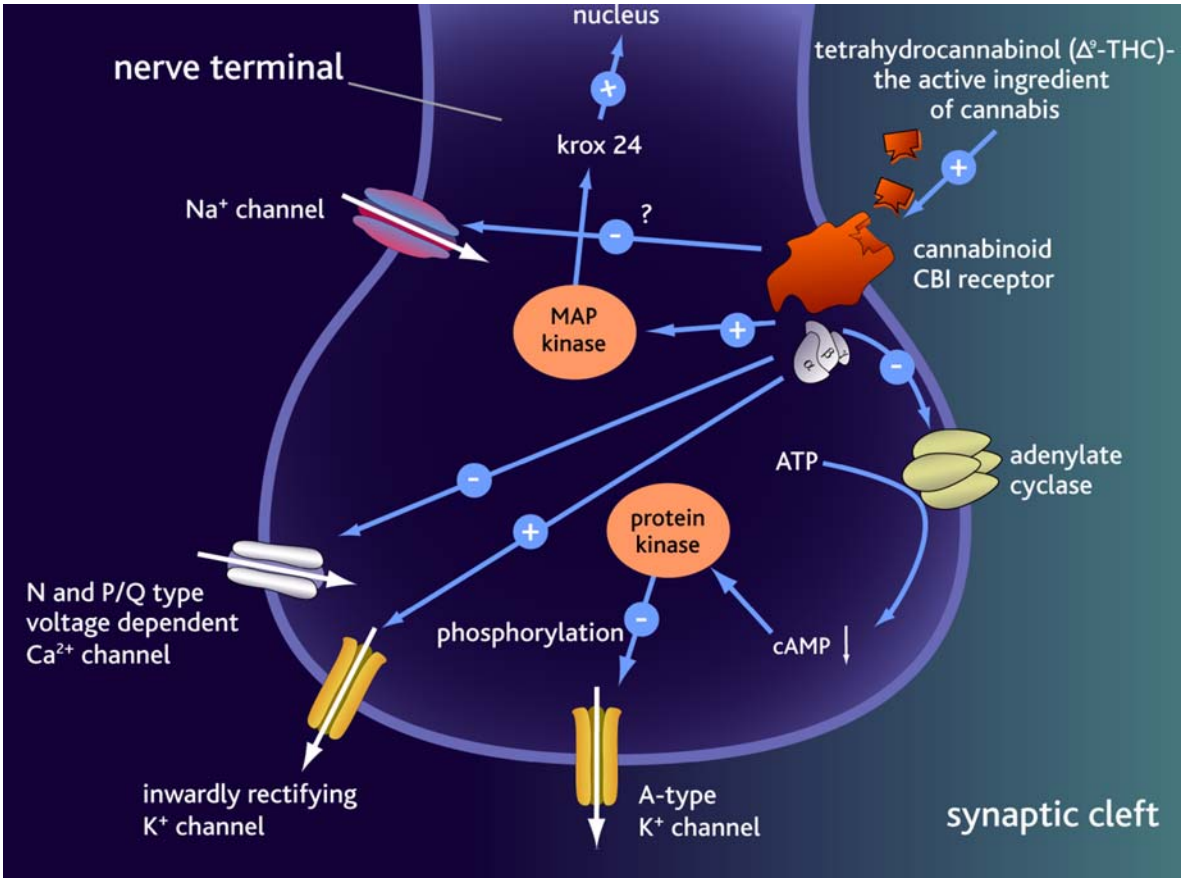

Fig. 1.7. CB1 receptor signaling.

Cannabinoid ligands act by binding to cannabinoid CB1 receptors on pre-synaptic nerve terminals in the brain. Δ^9-THC binding to CB1 receptors activates G proteins that activate/inhibit a number of signal transduction pathways. The G proteins directly inhibit N and P/Q-type voltage dependant calcium channels and sodium channels and indirectly inhibit A-type calcium channels via inhibition of adenylyl cyclase. Δ^9-THC binding and G protein activation also activates inwardly rectifying potassium channels and the MAP kinase signaling pathway. Figure is from www.cnsforum.com.

Fig. 1.8. Rhodopsin absorbance spectra and the extra-MII assay.

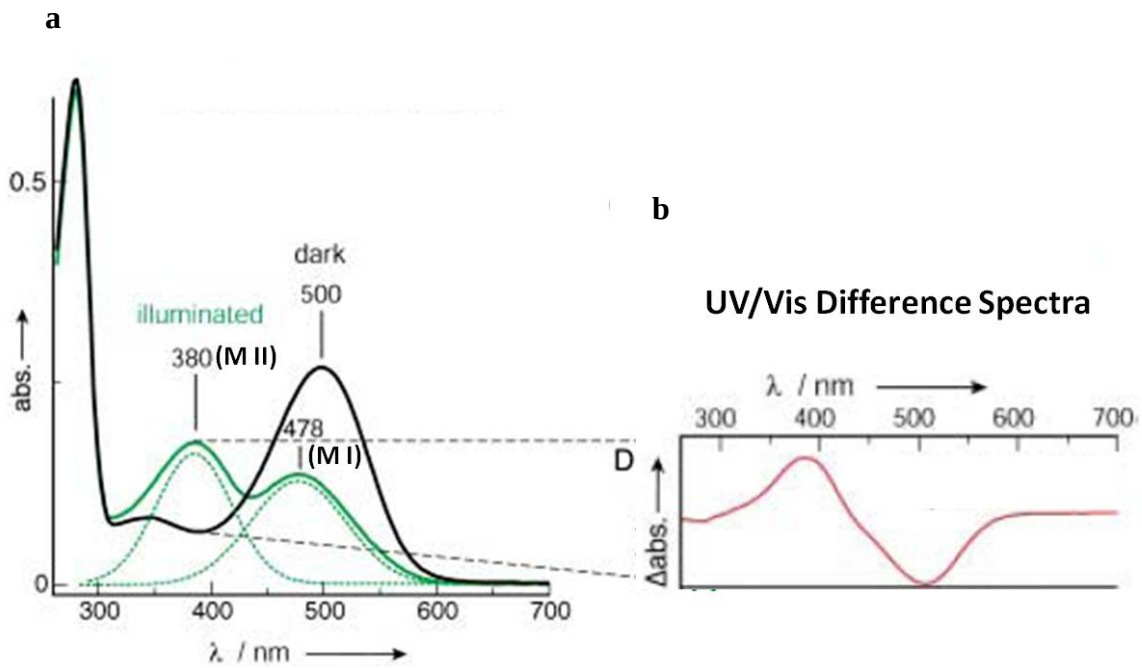

Fig. 1.8. Rhodopsin absorbance spectra and the extra-MII assay.

The absorbance spectra of rhodopsin can provide information about the functional state of the molecule. (a) In solid black line is the absorption spectrum of rhodopsin in the dark state, with a characteristic 500nm absorbance from the interaction of 11-cis-retinal with amino acids surrounding its binding pocket. Upon light activation, rhodopsin goes through various photointermediates, to arrive at the G protein coupling, active form, known as Meta-II (380nm), which is in equilibrium with the Meta-I form of rhodopsin (478nm), as depicted by the solid green line. The dotted green lines are Gaussian curves representing the Meta-I and Meta-II components. (b) The UV/Vis difference spectrum of rhodopsin is obtained by subtracting the dark state spectrum from the light-activated spectrum, and shows a dip at 500nm due to the loss of 500nm absorbance upon light activation, and a 380nm peak, resulting from the formation of Meta-II. Figure is adapted from (Ernst and Bartl, 2002).

Fig. 1.9. Retinal trapping assay to monitor arrestin binding to rhodopsin.

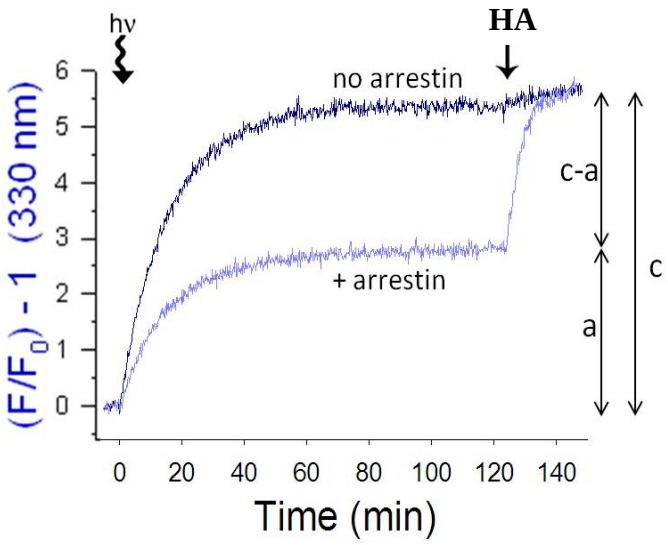

% Retinal Trapped = [(c-a)/(c)] x 100

Fig. 1.9. Retinal trapping assay to monitor arrestin binding to rhodopsin.

Meta-II decay can be monitored by the increase in intrinsic tryptophan fluorescence of rhodopsin due to the release of retinal. The dark blue spectrum shows the time-dependent increase in Trp fluorescence measured at 330nm, to a value ‘c’, upon light activation. Addition of hydroxylamine (HA) does not increase the fluorescence any further. However, in the presence of arrestin, the Trp fluorescence goes up only to about 50% to that in its absence, to a value ‘a’. Upon HA addition, the fluorescence increases to go up to the same value as in the absence of arrestin. The percent retinal trapped is calculated from as [(c-a)/c]*100 (Sommer et al., 2006).

Fig. 1.10. Tryptophan-Induced Quenching (TrIQ): Distance dependence.

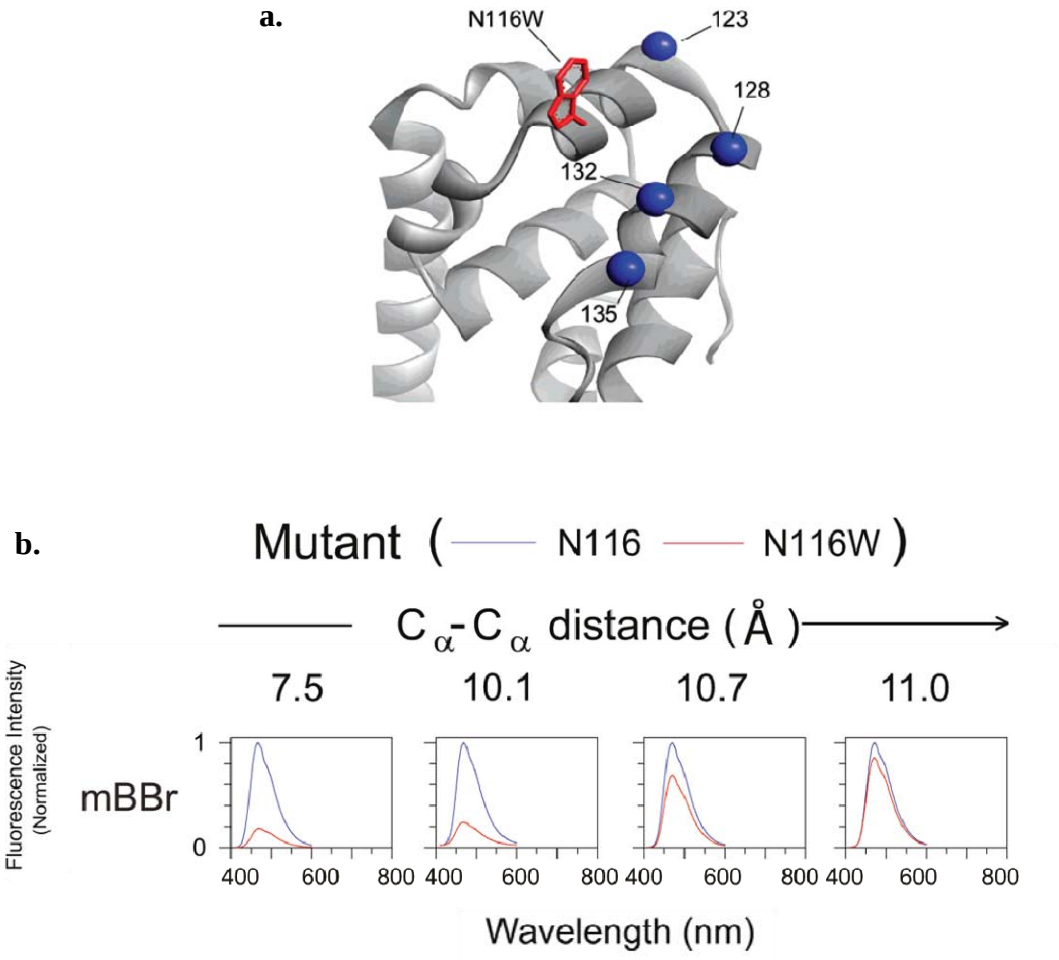

Fig. 1.10. Tryptophan-Induced Quenching (TrIQ): Distance dependence.

Tryptophan residue shows distance dependent quenching of mBBr fluorescence in T4 lysozyme (Mansoor et al., 2010). (a) Crystal structure of T4 lysozyme showing the site of mBBr attachment (on cysteines introduced at positions 123, 128, 132 and 135), represented by the Cα atoms as blue spheres. The quenching tryptophan was introduced my mutation of residue N116, shown as a stick model in red. (b) Distance dependent quenching of mBBr attached to cysteines introduced at positions 123, 128, 132 and 135 by N116W. Representative fluorescence emission spectra of mBBr-labeled lysozyme in the absence (blue) and presence (red) of the quenching tryptophan, N116W, show that tryptophan causes mBBr quenching in a distance dependent manner. The Cα-Cα distance between the labeled cysteine residues and the quenching tryptophan is given in Å on top of each spectrum. Figure is taken from Mansoor, et al (Mansoor et al., 2010).

Fig. 1.11. Components of fluorescence in the presence of a quencher.

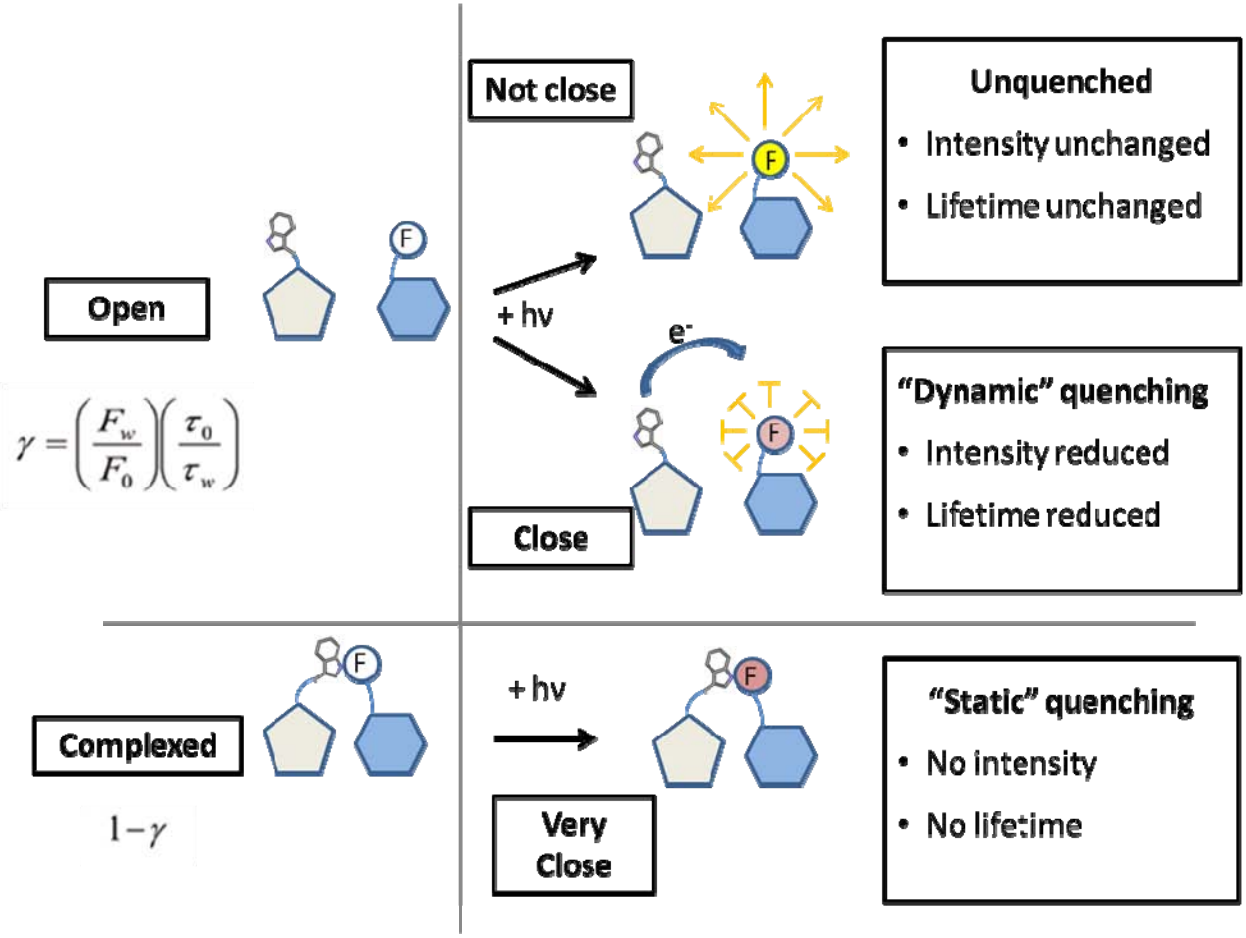

Fig. 1.11. Components of fluorescence in the presence of a quencher.

A schematic representation shows the different fates of a fluorophore in the presence of a quencher – unquenched, “dynamically” quenched or “statically” quenched. Steady state fluorescence emission data are combined with the fluorescence lifetime data to determine the amount static and dynamic quenching between bimane-Trp pairs. The top panel shows the fluorophore and quencher to be far apart, with no quenching seen, with no effect of either the intensity or the lifetime of the fluorophore. The middle panel depicts a fluorophore that is “dynamically quenched”. In this case, the quencher collides with the fluorophore during its excited state and reduces both the intensity and the lifetime of fluorescence. The above two are scenarios where the fluorophore and quencher are not in a pre-formed complex. The third component of fluorescence is depicted in the bottom panel, where the fluorophore and quencher are close enough to form a complex that is formed even before fluorescence excitation, within sub-nanosecond time-scale. This is called a static complex and indicates that the fluorophore and the quencher are “very close”, and these complexes do not contribute to any observed fluorescence intensity, nor do they affect the observed fluorescence decay (or lifetime) of the fluorophore..

For the bimane-Trp pair, studies with T4-lysozyme have shown static quenching to occur in case where the Cα-Cα distance between the quenching Trp and the labeled cysteine is less than 10 Å, while dynamic quenching occurs at distances less than 15Å (Mansoor et al., 2010).

Chapter 2

Two Distinct Sites on Arrestin Interact with the Base of TM6 of Rhodopsin

2.1. Summary

We report arrestin employs the same binding site on rhodopsin as the transducin C-terminal peptide, and thus localize one binding site for arrestin on the receptor as the cytosolic face of TM 5-6. We also show that arrestin in makes use of the hydrophobic patch on TM5 that gets exposed upon rhodopsin activation. Using a tryptophan-induced quenching (TrIQ) fluorescence approach, with Trp residues introduced in arrestin and monobromobimane (mBBr) attached to receptor cysteines, we identify two sites on arrestin that interact with the base of TM6 of the receptor. These two sites are the “finger” loop (residues 67-79) and the 160 loop (residues 155-165) of arrestin. The 160 loop residues cause a position-dependent static quenching of the fluorescence of bimane attached at T242 of opsin, indicating that some of these residues may come within 10Å of the bimane label on the receptor. Our data provide an unexpected contact site involving the 160 loop and the methodology can be used for further mapping of interaction sites between arrestin and rhodopsin.

All the sample preparation and experimental analysis reported in this chapter were performed by the author of this dissertation.

2.2. Introduction

G protein-coupled receptors (GPCR) are essential mediators for the transduction of a wide variety of extracellular signals to the inside of the cell. The general GPCR signaling paradigm includes activation of the membrane-embedded receptor upon binding of an agonist, which leads to structural changes in the receptor and subsequent binding of intracellular heterotrimeric G proteins. The latter then dissociate into α and βγ subunits and activate their downstream effectors. The key deactivation pathway for GPCRs involves the phosphorylation of the receptor by G protein coupled receptor kinase (GRK) on its cytosolic face and the subsequent recruitment of arrestin, which competitively inhibits G protein binding, and thus effectively turns off G protein-mediated signaling.

While the signaling paradigm described above is well elucidated, and the general surfaces of both arrestin and rhodopsin that are involved in their interaction have been defined, the detailed structural underpinnings behind the molecular interactions between a GPCR and arrestin have not been completely elucidated and the direct sites of interactions between the two proteins remain to be discovered (Gurevich and Gurevich, 2006). The interaction of arrestin with a GPCR has been most extensively studied with regards to the dim light photoreceptor, rhodopsin, and its interaction with visual arrestin. The covalently bound ligand, 11-cis-retinal, keeps rhodopsin in an inactive state. Upon photon absorption, the retinal undergoes a cis-trans isomerization to form all-trans-retinal and activates the receptor. Receptor activation involves the outward movement of TM 5 and 6 of rhodopsin (Farrens et al., 1996; Sheikh et al., 1996), and exposes a hydrophobic patch which is utilized by its G protein, transducin, to bind to the receptor (Janz and Farrens, 2004; Scheerer et al., 2008). Phosphorylation of the activated receptor by rhodopsin kinase (GRK1) leads to recruitment of arrestin, which competitively inhibits transducin and shuts

down the vision cascade. Mutagenesis, peptide inhibition, EPR spectroscopy and fluorescence spectroscopic studies have showed residues on the concave sides of both the N- and C-domain of arrestin as being involved in receptor binding (Dinculescu et al., 2002; Hanson et al., 2006; Kieselbach et al., 1994; Ohguro et al., 1994; Pulvermuller et al., 2000; Smith et al., 2004; Smith et al., 1999; Vishnivetskiy et al., 2011; Vishnivetskiy et al., 2004). One region of arrestin that has been implicated in receptor binding is the "finger" loop, a stretch of 13 amino acids in N-domain (residues 67-79), which sits in the middle of the N- and C-domains on the concave surface of the protein (Hirsch et al., 1999). Similarly, mutagenesis and peptide inhibition studies have implicated the receptor C-tail (with the GRK-catalyzed phosphates attached) as well as the intracellular loops 2 and 3 for arrestin binding (Krupnick et al., 1994; Raman et al., 1999; Shi et al., 1998). However, while these studies have indicated the importance of various arrestin and receptor elements for their interaction, they do not conclusively define where the two proteins interact.

Here, we set out to identify specific sites of direct arrestin-rhodopsin interaction using a combination of mutagenesis, biochemistry and fluorescence spectroscopy. We used fluorescently labeled cysteine mutants of rhodopsin constructed in a thermostable (N2C/D282C) background, which also contained the constitutive activating mutation, M257Y (Deupi et al., 2012; Han et al., 1998; Standfuss et al., 2007). The M257Y mutation allowed us to measure arrestin binding to opsin (rhodopsin without 11-cis-retinal) and thus circumvented the problem of rhodopsin photobleaching when subjected to the high intensity laser for fluorescence lifetime measurements. The N2C/D282C mutation was necessary because unliganded opsin is not stable in detergent micelles (Xie et al., 2003). We used a constitutively active form of arrestin (R175E) to circumvent problems in heterogeneity when using phosphorylated mutant receptors, as

heterogeneity in receptor phosphorylation could lower binding affinity of the phosphorylated receptor to the 1D4 antibody that is used for immuno-affinity purification of rhodopsin (Gurevich et al., 1995; Han et al., 1998; Molday and MacKenzie, 1983, 1985)

To specifically map sites of direct arrestin-opsin interactions, we introduced tryptophan residues at specific sites in arrestin and looked for tryptophan-induced quenching (TrIQ) (Mansoor et al., 2010) fluorescence from bimane fluorescent labels attached to specific cysteines in rhodopsin upon arrestin binding. Our results show that tryptophan introduced in the arrestin "finger" loop (residues 67-79) and the 160 loop can quench the fluorescence of mBBr attached to specific cysteines in TM6 of opsin. TrIQ analysis of the steady-state and time resolved fluorescence data identified several residues on arrestin that cause static quenching of receptor attached mBBr fluorescence, thus unequivocally identifying sites of direct physical interaction between the two proteins.

2.3. Materials and Methods

Materials

All restriction enzymes, ligase and DNA polymerase were from New England Biolabs. Tissue culture media was purchased from HyClone, while polyethyleneimine was from Polysciences, Inc. n-Dodecyl-β-D-maltoside (DM) was purchased from Anatrace and 1,2-dioleoyl-*sn*-glycero-3-phospho-L-serine was from Avanti Polar Lipids. Monobromobimane was obtained from Invitrogen. 1D4 antibody was obtained from the Monoclonal Antibody Core at the Vaccine and Gene Therapy Institute of Oregon Health and Science University and the competing

9-mer peptide was obtained from Biotechnology Core Facility Branch at the Centers for Disease Control and Prevention, Atlanta, GA. BL21 BL21-CodonPlus(DE3)-RP strain of *E. coli* was purchased from Agilent Technologies. Yeast extract and BactoTryptone were from BD Biosciences. Profinity eXact™ and HiTrap Heparin™ columns were from Bio-Rad and GE Healthcare Life Sciences respectively. Amicon Ultra protein concentrators (10kD cut-off) and nitrocellulose filters (0.45um) were from Millipore. GTP was purchased from Roche and **[**^{35}S]GTPγS was from PerkinElmer Life Sciences. Frozen bovine retinas were obtained from Lawson and Lawson, Inc. (Lincoln, NE). GBX red light filters were purchased from Eastman Kodak Co. Band pass filters and long pass filters were purchased from Oriel (Stratford, CT), while cuvettes were purchased from Uvonics (Plainview, NY). All other chemicals and reagents were obtained from Sigma-Aldrich.

Buffer definitions: ROS Buffer: 70 mM potassium phosphate, 1 mM magnesium acetate, pH 6.8; PBS: 137mM NaCl, 2.7mM KCl, 8mM Na_2HPO_4, 1.46mM KH_2PO_4, pH 7.4; MHE: 5mM MES, 50mM HEPES, 1mM EDTA, pH 6.8; Wash Buffer: 10mM Tris-HCl pH7.5, 0.1M NaCl, 5mM $MgCl_2$, 0.1mM EDTA, 1mM DTT, 0.01% DM.

Cloning and mutagenesis

The rhodopsin cysteine mutants were made in a "cys-less" background construct, θ, in which the native cysteines C140, C316, C322 and C323 are replaced with serines (Resek et al., 1993; Resek et al., 1994). The background construct M257Y/N2C/D282C were constructed using overlap extension PCR in the pMT4 vector. The mutants T242C and T243C were constructed in the M257Y/N2C/D282C background using QuikChange mutagenesis.

The arrestin Trp mutants were made in R175E background by QuikChange mutagenesis in the pG58 vector, which has been described previously (Huang et al., 2012; Tsukamoto et al., 2010). All of the mutations were confirmed by DNA sequencing.

Preparation of ROS Outer Segments (ROS) and rhodopsin phosphorylation

ROS were isolated from bovine retinas as described previously (Papermaster, 1982; Sommer et al., 2005). All the steps were carried out at 4 °C under red lights. Rhodopsin concentration was assessed by difference spectra in the presence of hydroxylamine (ε_{500} = 40,800 liter cm^{-1} mol^{-1}). Stocks were snap-frozen and stored at -80 °C.

Phosphorylated ROS (ROS-P) was prepared as described previously (Sommer et al., 2005)**.** Briefly, isolated ROS membranes were by suspended at 10μM concentration in ROS buffer containing 20 μM GTP and 3 mM ATP. Phosphorylation of rhodopsin by the native rhodopsin kinase in the ROS membranes was initiated by illumination with a 15-watt placed ~20 cm away, while rocking the sample on a nutator. After 2 hours, the reaction was stopped by a 4-fold dilution with ROS buffer containing 50 mM hydroxylamine and 2% bovine serum albumin. Phosphorylated opsin membranes were then collected by centrifugation at 40,000 x *g* for 1 hour and the levels of phosphorylation were quantified with the use of **[**γ-^{32}P]ATP (10–100 cpm/pmol) as a tracer (Kuhn and Wilden, 1982; Sommer et al., 2005). We consistently obtained between 5-6 phosphates per rhodopsin using this procedure.

Phosphorylated opsin membranes were then washed and homogenized in 5mM PIPES, 1 mM EDTA, pH7 and regenerated overnight at 4^{o}Cby the incubation with a 2-fold excess of 11-*cis*-retinal (4 °C). The regenerated samples were washed once with ROS buffer containing 2%

bovine serum albumin and 50 mM hydroxylamine, five times with 2% bovine serum albumin in ROS buffer, and three times with ROS buffer alone to remove any free 11-cis-retinal. Non-phosphorylated ROS membranes were prepared identically, except that no ATP was added during the phosphorylation procedure.

Opsin expression and purification

Rhodopsin mutants were expressed in COS-1 cells and purified as previously described (Dunham and Farrens, 1999; Janz and Farrens, 2004). Briefly, rhodopsin cysteine mutants were cloned in a thermostable (N2C/D282C) and constitutively active (M257Y) rhodopsin background by restriction cassette approach or by standard PCR approach. COS-1 cells were transfected with 30ug plasmid DNA/15cm plate using 0.1mg polyethyleneimine/plate. Cells were harvested after ~60 hours post transfection. Cells were solubilized using 0.6ml of 1% DM in 1X phosphate buffered saline (1X PBS) per plate of cells. After solubilization for 1hr, the lysates were clarified by centrifuging at 100,000 x g. The clear lysate was applied to 1D4 antibody-coupled sepharose beads and incubated for 4hrs at 4^{o}C. The beads were then washed sequentially first with PBS with 1M NaCl, 3mM $MgCl_2$, 0.05% DM, then 0.05%DM in PBS and finally with MHE Buffer with 0.025%DM. The opsin was then labeled with 10X molar excess of mBBr in the same buffer overnight at 4 deg C. The labeling reaction was quenched with 1mM L-cysteine for 30min on ice. The beads were washed sequentially with the following buffers: 0.025% DM in MHE Buffer, 0.2% DM in MHE Buffer, 0.025% DM in MHE Buffer and finally 0.05% DM in 5mM MES pH 6. The labeled opsin was eluted with 0.1mM rhodopsin 9-mer peptide (TETSQVAPA) in 5mM MES, 40mM NaCl, 0.05% DM, pH6.

Arrestin expression and purification

The visual arrestin R175E mutant, cloned at the C-terminal of a modified 77 amino acid prodomain region of subtilisin BPN' (proR8FKAM), in pG58 vector was a generous gift from Kevin Ridge (Huang et al., 2012)**.** The mutant was expressed in *E. coli* BL21(DE3)-RP cells (Stratagene) and purified using Profinity eXact column (Bio-Rad), followed by ion-exchange chromatography using HiTrap Heparin column (GE Healthcare) as described earlier **[**Tsukamoto, et al]. BL21(DE3)-RP cells harboring the pG58 expression vector containing the prodomain/arrestin R175E (or R175E with Trp mutation at specific sites) fusion were grown in 1L of LB media in the presence of 100 μg/ml ampicillin at room temperature to A_{550} of 0.6, and then induced with 30 μM IPTG for 16hr at 16 deg C. The cell pellet was resuspended in 50 mM Tris–phosphate, pH 7.2, containing 50 mM NaCl, 5 mM β-mercaptoethanol, 0.1 mM PMSF and protease inhibitor cocktail (Roche) and then disrupted by French press. The supernatant obtained by centrifugation of the cell lysate at 100,000 x g for 45 min was loaded onto a 5mL Profinity eXact column. The column was washed with 20 column volumes of 100 mM sodium phosphate, pH 7.2 and 20 column volumes of 100 mM sodium phosphate, 300 mM sodium acetate, pH 7.2. The cleavage of arrestin from the prosubtilisin tag was initiated by passing one column volume of 100 mM sodium phosphate, pH7.2 containing 100 mM sodium fluoride (elution buffer). The fluoride-mediated cleavage reaction was allowed to occur for 2hr on ice. Tag-free arrestin was eluted off the column by passing 5 column volumes of the elution buffer and was further purified by cation exchange chromatography using a 1ml HiTrap Heparin column. The resulting arrestin protein was >95% pure, as assessed by SDS-PAGE.

Arrestin functional pull-down assay

A previously described centrifugal pull-down assay was performed to test the binding of arrestin R175E to wild-type rhodopsin (Sommer et al., 2005, 2006). 12 μM ROS or ROS-P membranes were incubated with 3μM arrestin in 20mM HEPES, 140mM NaCl, pH7.4 for 15min at room temperature. The samples were either kept in the dark or light activated using a 150W fiber optic light source (>495nm) and the reaction was quenched immediately with 10-fold ice cold buffer. Bound arrestin was separated from free by centrifugation at 100,000 g for 10min. The membrane pellets were solubilized in loading dye and subjected to SDS-PAGE electrophoresis, followed by Coomassie staining to visualize the amount of arrestin that bound the receptor containing membranes. For the pull-down assay in the presence of G_t peptide, 100 μM of the peptide was pre-incubated with the receptor for 10 min at room temperature before arrestin addition.

Retinal release assay

The effect of mutation of rhodopsin hydrophobic patch residues on arrestin binding was studied by a retinal release assay, which was based on the observation that arrestin could inhibit retinal release from rhodopsin, upon light activation (Sommer et al., 2005, 2006)**.** Rhodopsin mutants T226C and V230C were expressed in COS-1 cells, regenerated and purified as above. 2μM of constitutively active arrestin R175E was incubated with 0.5μM of "wild-type", L226C or V230C rhodopsin in the a reaction mixture containing 20 mM HEPES, 140 mM NaCl, 0.05 %DM, 0.3 mM DOPS, pH 7.4 in the dark for 30 min at room temperature. The samples were placed in a 10mm fluorescence cuvette and the intrinsic Trp fluorescence was measured using λ_{ex} of 295nm and λ_{em} of 330nm. The slits were kept at 0.25nm to avoid photobleaching of the

samples. Fluorescence was measured over time. After an initial dark state fluorescence measurement, the samples were irradiated with >495nm light from a 150W fiber optic light source for 30s. The subsequent increase in fluorescence was measured over time. Once the increase in fluorescence reached a plateau, 10 mM hydroxylamine was added to cleave the Schiff base and convert all the remaining photoproducts to opsin and free retinaloxime, to arrive at the maximum fluorescence. From the values of the fluorescence in the dark state (F_o), the first plateau reached after light activation (F_1) and the final fluorescence after hydroxylamine addition (F_2), the percent retinal trapped was calculated by **[**$(F_2-F_1)/(F_2-F_o)$] x 100 (Sommer et al., 2006).

Steady state fluorescence spectroscopy measurements

All fluorescence measurements were made using a Photon Technologies QM-1 steady-state fluorescence spectrophotometer with a single excitation source and one emission detector. Temperature was controlled at 20^{o}C using a water-jacketed cuvette holder connected to a circulating water bath (VWR Scientific). Typically, a measurement involved using 0.25μM mBBr-labeled opsin in a 10mm black-jacketed cuvette, which was excited at 380nm, and the emitted fluorescence measured from 400 to 600nm using 1nm increments. Each data point was integrated for 0.2s, and the average of two scans yielded the final spectrum. Arrestin mutants were added at 5μM concentration and the fluorescence was monitored over time. The spectra were obtained every one minute to monitor the time-course of arrestin-induced fluorescence quenching (if any), till there was no further reduction in the mBBr fluorescence. The excitation band-pass was kept at 1 nm and emission band-pass at 5 nm. The 20-fold excess of arrestin over opsin, was found to be sufficient for complete arrestin binding. For the experiment with the G_t peptide, 100μM of the peptide was added to the opsin mix and incubated with the receptor for 10 min at room temperature before arrestin addition. Spectra were acquired and visualized using the

PTI software program Felix, and the fluorescence spectrum of buffer was subtracted as appropriate, and the dilution factor upon arrestin addition was taken into account during data analysis. The spectral data were plotted and analyzed using SigmaPlot.

Time-resolved fluorescence spectroscopy

The same sample in the same 10mm cuvette that was used for the steady state fluorescence measurement was used to measure the lifetime of mBBr fluorescence using FluoTime 200 spectrometer (PicoQuant GmbH). The samples were excited using a blue (405nm) diode laser passed through a neutral density filter to modulate the intensity. The measurements were made at "magic angle" settings (54.7^{o}) to avoid photoselection artifacts. The excitation aperture was set to minimum, while the emission slits were set to 1nm. To eliminate scattering, the emission was monitored at 490nm through three >470nm long pass filters. The decay spectra were collected over a range of 0 to 180ns using the PicoHarp 300 time-correlated single photon counting system. The instrument response function, which is deconvoluted from lifetime decay data, was determined from the scatter at 400nm from a solution of Ludox to be ~64ps FWHM. The system was controlled using the PicoHarp software and the obtained spectra were fit using software from the manufacturer (FluoFit). The "goodness of fit" was evaluated by plotting the residuals and a χ^2 value of 0.9-1.1 was considered acceptable (Lakowicz, 2006).

Transducin purification

Transducin was purified from bovine retina was carried out as previously described, with slight modifications (Goc et al., 2008; Matsuda and Fukada, 2000). ROS membranes were isolated from bovine retina as mentioned above, but were finally suspended in 10 mM Tris-HC1, 0.5 mM MgCI2, 1 mM DTT, 0.1 mM PMSF, 1X protease inhibitor cocktail (EDTA Free), pH

7.5 supplemented with 0.3 mM EDTA, flash frozen and stored at -80^{o}C. The frozen membranes were thawed, dounced in a tissue homogenizer and centrifuged at 70,000g for 30min. The pellets were washed with the same buffer twice and then twice with a hypotonic buffer (5 mM HEPES, pH 7.5 with 0.1 mM EDTA, and 1 mM DTT). G_t was then extracted by resuspending the washed pellet with hypotonic buffer containing 200μM GTP. After three rounds of extraction, the extracts were analyzed by SDS-PAGE. The extracts were pooled, concentrated and buffer exchanged into 20mM Tris-HCl, 0.2M NaCl, 2mM $MgCl_2$, pH7.5 containing 1mM DTT and 20μM GDP, in Amicon Ultra 15kD-cut-off centrifugal concentrator. To the concentrated protein, 10% glycerol was added and the protein and flash frozen and stored at -80^{o}C.

Transducin inhibition assay

Arrestin binding to opsin was assessed by testing its ability to inhibit opsin-induced transducin activation, as measured by the GTPγS incorporation assay (Kaya et al., 2011). Briefly, 0.25 μM mBBr-labeled opsin mutant was mixed with 0.3 mM DOPS, 1 mM MgCl2, 0.1 mM EDTA in 20 mM HEPES pH 8.0, and incubated with the 5 μM of the arrestin mutants for 30 min at room temperature. The reaction was started by adding G_t at 0.1μM and 4.5 μM GTPγS with **[**^{35}S]GTPγS as tracer (2000-10,000 cpm/pmol). The reaction was allowed to proceed for 10min at room temperature, following which the free nucleotide was removed from bound by applying the mix to 0.45um nitrocellulose filters in duplicate in a Brandel cell harvester attached to a vacuum pump and washing the filter with ice cold wash buffer. The filters were then removed and the bound radioactivity was measured in a scintillation counter. The data from at least two experiments, each measured in duplicate were averaged to determine the counts for each sample. The data were analyzed in SigmaPlot.

Quantitation of static and dynamic fluorescence quenching

The fraction of fluorophores undergoing static vs dynamic quenching upon arrestin binding to bimane-labeled opsin was done using the TrIQ method, as described by Mansoor et al (Mansoor et al., 2010)**.** Briefly, this approach analyzes the steady state fluorescence quenching data together with the measured fluorescence lifetimes of the fluorophore (mBBr attached to specific cysteines in opsin) in the presence and absence of a quenching tryptophan (introduced at specific sites in arrestin) in order to determine the fraction of static quenching component in a fluorophore-quencher pair. For this analysis, we calculated F_w/F_o and τ_w/τ_o, where F_w and F_o are the total fluorescence intensity of the samples with and without the quenching Trp residue, while (τ_w) and (τ_o) are the amplitude-weighted fluorescence lifetimes of the fluorophore with and without the quenching Trp residue.

The relative fraction of Trp-fluorophore pairs not in a static complex was calculated using

Eq.1: $\gamma = (F_w/F_o).(\tau_o/\tau_w)$

The relative fraction of Trp-fluorophore pairs involved in a static complex is given by

Eq. 2: $\gamma_{SQ} = (1- \gamma)$

while those undergoing dynamic quenching is

Eq. 3: $\gamma_{DQ} = (1-(\tau_w/\tau_o)).\gamma$

2.4. Results

Overview

A specific displacement of TM6 has been shown to be a key structural change in rhodopsin upon activation by a number of biophysical methods (Farrens et al., 1996; Sheikh et al., 1996). The G protein, transducin, was subsequently shown to employ the interhelical cavity that is created upon helix movement for its binding (Janz and Farrens, 2004)and these models were later confirmed by X-ray crystallography (Choe et al., 2011; Scheerer et al., 2008). Here, we tested the role of this region in arrestin binding. Our results show that arrestin also employs the same region of the receptor for binding, and we identify two distinct parts of arrestin that make contact with the base of TM6. Below, we report summarize the results of our studies on mapping the interaction sites between arrestin and rhodopsin.

Selection of sites of label attachment and introduction of Trp mutants

We tested two different regions of arrestin – the "finger" loop and the 160 loop, two regions that mark the extremities of the concave face of the N-domain of arrestin – for their ability to interact with the base of TM6 of rhodopsin. We introduced Trp mutations at sites Y67, I72 and F79 of the "finger" loop and at sites T157, D158, V159, E160, E161, D162, K163 and I164 of the 160 loop of arrestin R175E (Fig. 2.1C) to study the proximity of these arrestin sites to sites 242 and 243 on the receptor by monitoring tryptophan induced quenching (TrIQ) of mBBr fluorescence (Mansoor et al., 2010). The labeled samples did not have detectable free label (Fig. 2.S1).

Biochemical mapping of arrestin-rhodopsin interaction: Arrestin R175E utilizes the same binding site on rhodopsin as the transducin C-terminal peptide

As the first step in testing the hypothesis that arrestin uses the same (or similar) part of rhodopsin as G_t that is exposed upon receptor activation, we tested if a peptide corresponding to the C-terminal tail of G_t affects arrestin binding to rhodopsin. G_t binds rhodopsin via its C-terminal tail inside the cleft formed by TM6 movement, in part by interactions with a hydrophobic patch that is exposed upon rhodopsin activation (Choe et al., 2011; Farrens et al., 1996; Janz and Farrens, 2004; Scheerer et al., 2008; Sheikh et al., 1996). We tested the ability of arrestin R175E to bind rhodopsin in the presence of the peptide G_t by a well established centrifugal pull-down assay which measures the ability of arrestin to bind rhodopsin in native ROS membranes (Sommer et al., 2005, 2006). The pull-down data show that G_t peptide inhibits constitutively active arrestin (R175E) binding to light activated rhodopsin (R*) by almost 90% (Fig. 2.2a). It inhibits the binding to phosphorylated, light-activated receptor (RP*), but only by ~20%, presumably due to higher affinity imparted by phosphates. Together, the data indicate that arrestin utilizes the same patch on rhodopsin as the G_t tail peptide.

To further test the role of this region in interaction with arrestin, we mutated two residues on TM5 which form a part of the hydrophobic "patch" to which the G_t tail peptide binds and tested the ability of arrestin to trap retinal in rhodopsin using an assay developed by Sommer and Farrens (Sommer and Farrens, 2006). The assay is based on the observation that in the presence of arrestin, the retinal release from rhodopsin, that normally occurs as a result of Schiff base hydrolysis upon rhodopsin activation, does not go to completion. In fact, in most mixed-micellar preparations of rhodopsin, arrestin "traps" almost 50% of the retinal, and this trapping can be used as an indicator of arrestin binding. Arrestin binding to three different rhodopsin constructs -

Cys-less (θ), L226C and V230C - was measured. Both L226C as well as V230C showed very low levels of retinal trapping (~10%), indicated by the very slight increase in Trp fluorescence after hydroxylamine (HA) addition, compared to wild-type rhodopsin in which arrestin R175E trapped about 50% of the retinal (Fig. 2.2b). This suggests that arrestin could not bind well to these hydrophobic patch mutants. We next set out to further define arrestin binding sites using TrIQ fluorescence spectroscopy, as described below.

TrIQ mapping sites of arrestin "finger" loop interaction with rhodopsin TM5/TM6: Trp residues in arrestin "finger" loop quench mBBr fluorescence at T243C in opsin

Based on our results with the G_t peptide discussed above, we surmised that part of arrestin might directly bind to the same site on rhodopsin as does the G_t C-terminal peptide. A likely candidate for such binding is the "finger" loop of arrestin (Fig. 2.1c).

To test this, we made Trp mutations in arrestin at the base (Y67W and F79W) and the tip (I72W) of this loop and set out to test for direct evidence for interaction between these sites on arrestin, and this region on rhodopsin, by looking for instances of direct interaction between a Trp on arrestin and a fluorophore (bimane) on rhodopsin.

Specifically, we made two site-specific cysteine mutations at T242 and T243 on the cytosolic face of TM6 of a constitutively active and thermostable form of opsin. We then labeled the cysteines on the protein with the thiol-reactive fluorophore, mBBr (Fig. 2.1), and ensured that no free, unattached fluorophore was present in these samples (Fig. 2.S1a).

One clear indication of the interaction of the arrestin "finger" loop with opsin was with mBBr-labeled T243C. We found that Y67W causes ~40% quenching of 243mB fluorescence (Fig. 2.3). In contrast, the background mutant, R175E, with no non-native tryptophan, caused no

quenching of 243mB fluorescence. Also, it is apparent from the data that the fluorescence emission maxima show a slight blue shift from ~461nm to ~458nm in the presence of arrestin, indicating that the arrestin had bound to the receptor. Further, this shift is seen for both the arrestin mutants with and without the quenching tryptophan.

Defining direct sites of arrestin-rhodopsin interaction by TrIQ: Both the "finger" loop and the 160 loop Trp residues induce static quenching of fluorophores attached to the base of TM6

We next set out to define where in this area arrestin and rhodopsin interact, as well as another region in arrestin thought to have potential functional relevance (based on its conformational plasticity) (Hirsch et al., 1999). Thus, we expanded these initial studies to include more sites on arrestin, including the area around the "finger" loop, as well as the 160 loop. The residues that were mutated to Trp were Y67W, I72W and F79W in the "finger" loop, and T157W, D158W, V159W, E160W, E161W, D162W, K163W and I164W in the 160 loop of arrestin. All the mutants were tested to measure their ability to quench the fluorescence of opsin 242mB or 243mB. While the "finger" loop mutants Y67W and F79W both showed ~40% and ~35% fluorescence quenching, the third "finger" loop Trp mutant, I72W, caused minimal quenching of 243mB fluorescence (Fig. 2.4a). This is reasonable from a structural viewpoint, as both Y67 and F79 are physically closer by in space and I72 faces away from them. The 160 loop mutants show a more diffuse pattern of quenching at 243mB, and the amount of quenching varies between ~10-25%, with the residues in the middle – E160W and E161W showing ~20-25% quenching, while the flanking residues show lower amounts of quenching. Mansoor, et al have shown that free tyrosine can quench the fluorescence of mBBr, albeit not as effectively as tryptophan can (Mansoor et al., 2010)**.** Unpublished studies in our lab indicate that tyrosine can

cause quenching of mBBr fluorescence, if in close enough proximity. In fact, it is possible that some of the quenching (5-10%) shown by these residues might be coming from some native tyrosine in arrestin (e.g., Y67, Y250), as even R175E without any non-native tryptophans causes ~5-10% fluorescence quenching at 243mB.

Surprisingly, just one residue away, at 242mB, the "finger" loop Trp residues do not show any quenching (Fig. 2.4b). The 160 loop Trp mutants, on the other hand, show a strong site-specific quenching, with E160W and E161W showing almost 35% quenching. We assume amount of arrestin used in these experiments is saturating, since arrestin at 2μM at a ~2.5X lower concentration shows about the same amount of fluorescence quenching (Fig. 2.S2), although this concentration is not unequivocal evidence of saturating interaction. Unfortunately, we could not get arrestin at higher concentration without causing >10% dilution of the binding conditions.

Interestingly, the 160 loop mutants show a bell-shaped distribution for the amount of quenching from residue 157 to 164, with T157W and I164 causing almost no quenching, and the residues in the middle, E160W and E161W causing close to 35% quenching. This distribution might be indicative of the relative distances of these mutants from the labeled T243 site on opsin.

The various Trp mutants in arrestin display comparable binding to opsin

The foal of the TrIQ experiments was to produce a model for the physical interaction between arrestin and opsin, based on the pattern of site-specific quenching by Trp introduced at various positions in arrestin. In cases where we see measurable fluorescence quenching, we can propose that the Trp and bimane are in close proximity to each other. However, with respect to residues where we do not see a change, we cannot be certain if the lack of quenching is because the two sites are not close because the arrestin mutants are not binding in the first place. To address these concerns, we tested the binding of the arrestin Trp mutants to the labeled opsin

mutants by an independent assay, making use of the fact that arrestin competes with transducin for receptor binding (Krupnick et al., 1997; Pulvermuller et al., 2000), and the fact that the M257Y opsin mutant binds and activates transducin in the absence of any ligand (Han et al., 1998). We purified transducin from bovine retina (Fig. 2.S3) and performed a well established assay for receptor-mediated activation of transducin – the **[**^{35}S]GTPγS incorporation assay (Kaya et al., 2011). To monitor arrestin binding to the receptor, we tested if the arrestin mutants could inhibit transducin activation by monitoring the amount of **[**^{35}S]GTPγS incorporation.

Our results show that all the arrestin Trp mutants were able to bind opsin T243mB at roughly the same level, F79W and T158W, as judged by their ability to inhibit GTPγS incorporation (Fig. 2.4c). There were some notable variations, for example, F79W and T158W, which showed a slightly reduced inhibition of G_t activation. With T242mB, all the arrestin Trp mutants inhibited G_t activation to a large extent (>50%) (Fig. 2.4d). However, the 160 loop Trp mutants clearly inhibited G_t activation to a higher extent (80-90%) than the "finger" loop mutants (~50%). This would suggest a lower affinity of interaction between the "finger" loop mutants and T243mB opsin mutant than that between the 160 loop mutants and the receptor labeled at T243. It is possible that the lower affinity with the "finger" loop Trp mutants and T242mB could be part of the reason why we did not see any quenching by these 160 loop mutants.

TrIQ analysis shows arrestin 160 loop make physical contact with the base of TM6 in opsin.

The steady state fluorescence quenching data above indicate some of the various arrestin sites are in relative proximity to the bimane labeled sites on opsin. However, these data do not

prove direct interaction between the two sites. To get a more defined understanding of the proximity of these pairs of residues, we used the TrIQ approach to study fluorophore-quencher interactions (Mansoor et al., 2010). To do this, we also measured the fluorescence lifetime of the labeled opsin samples in the absence and presence of the Trp-containing arrestin bound to it. These experiments were carried out using the exact same samples and conditions used to measure the steady state fluorescence quenching by arrestin Trp mutants, thus reducing variability and improving the consistency of the results between the two sets of measurements. The lifetime data were fit to a three exponential decay (Fig. 2.S4) and the amplitude-weighted lifetime $< \tau >$ was calculated (Table 2.S1) used in combination with the steady state fluorescence quenching data to arrive at the fraction of fluorophore-quencher pairs that were in contact at the moment of light excitation (static quenching) (Mansoor et al., 2010)

Our results show that some static quenching can be observed, although the majority of quenching of 243mB fluorescence by the "finger" loop Trp residues is dynamic in nature. This indicates that the fluorophore and quencher come quite close to each other. Unfortunately, the data for the "finger" loop Trp mutants are quite noisy and cannot be interpreted too rigidly. The results also show that the arrestin 160 loop Trp residues form static quenching complexes (Fig. 2.5b), meaning these complexes were formed in the sub-nanosecond timescale and were in contact before the sub-nanosecond process of fluorescence excitation (<100ps for our instrument). This would suggest that some fraction (as much as ~20% in the case of E161W) of these bimane-tryptophan pairs is in contact with each other, at the moment of light excitation.

Arrestin binding to opsin also makes use of the G_t binding pocket

Our pull-down experiment with arrestin R175E and rhodopsin in ROS membranes in the presence of the G_t tail peptide had indicated that arrestin might be employing the same binding

pocket as the G_t tail (Fig. 2.2a). To test if the binding of the arrestin Trp mutants to the labeled opsin mutants in these detergent solubilized conditions is also inhibited by the G_t tail peptide, we kept the conditions identical to our previous experiments, but pre-incubated the opsin 242mB mix with the G_t peptide for 10 min before adding arrestin E160W in the R175E background. While the amount of fluorescence quenching was not too different with and without the peptide, the rate of arrestin-mediated fluorescence quenching was slower in the presence of the peptide (Fig. 2.S5). The $t_{1/2}$ of quenching in the absence of the peptide was ~1.5 min, while that in the presence of the peptide was slowed almost 6 fold to ~9 min. This indicates that the mode of arrestin binding to opsin under these conditions might not be too different from its binding to rhodopsin in ROS membranes.

2.5. Discussion

Here, we report two sites on the arrestin N-domain that make contact with the base of TM6 of opsin. An outward movement of TM6 is a major aspect of the activation of GPCRs (Choe et al., 2011; Farrens et al., 1996; Rasmussen et al., 2011; Sheikh et al., 1996) and this movement exposes a critical hydrophobic patch that provides crucial sites of contact for the binding cognate cytosolic proteins like G proteins (Choe et al., 2011; Janz and Farrens, 2004; Rasmussen et al., 2011). Since arrestin competes with G proteins for the occupation of activated receptor (Krupnick et al., 1997; Pulvermuller et al., 2000) and our results with the G_t C-terminal tail peptide further localized an area for this interaction, we tested if arrestin also makes use of the same or similar binding spot on rhodopsin by testing the interaction of arrestin with residues T242 and T243 on the receptor.

The putative interaction sites on arrestin whose interactions we tested are the "finger" loop (residues 67, 72 and 79) and the 160 loop (residues 157-164). Interestingly, the arrestin "finger" loop (Fig. 2.1c) has some sequence similarity to the transducin C-terminal tail (Fig. 2.S6), and, like the transducin C-tail, it adopts a helical structure upon binding rhodopsin (Feuerstein et al., 2009). This loop has also been shown to undergo movement upon receptor binding and its flexibility is important for interaction with rhodopsin (Hanson et al., 2006; Sommer et al., 2007; Sommer et al., 2005, 2006). Finally, arrestin competes with transducin in binding to activated rhodopsin, indicating the two proteins likely share a common binding site (Krupnick et al., 1997; Pulvermuller et al., 2000). Given these lines of evidence, we hypothesized that the arrestin "finger" loop might also employ the same binding pocket as the transducin C-tail.

In contrast, the 160 loop is on the far edge of the concave surface of the N-domain of arrestin. Like the "finger" loop, the 160 loop shows considerable conformational plasticity in the crystal isoforms of arrestin (Granzin et al., 1998; Hirsch et al., 1999), and its sequence belongs to a class of polypeptides termed "chameleons", whose structure is context dependent (Minor and Kim, 1996; Tan and Richmond, 1998). A peptide corresponding to residues 150-170 of arrestin inhibited arrestin binding to metarhodopsin II (Pulvermuller et al., 2000). Finally, a spin label attached to T157 in this region shows a change in mobility upon binding to phosphorylated rhodopsin (Hanson et al., 2006). Based on these lines of evidence, we hypothesized that this region might have a role in receptor binding and tested its interaction with the receptor. We used TrIQ fluorescence approach to define the sites of interaction between arrestin and opsin. The implications of our methodology and results are given below:

Rationale behind the use of constitutively active mutants

Direct physical studies aimed at mapping the interacting regions in the two proteins require the use of rhodopsin mutants. Such *in vitro* studies of rhodopsin-arrestin interactions using rhodopsin mutants provide a technical challenge of obtaining purified, phosphorylated receptor. The site of receptor phosphorylation is also the epitope for the 1D4 antibody used for purifying rhodopsin and receptor phosphorylation reduces the affinity of the antibody (Molday and MacKenzie, 1985). In fact, 1D4 antibody shows 10-fold higher K_D for phosphorylated rhodopsin compared to unphosphorylated rhodopsin. Further, phosphorylation may yield a heterogeneous mix of differently phosphorylated receptors – rhodopsin can have up to 9 phosphates per molecule (Aton et al., 1984; Wilden and Kuhn, 1982), which can make direct comparison of different mutants difficult. To get around the problem of phosphorylation, we used a constitutively active mutant of rhodopsin, M257Y, which has been shown to activate transducin even in the absence of any retinal ligand (Han et al., 1998) at ~30% the level of G_t activation as the wild-type receptor.

The use of the M257Y opsin form of the receptor is also useful for fluorescence studies as it does not have the problem of retinal photo-bleaching by the high intensity laser used for fluorescence lifetime studies and there is no issue of spectral overlap between the fluorophore, mBBr, and the retinal chromophore. However, the retinal-free opsin is quite unstable in detergent solubilized conditions and so our studies used a disulfide-linked thermostable mutant of opsin (N2C/D282C) that is stable in detergent (Xie et al., 2003). To increase the affinity of the interaction, we also used an arrestin mutant, R175E, which can bind rhodopsin even in the absence of phosphorylation (Gurevich et al., 1995).

Arrestin uses the same binding site on rhodopsin as the G_t C-terminal tail peptide

Two results suggest that arrestin binding overlaps with the site of transducin C-terminal tail binding. First, arrestin competes with G_t in binding light activated rhodopsin. The G_t tail peptide is known to bind the receptor on the TM5-TM6 face that is exposed upon receptor activation (Choe et al., 2011; Janz and Farrens, 2004; Scheerer et al., 2008). The inhibition of arrestin R175E binding to light activated rhodopsin, R*, by the G_t peptide in the pull-down experiment (Fig. 2.2a) is strongly suggestive that arrestin makes use of the same binding site as the peptide. The observation that the peptide did not inhibit arrestin binding to RP* can be explained on the basis of a multi-site interaction between the two proteins and the strong affinity of arrestin for RP*. The considerable decrease in the rate of arrestin E160W-mediated quenching of 242mB fluorescence in the presence of the G_t peptide (Fig. 2.S5) further bolsters the case for arrestin sharing the same binding site on the receptor as the G_t peptide.

Secondly, the reduced ability of arrestin to trap retinal in rhodopsin mutants V226C and V230C (Fig. 2.2b), which have the G_t-binding "hydrophobic patch" mutated, also suggests that some part of arrestin binds to the same area as the G_t peptide and also requires the hydrophobic interactions with these residues for binding. A similar reduced binding to rhodopsin V226C and V230C was seen for transducin (Yang et al., 1996) and V226A and V230A mutations lower the affinity of G_t tail peptide for rhodopsin by ~3 kCal/mol (Janz and Farrens, 2004). Together, these two lines of evidence suggest arrestin and the G_t C-terminal peptide share a common binding site on rhodopsin.

Arrestin "finger" loop and 160 loop make interactions with the base of TM6

Our mapping studies employed the fluorescence TrIQ approach, as TrIQ can be used to monitor interactions between a fluorophore and the quenching tryptophan in the 5-15Å distance range (Mansoor et al., 2010; Mansoor and Farrens, 2004). The fluorescence quenching profile at 243mB by arrestin Trp mutants in the "finger" loop indicates Y67 and F79 to be closer to T243 than I72, as Y67W and F79W cause almost 40 and 35% quenching, respectively, while I72W does not (Fig. 2.4a). This is understandable from a structural standpoint as both Y67 and F79 are close by at the base of the loop, in the arrestin crystal structure, while I72 is further away (Fig. 2.S7). The 160 loop Trp mutants show a diffuse quenching pattern at 243mB.

In order to confirm that for arrestin mutants that the residues that did not show TrIQ were actually bound to the receptor, we tested the ability of each arrestin mutant to inhibit M257Y opsin mediated activation of transducin, as measured by [^{35}S]GTPγS incorporation. All of the arrestin mutants appear to bind the receptor, as suggested by the similar levels of G_t inhibition. Therefore, the lack of fluorescence quenching is not because of lack of binding, and we can conclude the site-specific quenching we see reflects the proximity of the label to the quenching tryptophan. Further, all the arrestin mutants caused a slight blue-shift (~3nm) in the emission maxima of the bimane at 243, compared to the arrestin-free receptor (Fig. 2.3), further indicating that they had all bound arrestin.

One residue away, at T242mB, the fluorescence quenching by the "finger" loop Trp mutants was not seen. This might be due to slightly "weaker" binding of these mutants, as indicated by a lower inhibition of G_t activation. One possible cause for this could be some steric clash between the "finger" loop Trp residues and the bimane label attached to the receptor at the

interaction interface. The 160 loop mutants, however, bound well to the receptor and caused site-specific quenching of T242mB fluorescence (Fig. 2.4b, d).

The TrIQ data can be further analyzed to dissect static versus dynamic quenching of fluorescence by a quencher by comparing the steady state fluorescence data with fluorescence lifetime data (Mansoor et al., 2010; Mansoor and Farrens, 2004). Using this approach, a study of bimane probes on T4 lysozyme showed that Trp-bimane pairs that are 10-15Å apart show almost exclusively dynamic quenching, while those that are less than 10Å apart can exhibit considerable static quenching as well. We used this approach to identify specific sites of arrestin-opsin interactions. Our analysis indicates several 160 loop residues show static quenching, with E161W showing ~20-25% static quenching. This means that at least ~20-25% of opsin-arrestin complexes interact such that the bimane at T243 on opsin and Trp at E161 on arrestin form a pre-coupled non-fluorescent complex, an evidence of "very close" interaction (~5-10Å apart). Dynamic quenching, by the Trp residues, on the other hand, indicates that mBBr and the quenching tryptophan are likely ~10-15Å apart.

Overall, the results suggest that the arrestin "finger" loop and the 160 loop both lie near the base of TM6 of opsin. The involvement of the "finger" loop near this site of the receptor is not surprising, given the various lines of evidence pointing to its role in receptor binding (Feuerstein et al., 2009; Hanson et al., 2006; Sommer and Farrens, 2006; Sommer et al., 2007; Sommer et al., 2006). The role of the 160 loop in rhodopsin binding was a little surprising, as it has not been as rigorously tested so far. As mentioned earlier, this loop shows conformational plasticity in the crystal isoforms and belongs to a class of polypeptides that show context-dependent structure. EPR studies looking at the mobility of a spin label probe at residue T157 of arrestin found a slight loss of mobility of the probe upon binding phosphorylated rhodopsin

(Hanson et al., 2006), but no conclusions were drawn from that work. This is consistent with our result, as, while we see some quenching of fluorescence by T157W, we do not see a very strong quenching effect.

Gurevich and Benovic have proposed the presence of at least one “activation recognition” domain each within the residues 16-145 and between 145 and 191 of arrestin (Gurevich and Benovic, 1993). Since receptor activation exposes the TM5-TM6 cytosolic face which contains T242 and T243, it is possible that the two sites we have studied - the “finger” loop (67-79) and the 160 loop (157-164) - might be two of the proposed activation recognition domains.

However, how the two extreme ends of the N-domain interact with or lie near the same site of the receptor is difficult to explain. Providing distance constraints based on the static and dynamic quenching results to the online program PatchDock (Schneidman-Duhovny et al., 2005) provided one possible mode of interaction as shown in Fig. 2.6. It is also possible that arrestin interacts with the receptor in two possible orientations, with one binding mode positioning the “finger” loop near TM6 and the other positioning the 160 loop. Alternatively, it is possible that arrestin employs these two sites in the context of binding to a receptor dimer, with one protomer placing the T242-T243 near the “finger” loop, and the other near the 160 loop, or arrestin undergoes a large conformational rearrangement that enables both regions to be close.

While our results provide two sites of direct contact between arrestin and the receptor, more sets of interactions will need to be discovered to come with a more complete model of the complex. Finally, we note that our studies identified conditions under which ligand-free, constitutively active opsin and arrestin formed a stable, long lasting complex (Fig. 2.S8) , and

these mutants and conditions may be optimal for forming complexes which provides a possible method to obtain complexes that might be stable enough for co-crystallization or EM studies.

Fig. 2.1. Sites of labeling and introduction of tryptophan.

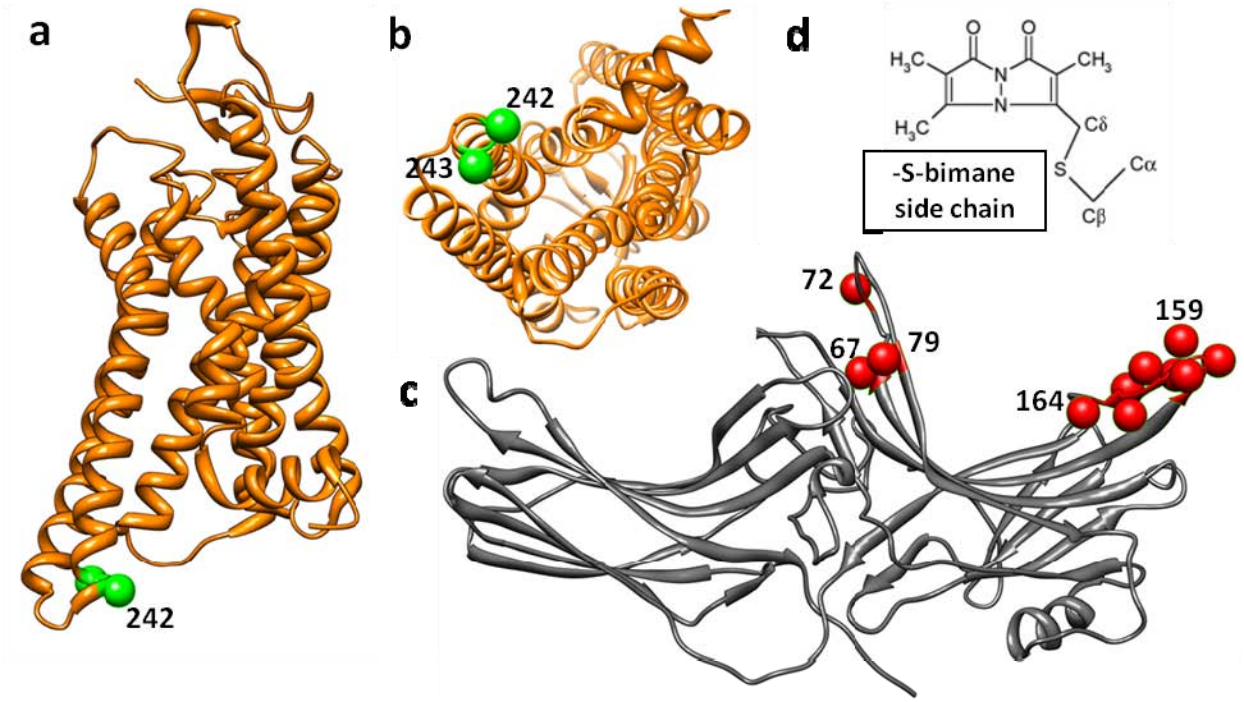

Fig. 2.1. Sites of labeling and introduction of tryptophan.

Crystal structure of opsin M257Y (PDB Id: 4A4M) with the alpha carbon atoms at T242 and T243 represented as green balls in shows as (a) transmembrane view and (b) cytoplasmic view. These residues were mutated to cysteines and labeled with mBBr. (c) Crystal structure of arrestin (PDB Id: 1AYR) with alpha carbons of residues Y67, I72 and F79 of the “finger” loop and those of residues T157-I164 of the 160 loop represented as red balls. These residues were mutated to Trp for the TrIQ studies. (d) Chemical structure of mBBr attached to the sulfhydryl group of cysteine. Models were made using UCSF Chimera.

Fig. 2.2. Arrestin employs the same binding pocket on rhodopsin as the G_t C-terminal tail peptide.

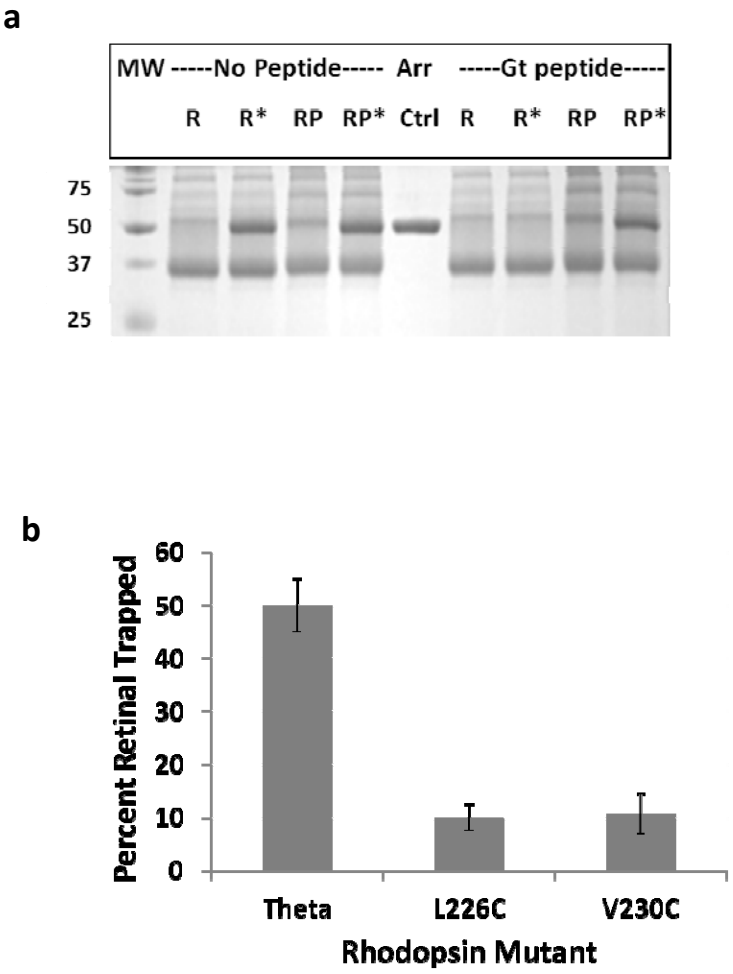

Fig.2.2. Arrestin employs the same binding pocket on rhodopsin as the G_t C-terminal tail peptide.

(a) The effect of G_t tail peptide on arrestin binding to rhodopsin studied tested by a centrifugal pull-down assay. G_t tail peptide inhibits the binding of arrestin R175E to light activated rhodopsin, R*. (b) The effect of mutations in the hydrophobic patch of rhodopsin on arrestin-mediated retinal trapping. Hydrophobic patch mutations L226C and T230C inhibit arrestin binding, indicated by the reduced amount of retinal trapped in these mutants in the presence of arrestin R175E.

Fig. 2.3. Site specific quenching of T243mB fluorescence by Trp residues in the arrestin "finger" loop.

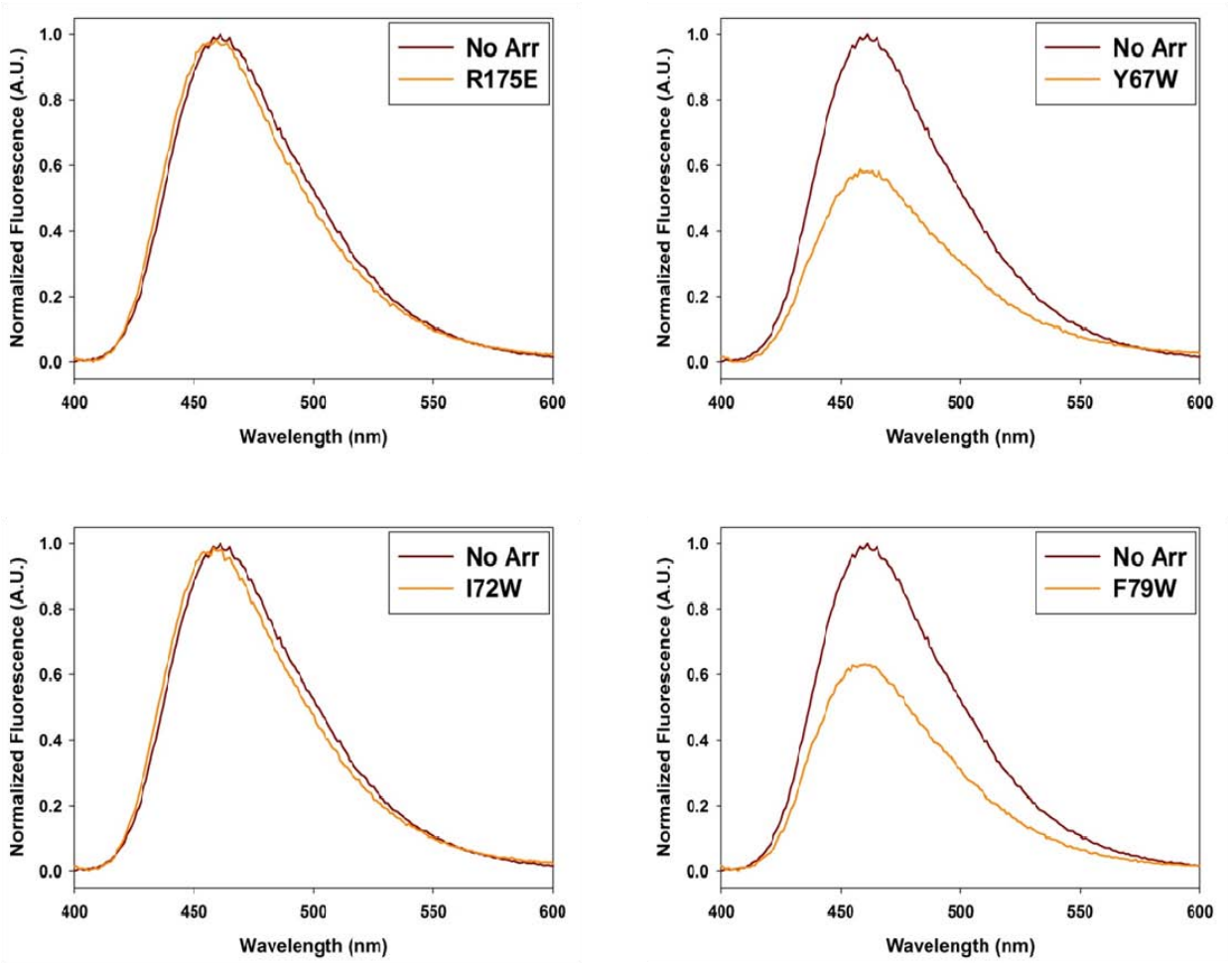

Fig. 2.3. Site specific quenching of T243mB fluorescence by Trp residues in the arrestin "finger" loop.

Steady state fluorescence emission spectrum of opsin T243mB in the absence (in brown) and presence (in orange) of arrestin mutants. Arrestin mutant R175E with no non-native Trp or with Trp at I72 does not show any quenching (left panels). However, the presence of Trp at residues Y67 and F79 in arrestin causes ~35-40% quenching T243mB fluorescence, indicating the proximity of these two residues to T243mB. In all the panels, there is a slight blue shift in the emission maxima of bimane fluorescence in the presence of arrestin, compared to that in absence, reflecting a change in the local environment around the probe, possibly as a result of arrestin binding.

Fig. 2.4. Arrestin "finger loop" and 160 loop interact with the base of TM6 of opsin.

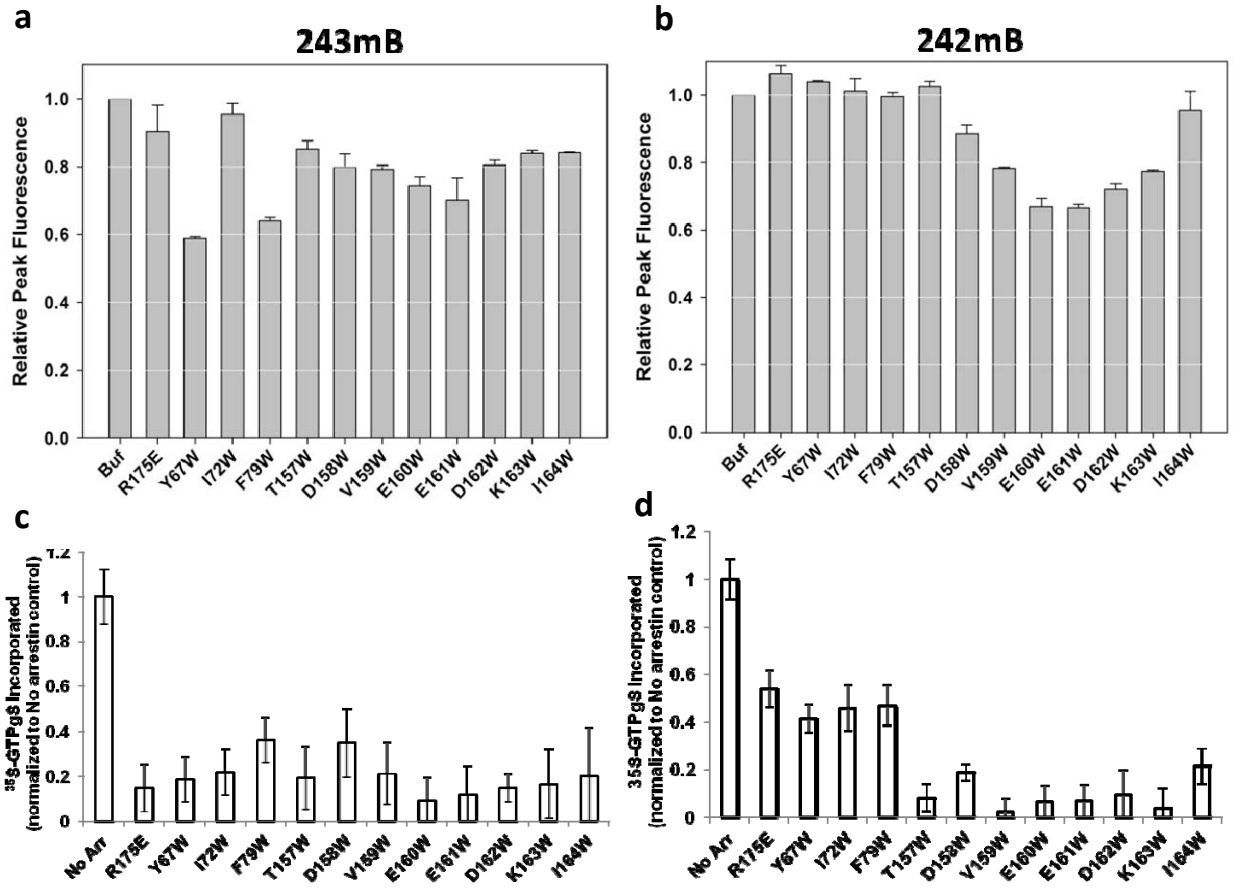

Fig. 2.4. Arrestin "finger loop" and 160 loop interact with the base of TM6 of opsin.

Arrestin-mediated steady state fluorescence quenching and inhibition of G_t activation. Fluorescence quenching of (a) T243mB and (b) T242mB of opsin N2C/D282C/M257Y by Trp residues introduced in the arrestin "finger" loop (Y67W, I72W and F79W) and the 160 loop (T157W – I164W) show that both these regions of arrestin bind near the base of TM6 of opsin and quench mBBr fluorescence in a site-specific manner. 0.25μM opsin and 5μM arrestin were used in these experiments. (c and d) Arrestin mutants retain their ability to bind the labeled opsin mutants, as tested by their ability to inhibit transducin activation by opsin in a [^{35}S]GTPγS incorporation assay.

Fig. 2.5. Arrestin "finger" loop and 160 loop make direct physical contact with the base of TM6 of opsin.

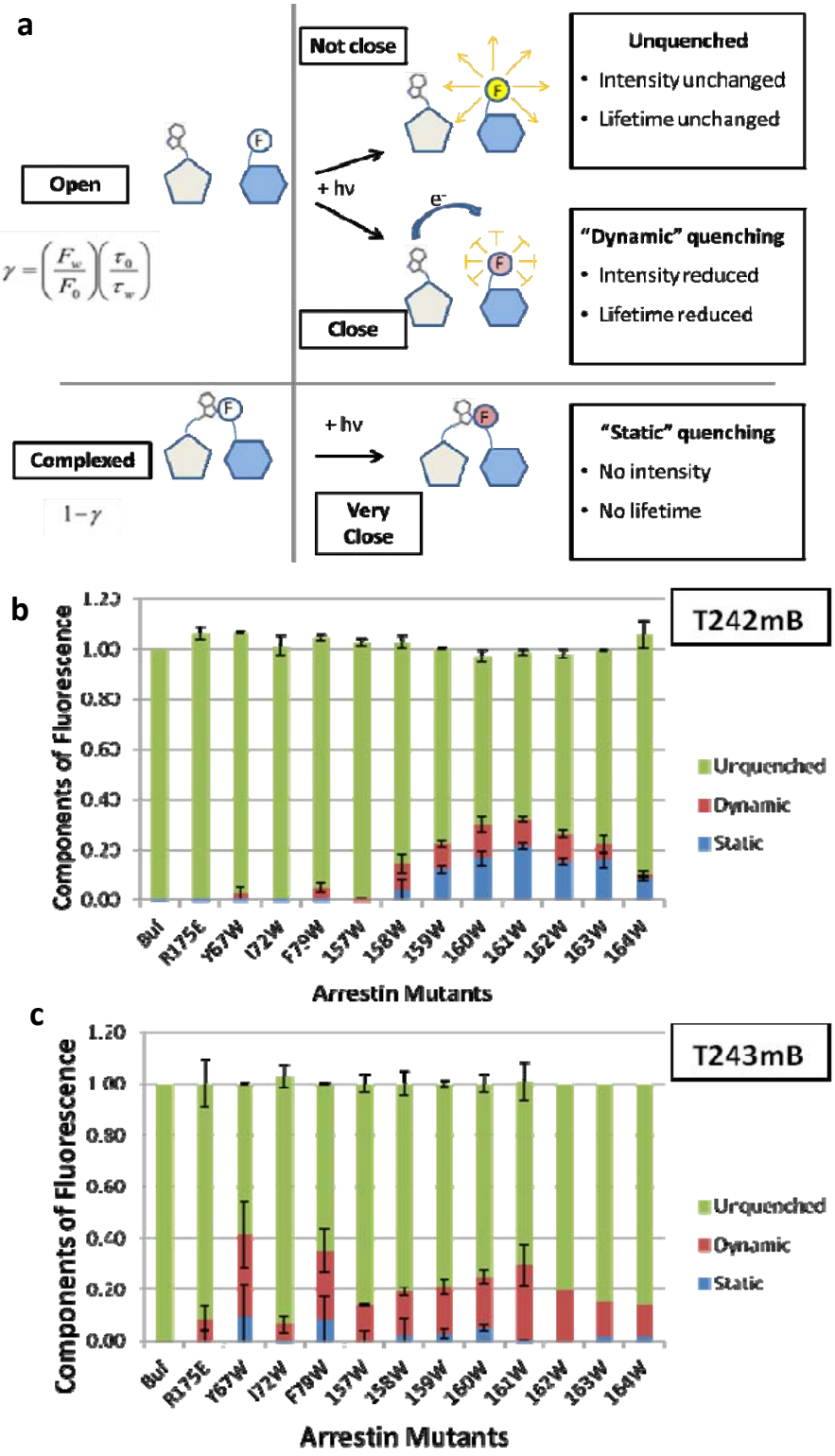

Fig. 2.5. Arrestin “finger” loop and 160 loop make direct physical contact with the base of TM6 of opsin.

(a) Schematic illustration of the concept of static vs dynamic quenching of fluorescence. (b) Combination of steady state quenching and fluorescence lifetime data shows that the 160 loop of arrestin makes direct contact with 242mB, as some residues show upto 20% static quenching. (c) The same analysis indicated that the arrestin “finger” loop, too, interacts with the base of helix, as seen by the quenching of 243mB fluorescence.

Fig. 2.6. A possible model of arrestin interaction with opsin.

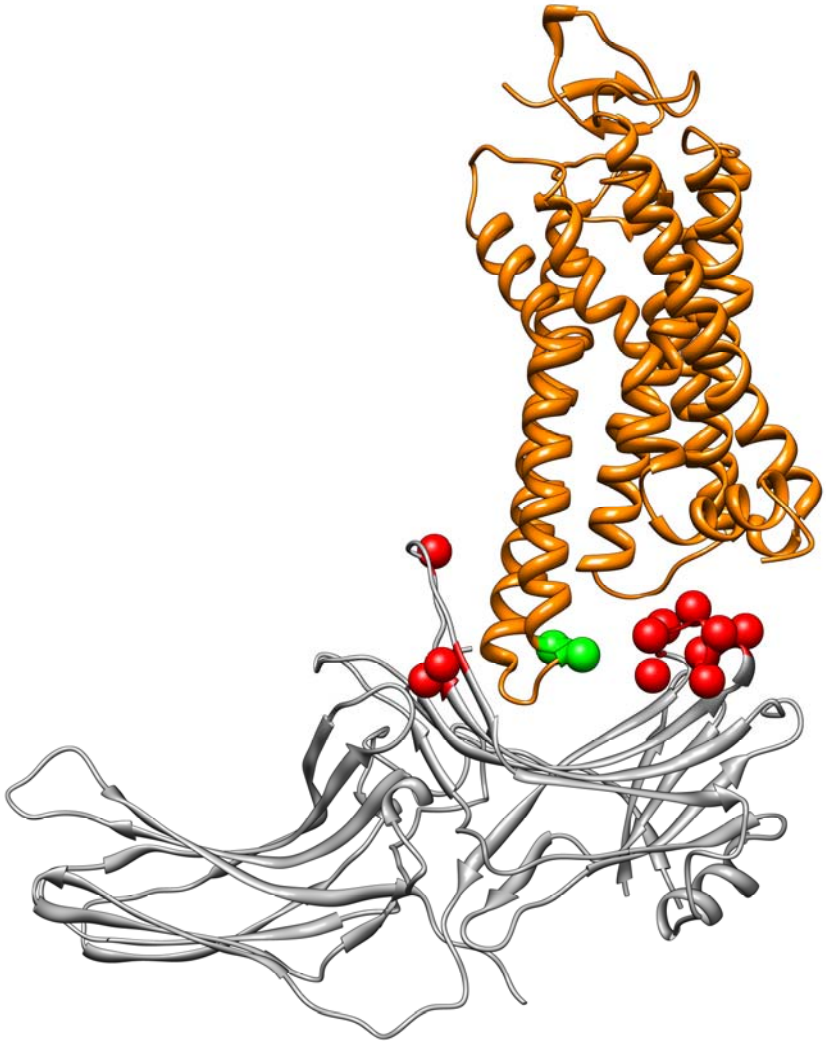

Fig. 2.6. A possible model of arrestin interaction with opsin.

One possible model of arrestin-rhodopsin interaction based on our data, obtained by providing distance constraints based on the static vs dynamic quenching analysis to the online server PatchDock shows the base of TM6 of rhodopsin lying between the finger loop and the 160 loop of arrestin. However, there are other possible modes of interaction that are outlined in the main text.

Table 2.S1. Life-time decay data for mBBr labeled opsin in the presence of arrestin mutants.

Mutant	α_1	τ_1 (ns)	α_2	τ_2 (ns)	α_3	τ_3 (ns)	χ^2	$<\tau>$(ns)
242mB								
Buf	318.3	15.891	364.2	7.987	239	0.474	0.93	8.77
R175E	359.6	16.497	337.4	6.817	261	0.442	0.94	8.72
Y67W	312.1	16.318	324.4	7.816	257.4	0.665	0.92	8.72
I72W	377.8	15.961	333.4	6.818	244	0.534	0.93	8.83
F79W	350.7	15.613	290.9	6.677	251	0.486	0.90	8.45
T157W	315.4	16.723	311.1	7.824	243.6	0.775	0.94	9.08
D158W	338.2	16.328	317.8	7.693	252.8	0.522	0.92	8.10
V159W	320.1	15.039	222	6.16	270	0.538	0.97	7.79
E160W	267.5	15.95	280.1	6.918	306	0.549	0.95	7.47
E161W	241.24	15.774	246	6.602	267.4	0.525	0.97	7.38
D162W	299.6	15.726	313.2	6.684	299	0.515	0.98	7.63
K163W	306.5	15.438	263	0.374	244.8	5.924	0.97	7.71
I164W	340.2	15.629	296.9	6.84	248	0.541	0.96	8.46
243mB								
Buf	497.3	16.954	299.1	8.034	234	0.572	0.96	10.65
R175E	564.4	16.922	372.6	7.837	290	0.589	0.97	10.31
Y67W	432.6	15.658	345	0.468	362.1	6.35	0.94	8.10
I72W	616.8	16.321	264.5	7.29	288	0.373	0.93	10.35
F79W	485.1	15.445	384.9	6.357	352	0.559	0.95	8.30
T157W	444.2	16.705	262.3	6.625	308	0.53	0.92	9.19
D158W	368.9	15.948	330.1	7.242	271.1	0.816	0.94	8.76
V159W	497.3	14.997	339	6.056	323	0.521	0.97	8.35
E160W	236.2	5.92	345.9	15.414	200	0.392	0.94	8.71
E161W	310.3	15.281	243	6.047	206.7	0.714	0.92	8.37
D162W	487.4	15.557	348.1	6.32	325	0.54	0.96	8.58
K163W	343.1	15.524	246	6.598	172	0.381	0.94	9.22
I164W	488.5	16.619	258.9	6.685	325	0.389	0.90	9.30

Table 2.1. Life-time decay data for mBBr labeled opsin in the presence of arrestin mutants.

Life-time decay data for mBBr labeled opsin mutants in the absence (Buf) or presence of different arrestin mutants. The data was fit to a three exponential decay. τ_1, τ_2 and τ_3 are the fluorescence lifetimes in nanoseconds; α_1, α_2 and α_3 are the normalized pre-exponential factors such that $\alpha_1 + \alpha_2 + \alpha_3 = 1.0$; χ^2 is chi-squared value of the fit. $< \tau > = \alpha_1\tau_1 + \alpha_2\tau_2 + \alpha_3\tau_3$, the amplitude-weighted average fluorescence lifetime.

Fig. 2.S1. The labeled sample does not have free label.

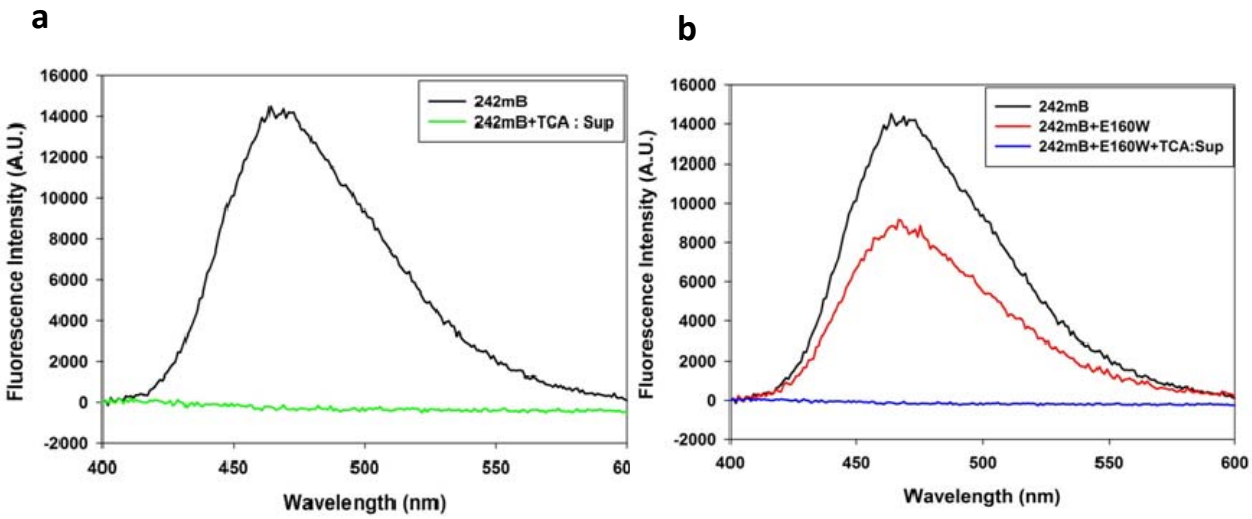

Fig. 2.S1. The labeled sample does not have free label.

(a) TCA precipitation of 243mB indicates there is not free label contamination in the supernatant, i.e., all the label is attached to opsin. (c) Binding of arrestin does not cause the label to get reduced off the receptor. TCA precipitation of arrestin bound 242mB shows no free label. Therefore, the reduction in fluorescence is due to Trp-mediated quenching.

Fig. 2.S2. Fluorescence quenching by 2μM arrestin mutants.

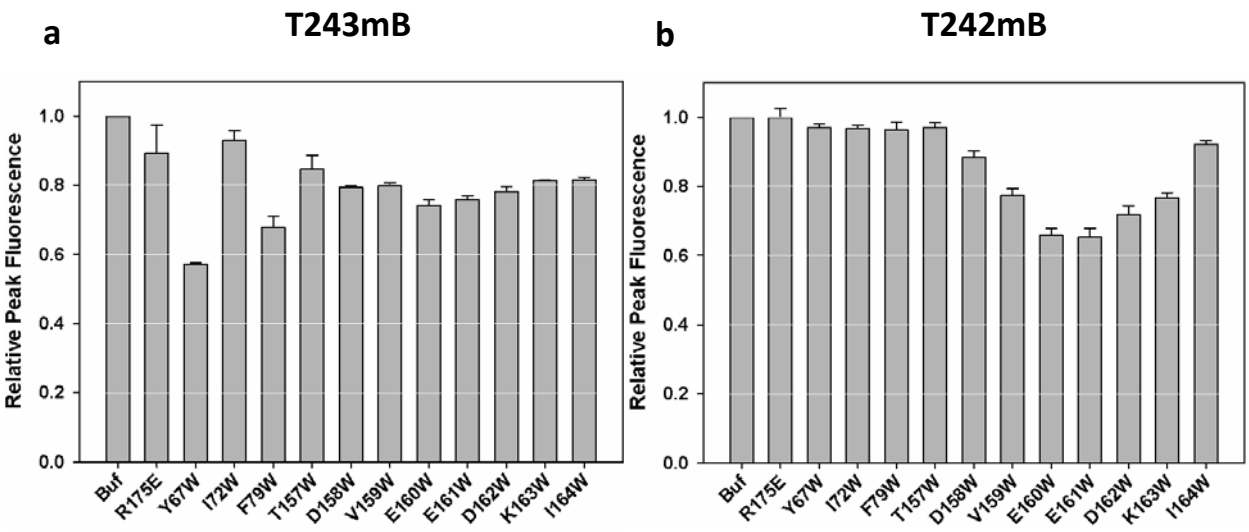

Fig. 2.S2. Fluorescence quenching by 2μM arrestin mutants.

Fluorescence quenching of mBBr attached to residue (a) T243C and (b) T242C of opsin N2C/D282C/M257Y by Trp residues introduced in the arrestin "finger" loop (Y67W, I72W and F79W) and the 160 loop (T157W – I164W) shows that both these regions of arrestin bind near the base of helix VI of opsin and quench mBBr fluorescence in a site-specific manner. 0.25μM opsin and 2μM arrestin were used in these experiments. The amount of quenching by 2μM arrestin is comparable to that seen by 5μM arrestin mutants.

Fig. 2.S3. Purification of G_t from bovine retina.

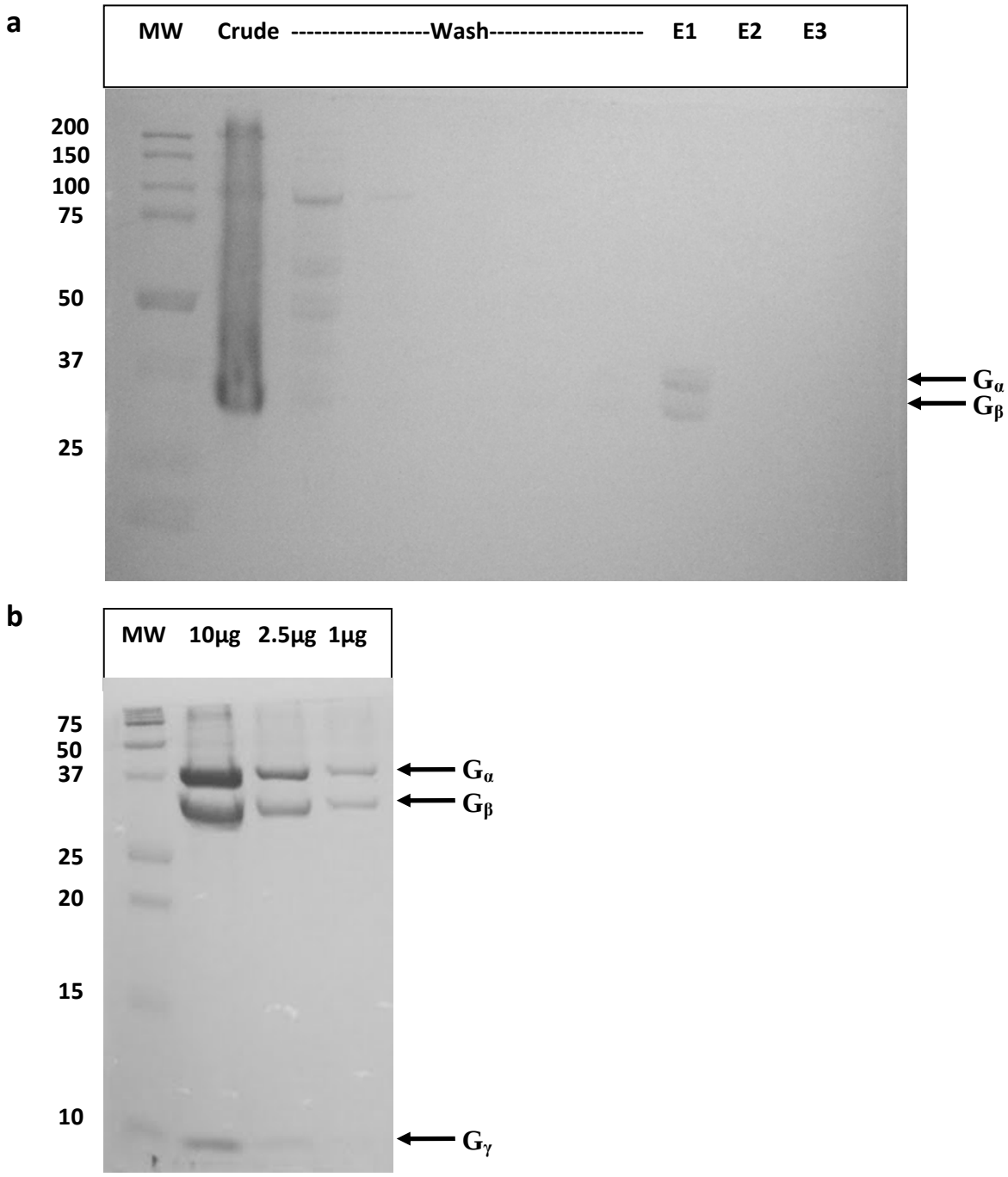

Fig. 2.S3. Purification of G_t from bovine retina.

Gt was purified from the ROS membranes of bovine retina as described in the text.

(a) Coomassie stained gel showing samples from different steps of purification. Samples were loaded on a 10% tricine gel as indicated. E1, E2 and E3 lanes represent first, second and third extracts, respectively. The α subunit runs at 38 kDa and the β subunit at 36 kDa. The γ subunit s not observed on this gel. E1 was the cleanest of the three and was concentrated, buffer exchanged and frozen with 10% glycerol for use in GTPγS incorporation assays. (b) Three different amounts of concentrated G_t protein (10μg, 3μg and 1μg) were analyzed by a Coomassie-stained 15% tricine gel. All the three subunits - α (38kDa), β (36kDa) and γ (8kDa) – can be seen in this gel.

Fig. 2.S4. Fluorescence life-time decay analysis.

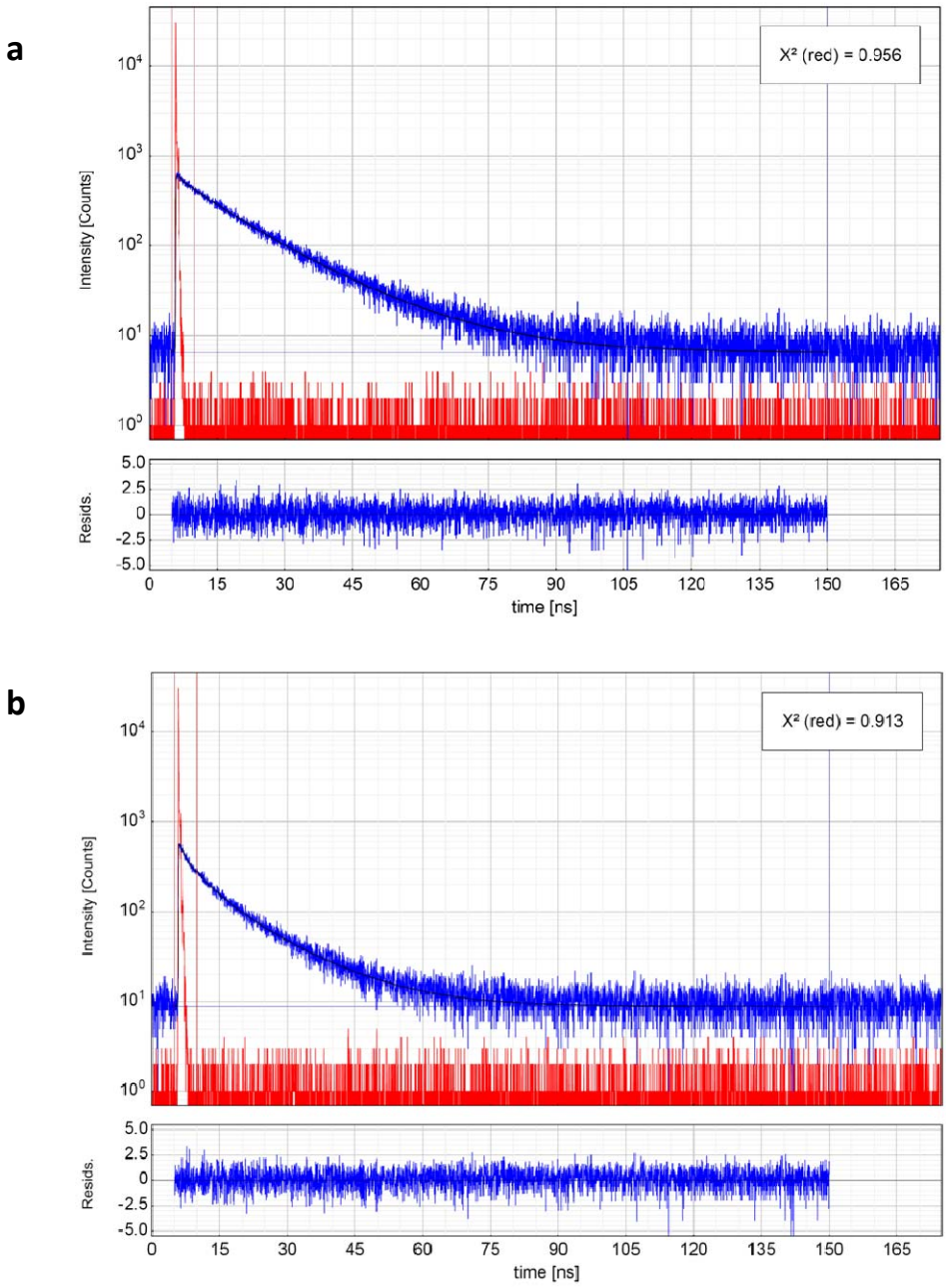

Fig. 2.S4. Fluorescence life-time decay analysis.

Representative fluorescence lifetime decay spectra and fit of opsin 243mB with (a) no arrestin (b) arrestin R175E/Y67W. The top panel for both (a) and (b) s the fluorescence decay spectrum of the bimane labeled opsin sample in blue and the instrument response function (IRF) as determined by the scatter of a solution of Ludox is in blue. The lifetime decay spectrum was fit to a three exponential decay and the fit is overlaid as a black solid line on top of the blue decay spectrum. The "goodness of fit" is given by the reduced χ^2 value, χ^2(red). The residuals from the fit are plotted in blue in the bottom panel for both (a) and (b).

Fig. 2.S5. G_t tail peptide inhibits the rate of quenching of T242mB fluorescence by arrestin R175E/E160W.

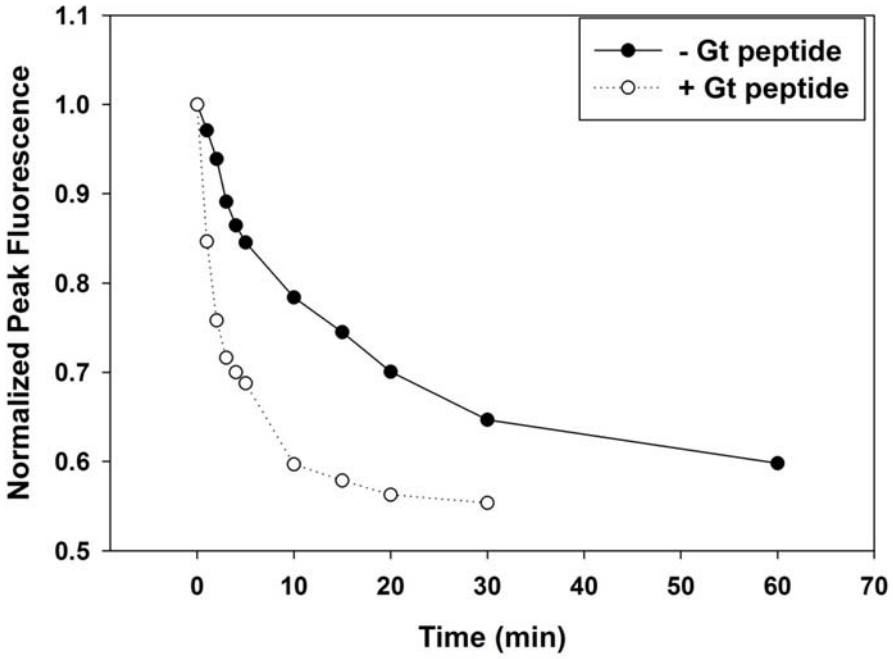

Fig. 2.S5. G_t tail peptide inhibits the rate of quenching of 242mBBr fluorescence by arrestin R175E/E160W.

The time-course of arrestin E160W-mediated decrease in the fluorescence of mBBr attached to T242 in opsin was measured in the absence ("-G_t peptide") or presence ("+G_t peptide") of a high affinity peptide derived from the C-terminal tail of G_t. upon The $t_{1/2}$ of quenching in the presence of the G_t peptide is ~9min, while it is about 1.5 min in the absence of the peptide.

Fig. 2.S6. ClustalW sequence alignment of G_t C-tail with the arrestin "finger" loop.

```
Gt_C-Tail.         IKENLKDCGL-F 11
Arr_Finger-Loop.   GQEDIDVMGLSF 12
                    :*::.  ** *

SeqA Name            Len(aa)  SeqB Name               Len(aa)  Score
==========================================================================
1    Gt_C-Tail.      11       2    Arr-Finger-loop.   11       27
==========================================================================
```

Fig. 2.S6. ClustalW sequence alignment of G_t C-tail with the arrestin "finger" loop.

Sequence alignment of the C-terminal tail region of G_t with the "finger" loop of arrestin shows considerable similarity between the two sequences. The sequences were aligned using ClustalW and an alignment score of 27 was obtained.

Fig. 2.S7. Arrestin "finger" loop residues Y67 and F79 are close together in space.

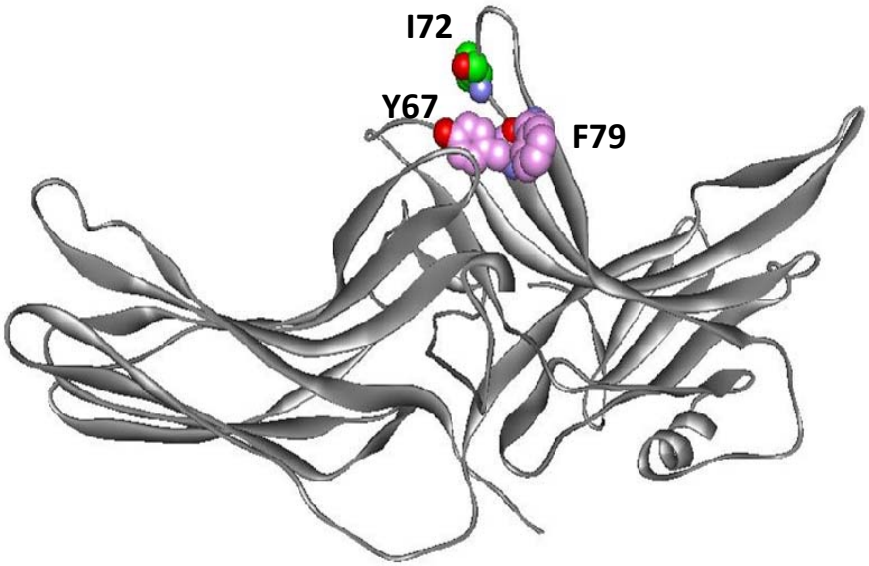

Fig. 2.S7. Arrestin "finger" loop residues Y67 and F79 are close together in space.

Crystal structure of visual arrestin (PDB Id: 1AYR) showing Y67, I72 and F79 as space filling atomic models. Y67 and F79 are next to each other in space at the base of the "finger" loop, as shown in pink space-filling models, while (I72 in green) is further away. The model was made using Discovery Studio Visualizer.

Fig. 2.S8. Arrestin forms stable complex with labeled opsin mutants.

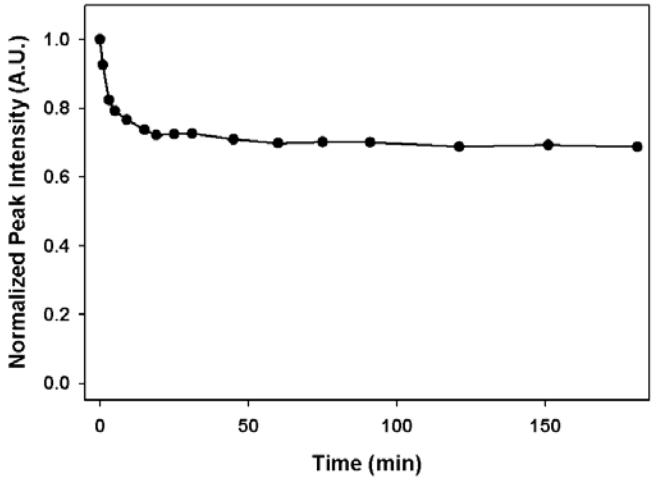

Fig. 2.S8. Arrestin forms stable complex with labeled opsin mutants.

The time course of fluorescence quenching of opsin T242mB by arrestin E161W monitored for 3 hours. The quenching profile does not change much after about 30min and stays stable for at least 180 min, indicating that the complex is stable for at least 3 hours at 20^{o}C.

Chapter 3

Purification and Analysis of the Interaction of Rhodopsin Kinase with Rhodopsin

3.1. Summary

We describe a fast and simple, one-step purification method for rhodopsin kinase expressed in mammalian cells. We tested its functionality and found it to phosphorylate membrane bound or detergent-solubilized/purified rhodopsin at roughly the same level. We report that RK could phosphorylate monomeric rhodopsin nanodiscs, which shows that the kinase does not need a multimeric receptor species for a "productive" interaction with the receptor, a result reported recently by another group as well (Bayburt et al., 2011). We found that the transducin C-terminal tail peptide inhibited rhodopsin kinase mediated phosphorylation, indicating a common site on binding site on rhodopsin for both the transducin peptide, as well RK. We also report that RK can phosphorylate M257Y opsin, at a rate that is accelerated by the presence of the agonist, all-trans-retinal, thus reflecting the functional interaction of G_t with the M257Y mutant. Also, arrestin could compete with RK in binding to the opsin mutant, again pointing to possible common binding site on the receptor.

The author of this dissertation set up and standardized the purification protocol and the radioactivity assays to study RK function. Most of the experiments and analysis were performed by the author. Some opsin experiments were done in conjuction with Amber Jones-Hackathorne.

3.2. Introduction

G Protein-Coupled Receptors (GPCRs) are essential mediators of signal transduction across the cell membrane. Receptor-mediated G protein signaling, initiated by the binding of a wide array of cognate ligands (agonists), is central to the development of a phenotypic response to a triggering stimulus. While receptor activation is important, so is its deactivation, which modulates the duration and amplitude of the cellular response. In fact, disruption of the both the activation and deactivation of GPCRs can lead to various diseases (Schoneberg et al., 2004; Thompson et al., 2008). GPCR desensitization involves phosphorylation of the activated receptor by a G protein coupled receptor kinase (GRK), followed by the binding of arrestin, which inhibits G protein binding and shuts down G protein-mediated signaling.

Rhodopsin, the dim light photoreceptor of rod cells, is probably the best studied GPCR (Palczewski, 2006). The kinase involved in its desensitization is GRK1 or rhodopsin kinase (RK). RK recognizes the active state of rhodopsin (like transducin and arrestin) and phosphorylates the C-terminal tail at up to seven Ser/Thr phosphorylation sites (Palczewski et al., 1991). The kinase, like other members of the GRK family, is a member of the AGC family of kinases, and consists of an N-terminal helical element, followed by a regulator of G protein signaling (RGS) homology (RH) domain (Singh et al., 2008). A kinase domain, closely related to protein kinase A (PKA), is inserted into one of the loops of the RH domain and has the active site placed between the N- and C- lobes of the kinase domain.

While the structure of the inactive enzyme has been solved, the interaction of RK with rhodopsin is not well defined. The kinase N-terminal helix is reported to interact with the kinase domain and might be involved in mediating interaction with the receptor via a patch of hydrophobic residues at its distal end (Huang et al., 2011). In fact, the N-terminal helix, is

proposed to be the major determinant of the binding of GRK family members to their cognate receptors, analogous to the binding of G proteins to the receptors via their C-terminal α-helix (Boguth et al., 2010). The kinase domain C-tail has also been implicated in mediating receptor induced activation of GRKs, possibly by forming a receptor docking site in conjunction with the small lobe of the kinase domain (Huang et al., 2009). However, experiments showing direct interaction between these regions and rhodopsin are lacking. The activation of RK by rhodopsin is thought to result from a conformational change in the enzyme, upon interaction with the receptor, the exact nature of which is also not known.

Short of co-crystallization of rhodopsin-RK complexes, filling in the above mentioned gaps in our understanding of RK dynamics and activation/interaction mechanism will need mutagenesis and/or spectroscopic studies with labeled proteins. As such, a fast and easy method for RK purification will be highly beneficial, since the commonly used approach for RK purification involves nickel affinity chromatography followed by cation exchange chromatography and finally size exclusion chromatography, making the purification a long and involved process (Bruel et al., 2000; Singh et al., 2008). Given that RK is inherently unstable and loses activity over time (Bruel et al., 2000; Palczewski et al., 1988a), a shorter purification would provide a longer window of functional enzyme. Further, the methods used previously for recombinant RK purification commonly employ an N-terminal hexahistidine tag on the protein (Bruel et al., 2000; Cha et al., 1997; Singh et al., 2008), which might affect the interaction of RK with rhodopsin.

We report here the expression and purification of rhodopsin kinase expressed in mammalian cells by a one-step purification, using a relatively recent purification technique which involves the expression of the protein with an N-terminal mutant prosubtilisin tag. The

approach exploits the picomolar affinity between prosubtilisin and its cognate mature subtilisin variant (Huang et al., 2012; Ruan et al., 2004; Tsukamoto et al., 2010), for a quick and simple purification of RK and yielded purified RK which retained its functionality. We found the kinase was also able to phosphorylate rhodopsin in a monomeric form, as was also reported recently by another group (Bayburt et al., 2011). We also localized a potential interaction site of RK on rhodopsin as being the same site used by the transducin C-tail for binding to the receptor. We also report that RK can phosphorylate a constitutively active mutant of unliganded opsin (M257Y), at a rate that is accelerated by the presence of the agonist, all-trans-retinal, and that arrestin can inhibit RK-mediated phosphorylation of the receptor.

3.3. Materials and Methods

Materials

All restriction enzymes, ligase and DNA polymerase were from New England Biolabs. Tissue culture media was purchased from HyClone, while polyethyleneimine was from Polysciences, Inc. n-Dodecyl-β-D-maltoside (DM) was purchased from Anatrace and 1,2-dioleoyl-*sn*-glycero-3-phospho-L-serine was from Avanti Polar Lipids. 1D4 antibody was obtained from the Monoclonal Antibody Core at the Vaccine and Gene Therapy Institute of Oregon Health and Science University and the competing 9-mer peptide was obtained from Biotechnology Core Facility Branch at the Centers for Disease Control and Prevention, Atlanta, GA. High affinity G_t C-terminal tail peptide (Janz and Farrens, 2004) was synthesized by Emory Microchemical Facility. Protease Inhibitor Cocktail (EDTA Free) was purchased from Roche Diagnostics. Profinity eXact^{TM} column was from Bio-Rad. Amicon Ultra protein concentrator

(10kD cut-off) was from Millipore. [^{32}P]-ATP was from Perkin Elmer. Frozen bovine retinas were obtained from Lawson and Lawson, Inc. (Lincoln, NE). GBX red light filters were purchased from Eastman Kodak Co. Band pass filters and long pass filters were purchased from Oriel (Stratford, CT), while cuvettes were purchased from Uvonics (Plainview, NY). All other chemicals and reagents were obtained from Sigma-Aldrich.

Cloning of rhodopsin kinase

To purify rhodopsin kinase using the prosubtilisin affinity tag method, we sub-cloned the 77-amino acid long ProR8FKAM subtilisin BPN' prodomain coding sequence (Abdulaev et al., 2005; Ruan et al., 2004) into pCMV5-RK$(His)_6$ plasmid from the Khorana group (Bruel et al., 2000). We removed the N-terminal hexahistidine tag from rhodopsin kinase and replaced it with the ProR8FKAM sequence by overlap extension PCR, while maintaining the Kozak sequence (GCCACC) preceding the start codon of the prodomain, to make the pCMV5 Prosub-RK construct.

Expression and purification of rhodopsin kinase

90% confluent COS-1 cells in 15cm plates were transfected with 30ug pCMV5 Prosub-RK construct using 100ug polyethyleneimine (PEI) per plate. 12 hours post transfection, the transfection media was changed and 4mM mevalonolactone was added to the cells with fresh complete media. Cells were incubated for 36-48 hours more before harvesting with 20mM HEPES, 140mM NaCl, pH7.4 (Buffer A). All the purification steps except elution were carried out at 4^{o}C. The harvested cell pellet was solubilized for 1 hour with Buffer A containing 1% dodecyl maltoside, 1X protease inhibitor cocktail and 0.1mM PMSF. The lysate was dounced for 20 strokes with a Teflon homogeizer. The lysate was clarified by centrifuging at 100,000g for 30

min. The supernatant was filtered through a 0.45um filter and applied to a 1ml Profinity eXact column, equilibrated with Buffer A. The column washed extensively with 5ml of each of the following (in Buffer A): 2 x 0.3% DM; 0.3% Tween-20; 5mM MES pH 6.5; 1mM EGTA; 1mM $CaSO_4$; 2 x 5ml Buffer A; 2 x 5ml Buffer A with 0.3M CH_3COONa and 5ml of Buffer A. Following these washes, the protein was eluted by passing Buffer A containing 10mM NaF. Most of the RK was present in the first 10ml of the elution volume. These fractions were pooled, concentrated and stored at 4^oC for use within 2-3 weeks.

Isolation of ROS membranes and preparation of urea stripped ROS

ROS were isolated from bovine retinas as described previously (Papermaster, 1982; Sommer et al., 2005). All the steps were carried out at 4 °C under red lights. Rhodopsin concentration was assessed by difference spectra in the presence of hydroxylamine (ε_{500} = 40,800 liter cm^{-1} mol^{-1}). Stocks were snap-frozen and stored at -80 °C.

Urea stripped ROS (USR) was made as described (Shichi and Somers, 1978). Briefly, ROS membranes were washed with 5M urea in 50mM Tris-HCl, pH8 containing 50mM EDTA for 15min at 4^oC. The membranes were then centrifuged at 13,000g for 15min and washed five times with 50mM Tris-HCl pH 7.4 before freezing in liquid nitrogen.

Isolation of "crude", soluble RK from bovine retina

Soluble rhodopsin kinase was extracted from ROS membranes as previously described (Palczewski et al., 1988a). Briefly, we first extracted cAMP-dependent protein kinase and protein kinase C, by light activating rhodopsin in the presence of Mg2+, to enable rhodopsin kinase to stay bound to the rhodopsin containing membranes. We then extracted rhodopsin

kinase from the membrane by washing the membranes with KCl in the dark for 12 hr. This “KCl extract” was used as a source of native rhodopsin kinase.

Purification of wild-type rhodopsin and constitutively active mutant opsin

Wild-type rhodopsin was purified from the isolated ROS membranes using ConA affinity chromatography as described previously (Mansoor et al., 2006). Constitutively active, thermostable opsin mutant N2C/D282C/M257Y was purified using 1D4 immuno-affinity chromatography as described for mutant rhodopsins (Janz and Farrens, 2004), except that the opsin was not regenerated with 11-cis-retinal before solubilization.

Preparation of monomeric rhodopsin in nanodiscs

Monomeric rhodopsin in nanodisc were prepared as described (Tsukamoto et al., 2010). Briefly, wild-type rhodopsin (solubilized in 1.46% octyl glucoside), MSP, and lipid (solubilized in 0.5M sodium cholate) were mixed with ~2/3 volume of Bio-Beads SM-2 (Bio-Rad) overnight at 4 °C. The Rh/MSP/lipid molar ratio was set to 0.1:1:75. The Bio-Beads were removed by centrifugation (1000g, 1 min). The samples were then injected onto a Superdex 200 column (GE Healthcare; column volume, 23.55 mL) run at 0.5mL/min. For the nanodisc samples, a fraction corresponding to a diameter of ~12 nm was collected. The diameter of nanodiscs was estimated by comparison to a Gel Filtration Calibration Kit HMW (GE Healthcare). The collected sample was concentrated by Amicon Ultra 0.5-mL Centrifugal Filters (10 kDa molecular weight cutoff).

Expression and purification of arrestin R175E

The visual arrestin R175E mutant, cloned at the C-terminal of a modified 77 amino acid prodomain region of subtilisin BPN' (proR8FKAM), in pG58 vector was a generous gift from Kevin Ridge (Abdulaev et al., 2005; Huang et al., 2012; Ruan et al., 2004). The mutant was expressed in *E. coli* BL21(DE3)-RP cells (Stratagene) and purified using Profinity eXact column (Bio-Rad), followed by ion-exchange chromatography using HiTrap Heparin column (GE Healthcare) as described earlier (Tsukamoto et al., 2010) BL21(DE3)-RP cells harboring the pG58 expression vector containing the prodomain/arrestin R175E (or R175E with Trp mutation at specific sites) fusion were grown in 1L of LB media in the presence of 100 ug/ml ampicillin at room temperature to an A_{550} of 0.6, and then induced with 30 μM IPTG for 16hr at 16 deg C. The cell pellet was resuspended in 50 mM Tris–phosphate, pH 7.2, containing 50 mM NaCl, 5 mM β-mercaptoethanol, 0.1 mM PMSF and protease inhibitor cocktail (Roche) and then disrupted by French press. The supernatant obtained by centrifugation of the cell lysate at 100,000 x g for 45 min was loaded onto a 5mL Profinity eXact column. The column was washed with 20 column volumes of 100 mM sodium phosphate, pH 7.2 and 20 column volumes of 100 mM sodium phosphate, 300 mM sodium acetate, pH 7.2. The cleavage of arrestin from the prosubtilisin tag was initiated by passing one column volume of 100 mM sodium phosphate, pH7.2 containing 100 mM sodium fluoride (elution buffer). The fluoride-mediated cleavage reaction was allowed to occur for 2hr on ice. Tag-free arrestin was eluted off the column by passing 5 column volumes of the elution buffer and was further purified by cation exchange chromatography using a 1ml HiTrap Heparin column. The resulting arrestin protein was >95% pure, as assessed by SDS-PAGE, and was concentrated using a 10kDa cut-off centrifugal concentrator and frozen in liquid nitrogen.

Rhodopsin kinase activity assay

For assays with wild-type rhodopsin in membranes, detergent or nanodiscs, 8μM of rhodopsin was incubated with 0.3μM RK in 75mM Tris-HCl pH7.5, containing 3mM ATP (with ^{32}P-ATP as a radioactive tracer), 1mM $MgCl_2$ and 1mM DTT at pH7.5 at 20^{o}C. The sample were either kept in the dark (dk) or light activated (hv) for 15, 60 or 120 min. The samples were analyzed by SDS-PAGE, followed by phosphor imaging to detect phosphorylated proteins. Densitometry was performed on the phosphorylated protein bands to determine relative phosphorylation between the bands.

The number of phosphates that were added on rhodopsin by RK was measured by precipitating the phosphorylated protein with 10% trichloroacetic acid containing 10mM phosphoric acid (Palczewski et al., 1988b), centrifuging the sample at 100000 x g for 15min and washing the precipitated protein. The amount of incorporated ^{32}P was measured by radioactive scintillation counting and then comparison to a standard curve generated from known amounts of ^{32}P-ATP. The number of moles of phosphates added was divided by the number of moles of receptor present in the reaction mix to get the number of phosphates per receptor.

For the opsin mutant, the receptor concentration was lowered to 0.25μM and RK concentration, to 0.1μM, while keeping other conditions the same as above. For studying the all-trans-retinal (ATR) effect, the opsin was incubated with 10μM ATR for 15min at 20^{o}C before adding arrestin or the kinase. In experiments with arrestin, 2μM arrestin was pre-incubated with the receptor for 30 min at 20^{o}C before adding the kinase.

3.4. Results and Discussion

Purification of rhodopsin kinase

The N-terminus of rhodopsin kinase and other GRKs has been shown to be critical in the phosphorylation of their cognate receptor, wherein receptor docking activates a GRK by stabilizing the interaction of its N-terminal region with the kinase domain (Boguth et al., 2010; Higgins et al., 2006; Huang et al., 2011; Huang et al., 2009; Palczewski et al., 1993). It is possible that having the hexahistidine tag at the N-terminus adversely affects its interaction with rhodopsin. In fact, a comparison of pH on the activity of untagged and $(His)_6$-RK shows that the two forms of RK have considerably different pH profiles, with the optimal pH being almost 1 pH unit apart for the two enzyme forms (Bruel et al., 2000). The prosubtilisin tag, on the other hand, acts as a high-affinity purification tag, and gets cleaved off during the elution from the Bio-Rad Profinity eXact column (Abdulaev et al., 2005; Huang et al., 2012; Ruan et al., 2004; Tsukamoto et al., 2010) (Fig. 3.1a). Thus, it leaves the N-terminus untagged, free to interact with the receptor in a manner akin to native RK.

From the purification gels, it is clear that we get ~80% pure RK from a single step purification (Fig. 3.1b). The purification yield was ~4-5 ug RK per 15cm plate of cells. The purification scheme is a lot more facile than traditional purification of RK, which require at least two chromatographic steps with long incubation, which might be deleterious to enzyme activity (Bruel et al., 2000). In fact, rhodopsin kinase has been shown to be quite unstable, with most labs storing the kinase for a couple of weeks at 4^oC, before declaring it unusable (Rim and Oprian, 1995). Our purification method is very fast and can be completed within 4-5 hours. The ease of

purification will enable purification of multiple enzyme mutants at once, and can significantly increase the throughput of the research.

Purified RK is functional

The functionality of the purified RK was measured by its ability to phosphorylate wild-type rhodopsin, as assessed by an autoradiographic analysis. The autoradiograph shows that the kinase is quite functional and causes robust light-dependent phosphorylation of wild-type rhodopsin in urea-stripped ROS membranes (Fig. 3.2a). There is < 5% phosphorylation of the receptor in the dark state in 2 hours. It also shows there is a small amount of autophosphorylation of RK, as has been observed previously (Buczylko et al., 1991; Palczewski et al., 1992a; Palczewski et al., 1995).

A key role of rhodopsin phosphorylation is to induce the recruitment of arrestin and the subsequent complete inhibition of G protein binding and turning off G protein-mediated signaling. While rhodopsin can have as many as 9 phosphates per receptor (Wilden et al., 1986), high affinity arrestin binding to rhodopsin requires 3 phosphates per receptor (Bayburt et al., 2011; Gurevich and Benovic, 1993). Estimation of the number of phosphates (based on comparison with a standard curve with known amounts of [^{32}P]-ATP) shows the incorporation of about 5 phosphates per rhodopsin on an average (Fig. 3.2b), which is above the level of phosphorylation required to achieve the key physiological role of receptor phosphorylation, i.e., recruitment of arrestin.

RK can phosphorylate monomeric rhodopsin

There a growing evidence for GPCR dimerization and/or oligomerization. Atomic force microscopy and electron microscopy have shown rhodopsin to exist in dimeric arrays in native

membranes (Fotiadis et al., 2003, 2004). Also, rhodopsin can self associate into dimers or higher order oligomers when reconstituted into lipid vesicles, as studied by resonance energy transfer approaches like LRET and FRET (Mansoor et al., 2006). Also, FRET analysis has showed that rhodopsin expressed in COS-1 cells forms dimers (Kota et al., 2006). This raises the question of the minimal functional unit of rhodopsin. Using "nanodiscs", which are flat, discoidal membranes surrounded by a belt of amphipathic helices made of variants of apolipoprotein A (Bayburt et al., 2011), we have previously shown that monomeric rhodopsin is sufficient for arrestin binding (Tsukamoto et al., 2010). Here, we report that monomeric rhodopsin (encapsulated in nanodiscs) is sufficient for activating RK as well (Fig. 3.3a). A similar conclusion was recently reported by Bayburt, et al (Bayburt et al., 2011). This previous study monitored RK phosphorylation of monomeric rhodopsin in nanodiscs composed of POPC lipid, with varying amounts (0-50%) of POPS. In our study, we have used POPC and POPG in a 3:2 ratio, (a mixture that reflects the zwitter-ionic environment of the cell membrane) as has been used previously to study G_t and arrestin binding to rhodopsin (Tsukamoto et al., 2010; Whorton et al., 2008). Also, like the previous study (Bayburt et al., 2011), we see higher levels of phosphorylation of rhodopsin in nanodisc, compared to those in native membranes. This could be due to the crowding of native membranes with very high density of receptors, which limits the access of RK to its substrates. Alternatively, it could be the result of a difference in the membrane composition of the two rhodopsin samples.

RK competes for the same site on rhodopsin as the G_t C-terminal tail peptide

The G_t C-terminal tail binds a hydrophobic patch on the cytosolic face of TM5-6 that is exposed upon rhodopsin activation (Choe et al., 2011; Janz and Farrens, 2004; Scheerer et al., 2008). We tested if this peptide affects RK-mediated phosphorylation of rhodopsin. Clearly, the

G_t peptide inhibited rhodopsin phosphorylation to a large extent (Fig. 3.4), indicating that rhodopsin kinase probably competes for the same site as the G_t peptide for interacting with rhodopsin (i.e., the hydrophobic patch exposed on TM6 movement). Both the purified kinase as well as the native kinase from crude extract from ROS membranes caused a similar inhibition (~90-95%) of rhodopsin phosphorylation, presumably by competing with RK for the binding site on the activated receptor. Given the various lies of evidence indicating to the formation of an alpha helix at the N-terminus of rhodopsin kinase (Ames et al., 2006; Higgins et al., 2006) its role in interaction with the rhodopsin (Boguth et al., 2010; Huang et al., 2011) and the fact the the G_t peptide adopts a helical conformation upon binding rhodopsin (Brabazon et al., 2003; Kisselev et al., 1998), it is tempting to speculate that the N-terminus of the kinase binds the same site on rhodopsin as the G_t peptide (Huang et al., 2011; Singh et al., 2008).

RK binding to constitutively active M257Y opsin is accelerated by all-trans-retinal

M257Y is a activating mutation in rhodopsin that disrupts the stabilizing interactions in the highly conserved NPxxY and the E(D)RY motifs of rhodopsin, and stabilizes the G protein binding site (Deupi et al., 2012; Han et al., 1998). This mutant causes G_t activation even in the absence of a ligand. The crystal structure of M257Y with all-trans-retinal in the ligand binding pocket and the G_t C-terminal peptide in the TM5-6 cavity shows the structure to be almost indistinguishable from that of Meta II-G_t peptide complex, indicating that this mutant adopts a native-like structure and its interactions with other cytosolic proteins might be native-like, too.

So, we tested if the purified rhodopsin kinase can phosphorylate this opsin mutant in the absence of any ligand, as is the case with transducin. Our results show that RK does phosphorylate M257Y in its ligand free, opsin form (Fig. 3.5), and the rate of phosphorylation is

enhanced by the pre-incubation of the receptor with its agonist, all-trans-retinal, indicating that RK has higher affinity for the fully activated form of the protein. Similar result was seen for transducin where addition of all-trans-retinal increased transducin activation from 30% to 100% (wild-type rhodopsin levels) (Han et al., 1998). That RK can phosphorylate the receptor even in the absence of any ligand, though, might enable fluorescence studies to monitor its interaction with the opsin form of the receptor, without energy transfer issues between the fluorophore and the retinal chromophore. This result also suggests that obtaining a co-crystal of RK bound to M257Y for X-ray crystallographic studies might be a possibility.

Arrestin competition

Arrestin can modulate the kinetics of rhodopsin phosphorylation by competing with RK (Doan et al., 2009). So, we tested if RK interaction with/phosphorylation of M257Y opsin is sensitive to a similar inhibition by arrestin. We pre-incubated M257Y with arrestin R175E (a constitutively active mutant of arrestin) and tested the ability of RK to phosphorylate the receptor. We found that arrestin inhibits RK-mediated phosphorylation of M257Y. (Fig 3.6). This indicates that the interaction of RK with M257Y is sensitive to arrestin in a manner similar to its interaction with wild-type rhodopsin. These results combined with the interaction of G_t with M257Y suggest that G_t, RK and arrestin might interact with the same region of M257Y.

In summary, we report a new purification method to obtain tag-free rhodopsin kinase using a very quick and simple one-step purification strategy. We show that the kinase is functional and confirm that monomeric rhodopsin is sufficient for RK activation. Further, we also show that RK competes with the transducin C-terminal tail in binding activated receptor, which suggests that rhodopsin kinase likely binds the same face of rhodopsin as the G_t peptide.

Finally, we report that RK can phosphorylate constitutively active receptor M257Y in its ligand free form, but the rate of phosphorylation is enhanced in the presence of the agonist, all-trans-retinal, in a manner akin to the interaction of M257Y with G_t. Finally, arrestin also competes with RK for the constitutively active receptor, which suggests that G_t, RK and arrestin all bind the same area on rhodopsin.

Figure 3.1 Purification of rhodopsin kinase.

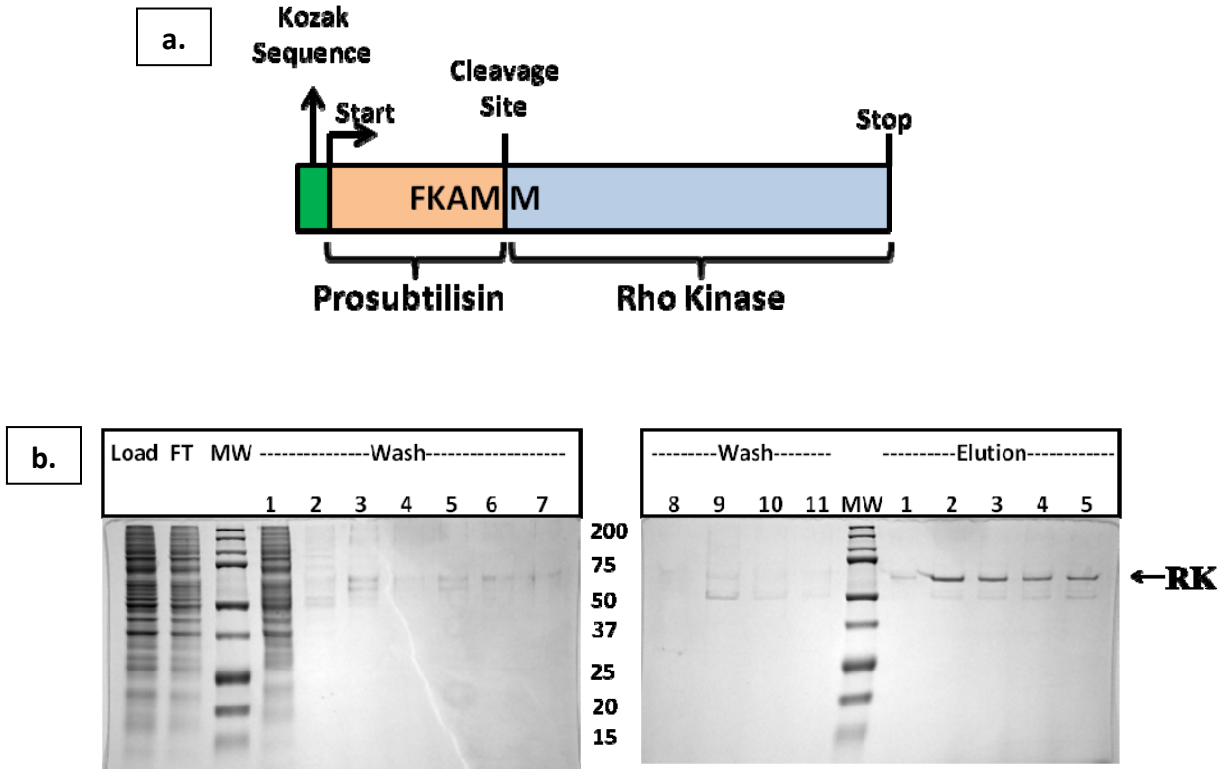

Figure 3.1 Purification of rhodopsin kinase.

Rhodopsin kinase (RK) was purified making use of the affinity between the subtilisin prodomain (prosubtilisin) and the mature subtilisin enzyme (Profinity eXact system) (Ruan, et al., 2004). (a) RK was cloned as a fusion construct with prosubtilisin fused to its N-terminus in pCMV5 vector, with a Kozak sequence maintained at the 5'-end of the prodomain. The subtilisin cleavage site is between the prodomain and RK. (b) SDS-PAGE analysis of the purification of RK using the Profinity system shows that the simple, one-step purification yielded ~80% pure protein. Extensive wash protocol was followed and the different wash fractions are numbered 1-11, where the numbering stands for different kinds of wash steps. 1, 2: 0.3% DM, 3: 0.3% Tween-20, 4: pH 6.5 buffer, 5: 1mM EGTA, 6: 1mM Ca^{2+}, 7, 8: Wash buffer 1; 9, 10: Wash Buffer 2; 11: Wash Buffer 1.

Figure 3.2. Purified rhodopsin kinase is functional.

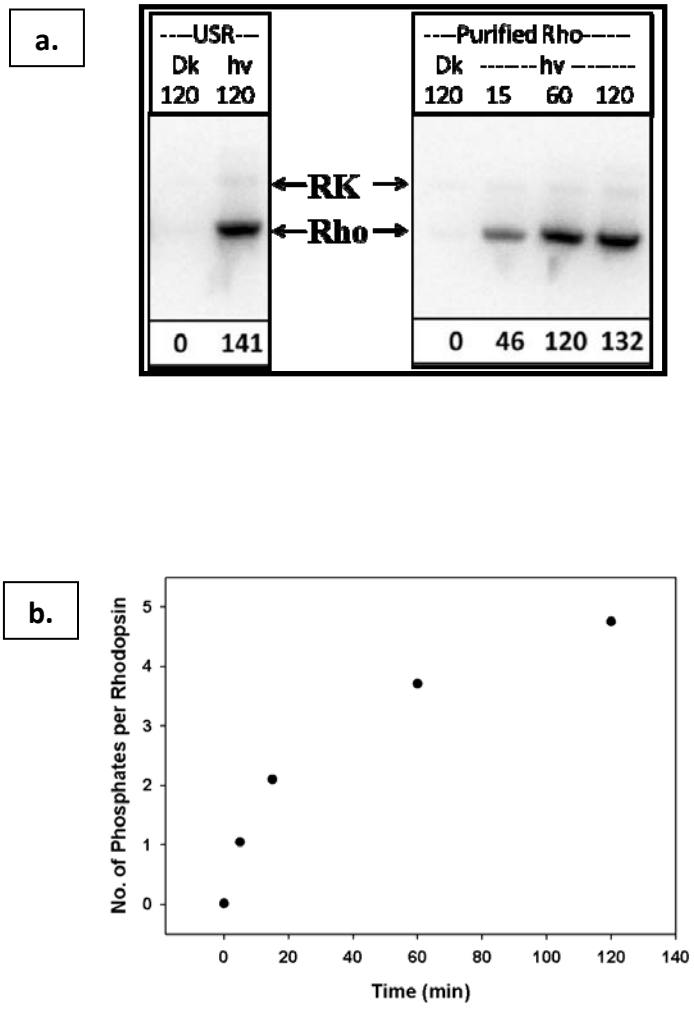

Figure 3.2. Purified rhodopsin kinase is functional.

The functionality of the purified rhodopsin kinase was tested by studying its ability to phosphorylate rhodopsin in a light dependent manner. (a) 8uM rhodopsin in urea-stripped ROS (rod outer segment), USR, or in DM-solubilized form after purification, was phosphorylated by 0.3uM rhodopsin kinase in the presence of 3mM ATP (with ^{32}P-ATP as a radioactive tracer), 10mM $MgCl_2$ and 1mM DTT at pH7.5. The sample were either kept in the dark (dk) or light activated for 15, 60 or 120 min. The samples were analyzed by SDS-PAGE, followed by ^{32}P autoradiography to detect phosphorylated proteins. The purified protein does exhibit a robust light-dependent phosphorylation of rhodopsin, both in native membranes as well as in purified, detergent-solubilized form. Some amount of RK autophosphorylation is also seen. (b) The number of phosphates that were added on rhodopsin in USR by the purified rhodopsin kinase was measured by precipitating the phosphorylated protein by trichloroacetic acid, and then measuring the incorporated ^{32}P radioactivity using radioactive scintillation counting and comparing it with that of a known amount of ^{32}P-ATP. The number of moles of phosphates added was divided by the number of moles of receptor present in the reaction mix to get the number of phosphates per receptor. The purified rhodopsin kinase added ~5 phosphates per receptor over the time course of the experiment (2 hours).

Fig. 3.3. Rhodopsin kinase can phosphorylate monomeric rhodopsin.

a.

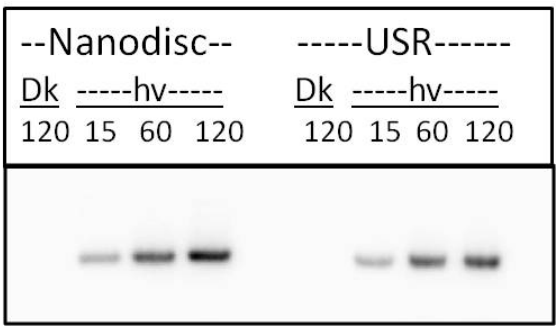

b.

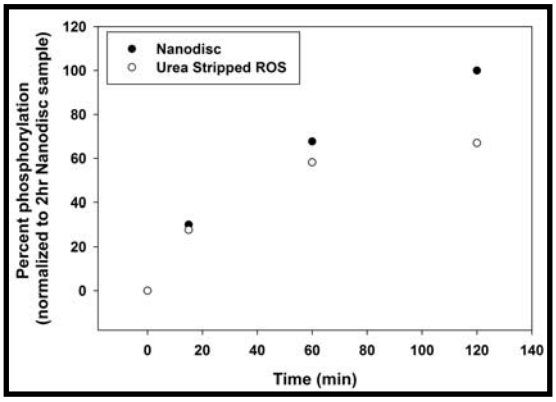

Fig. 3.3. Rhodopsin kinase can phosphorylate monomeric rhodopsin.

The ability of purified RK to phosphorylate monomeric rhodopsin was tested using monomeric rhodopsin in nanodiscs. The phosphorylation of monomeric rhodopsin was compared to that of rhodopsin in urea-stripped native membranes. (a) Autoradiograph analysis shows that RK causes light-dependent phosphorylation of rhodopsin in nanodiscs, showing that monomeric rhodopsin is sufficient for RK binding and activity. (b) Densitometric quantitation of the phosphorylated confirms that RK can phosphorylate monomeric rhodopsin at least as well as rhodopsin in membranes. The reaction conditions were the same as that for the reaction is Fig. 2.

Fig. 3.4. Transducin C-terminal tail peptide inhibits rhodopsin kinase activity.

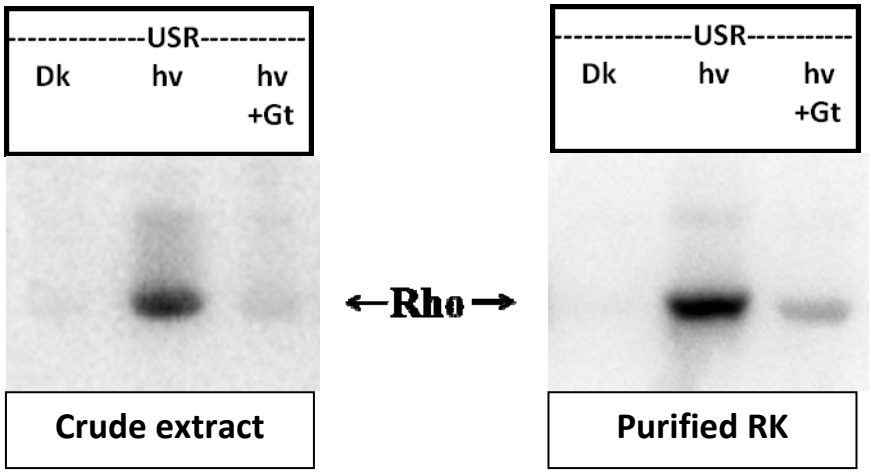

Fig. 3.4. Transducin C-terminal tail peptide inhibits rhodopsin kinase activity.

The ability of the transducin (G_t) C-terminal tail to compete with RK for active rhodopsin was tested by measuring the ability of RK to phosphorylate rhodopsin in the presence of a peptide corresponding to the G_t C-terminal tail. 100uM G_t effectively competed with RK for the activated receptor. The amount of phosphorylation was much lower (~90%) in the presence of the G_t peptide. This effect was seen with both purified RK as well as RK from a crude ROS extract. It indicates that RK probably uses the same site as the G_t tail peptide for receptor binding.

Fig. 3.5. Effect of all-trans-retinal on rhodopsin kinase-mediated phosphorylation of opsin M257Y.

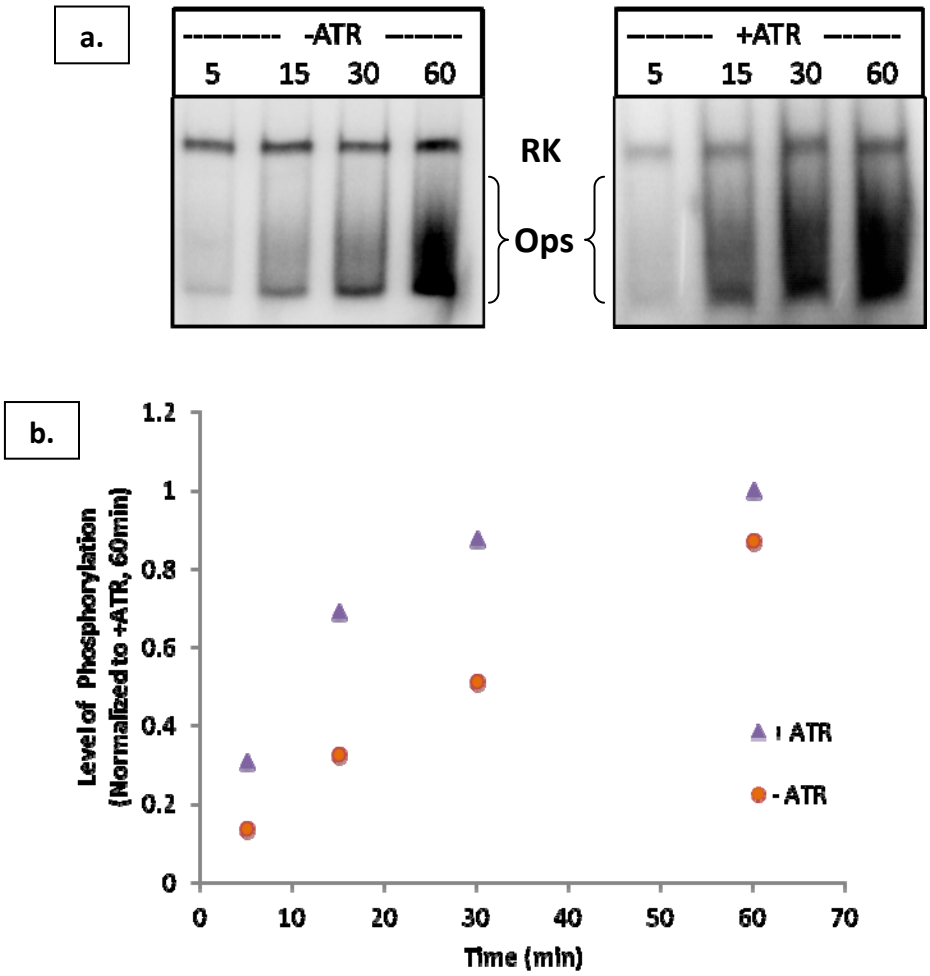

Fig. 3.5. Effect of all-trans-retinal on rhodopsin kinase-mediated phosphorylation of opsin M257Y.

The ability of RK to phosphorylate a constitutively active mutant of rhodopsin, M257Y, was measured. The effect of 10uM all-trans-retinal was studied over a 60 min time course. (a) All-trans-retinal increases the rate of phosphorylation by the kinase. The receptor runs as a diffuse band, owing to heterogeneous glycosylation (Standfuss et al., 2007). (b) Densitometry of the phosphorylated bands in (a).

Fig.3.6. Effect of arrestin on rhodopsin kinase-mediated phosphorylation of opsin M257Y.

a.

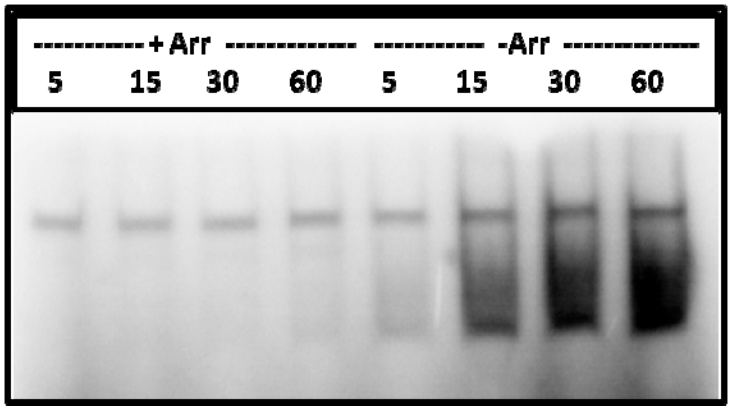

b.

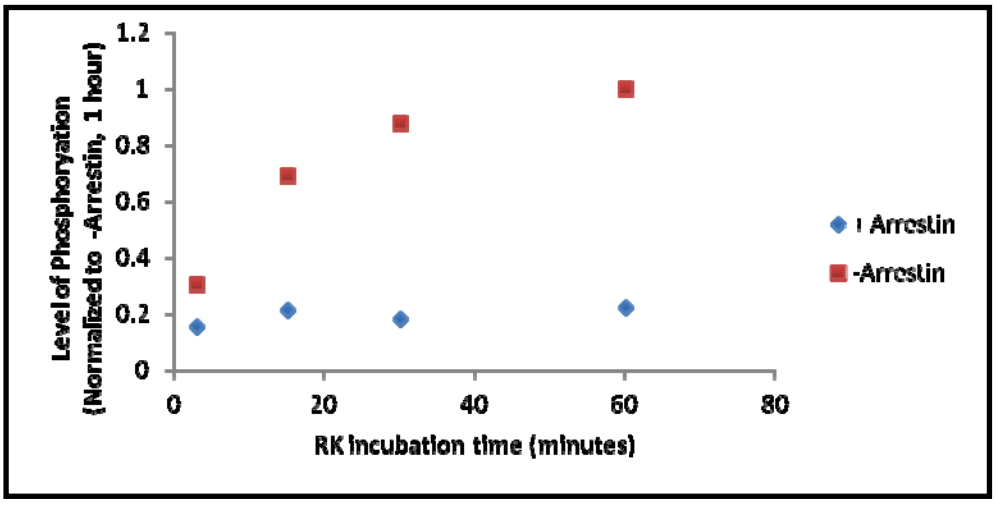

Fig.3.6. Effect of arrestin on rhodopsin kinase-mediated phosphorylation of opsin M257Y.

Arrestin can modulate rhodopsin phosphorylation by competing with RK (Doan et al., 2009). We tested whether it holds true for the constitutively active opsin mutant M257Y as well, in the presence of all-trans-retinal. (a) Autoradiograph shows the phosphorylation of opsin M257Y by RK is inhibited in the presence of arrestin. (b) Densitometry of the phosphorylated receptor bands shows that pre-coupling of the receptor by arrestin reduces the RK-mediated receptor phosphorylation by almost 80%.

Chapter 4

Summary and Conclusions

This dissertation reports on the interactions between GPCRs and proteins involved in the attenuation of their signaling. The biochemical and spectroscopic studies were carried out using defined, purified proteins to gain new insights into the interactions of these proteins with the receptor. The main conclusions of these studies, along with the future direction of the research are summarized below.

4.1. Both rhodopsin kinase and arrestin binds monomeric rhodopsin

Rhodopsin has been shown to exist as dimers and/or higher order oligomers in native membranes as well as in liposomes or in COS-1 cells (Fotiadis et al., 2004; Knepp et al., 2012; Kota et al., 2006; Mansoor et al., 2006). Arrestin, too, forms dimers or tetramers in a concentration-dependent manner (Hanson et al., 2007b; Hirsch et al., 1999; Imamoto et al., 2003; Shilton et al., 2002). As outlined in Chapter 3 and Appendix A1, we tested if rhodopsin oligomerization is required for RK and arrestin binding, respectively. We encapsulated rhodopsin in monomeric form in phospholipid containing disc-like particles called nanodiscs (Bayburt et al., 2007; Bayburt and Sligar, 2010). As reported in Chapter 3, we found that monomeric rhodopsin in nanodiscs can bind rhodopsin kinase, and this was reported recently by another lab (Bayburt et al., 2011). We also found both visual arrestin and β-arrestin 1 can bind monomeric rhodopsin (Appendix A1). In fact, visual arrestin bound monomeric rhodopsin in nanodiscs with a higher affinity than oligomeric rhodopsin in nanodiscs or liposomes. Our data clearly show rhodopsin self assembly is not required for arrestin binding. Moreover, our finding that arrestins can bind monomeric rhodopsin, coupled with the results from spin-labeling studies that show only monomeric arrestin binds rhodopsin (Hanson et al., 2007a), together strongly suggest a 1:1 stoichiometry between rhodopsin and arrestin, although it is possible this ratio can

change in response to different external events (Sommer et al., 2011). Previous studies show that G proteins can also bind monomeric GPCRs (Banerjee et al., 2008; Bayburt et al., 2007; Whorton et al., 2007).

Thus, at least for rhodopsin, all the three important cytosolic interacting partners can recognize and bind with a monomeric receptor. Our results, combined with previous studies with G proteins and RK, rule out an obligate need of multimeric receptor interaction with these three key cytosolic binding partners. However, while it is tempting to speculate that other (class A) GPCRs, too, might have such 1:1 stoichiometry, further experiments need to be performed to make a generalized claim about all GPCRs.

4.2. Arrestin interacts with the base of TM6 of rhodopsin

Rhodopsin activation involves the outward movement of TM6 (Farrens et al., 1996; Sheikh et al., 1996), which opens up a hydrophobic cavity on the cytosolic face of TM5-6 that is utilized by G protein to bind to the activated receptor (Choe et al., 2011; Janz and Farrens, 2004; Scheerer et al., 2008). Arrestin is a known competitor of G protein for the binding the activated receptor, indicating some shared site(s) of interaction within the receptor by both arrestin and G proteins. As reported in Chapter 2, we have localized one such common binding site on the receptor as the base of TM5-6. We showed that the G_t C-terminal tail peptide, which binds this particular region of rhodopsin, inhibits arrestin binding to the receptor, indicating a competition between arrestin and the peptide for the base of TM5-6 in rhodopsin (Fig. 3.2a, 3.S5). Also, mutation in the hydrophobic patch of rhodopsin inhibits arrestin-mediated trapping of retinal in activated rhodopsin, a likely indicator of reduced arrestin binding. Thus these lines of evidence indicate that arrestin interacts with the base of TM5-6 of rhodopsin.

4.3. Two sites on arrestin make contacts with the base of TM6 of rhodopsin

The arrestin "finger" loop has long been implicated in receptor binding by a variety of approaches, including peptide competition, EPR, fluorescence spectroscopy and NMR among others (Feuerstein et al., 2009; Hanson et al., 2006; Pulvermuller et al., 2000; Sommer et al., 2007). Using a Tryptophan Induced Quenching (TrIQ) approach , we measured the ability of tryptophan residues introduced in the "finger" loop of arrestin to quench the fluorescence of mBBr attached to specific sites on a thermostable (N2C/D282C), constitutively active form (M257Y) of opsin. We detected ~30-40% quenching of 243mB fluorescence by two of the three "finger" loop Trp mutants tested, indicating a likely proximity between the two sites involved, which is along expected lines. A surprising finding from these quenching experiments was the quenching of 242mB fluorescence by Trp residues introduced in the distal N-terminal lobe of arrestin (residues 157-164), indicating that this region of arrestin, too, was involved in interacting with the base of TM6 of rhodopsin. Combination of the steady state quenching data with fluorescence lifetime data enables us to quantify the fraction of Trp-fluorophore pairs that are unquenched, or show static or dynamic quenching (Mansoor et al., 2010; Mansoor and Farrens, 2004). The residues in the 160 loop show a site specific pattern of quenching at 242mB and, in fact, two of these residues (E160W and E161W) show ~20-25% static quenching, which indicates that the fluorophore, mBBr, and the quenching tryptophan may be less than 10Å apart. These pieces of data show that the "finger" loop and the 160 loop on arrestin both come in the proximity of the base of TM6 upon receptor binding.

Arrestin might interact with the receptor in two possible orientations, with one binding mode positioning the "finger" loop near TM6 and the other positioning the 160 loop. It is also

possible that arrestin employs these two sites in the context of binding to a receptor dimer, with one protomer placing T242-T243 near the “finger” loop, and the other near the 160 loop. Yet another possible mechanism might be a large conformational rearrangement in arrestin that enables both regions to be close, thus explaining the large Arrhenius activation energy (165kJ/mol) associated with arrestin binding to phosphorylated metarhodopsin II (Schleicher et al., 1989).

4.4. G_t C-terminal peptide inhibits RK-mediated phosphorylation of rhodopsin

We report a fast and simple, one-step purification method for rhodopsin kinase expressed in mammalian cells. We used RK purified by this method to achieve high-level phosphorylation of rhodopsin, with ~5 phosphates per receptor. We found the kinase was also able to phosphorylate rhodopsin in a monomeric form in nanodiscs, as was also reported recently by another group (Bayburt et al., 2011). We also localized a potential interaction site of RK on rhodopsin as being the same site used by the transducin C-tail for binding to the receptor, based on the inhibition of RK-mediated phosphorylation of rhodopsin in the presence of the G_t C-terminal peptide. We also report that RK can phosphorylate a constitutively active mutant of unliganded opsin (M257Y), at a rate that is accelerated by the presence of the agonist, all-trans-retinal, thus reflecting the functional interaction of G_t with the M257Y mutant (Han et al., 1998). Finally, we found that constitutively arrestin can inhibit RK-mediated phosphorylation of the M257Y receptor, again their competition reflecting a physiological scenario where arrestin is known to modulate the rhodopsin phosphorylation by competing with RK *in vivo* (Doan et al., 2009). Interaction of both arrestin and RK with rhodopsin is inhibited by the G_t C-terminal tail

peptide. This indicates that all the three proteins likely have at least one common binding region on rhodopsin – the cytosolic face of TM 5-6 that gets exposed upon receptor activation.

4.5. CRIP1a, a novel inhibitor of CB1 receptor constitutive activity, is a well-structured, stable protein with high β-sheet content.

Rhodopsin is a very tightly regulated receptor that acts as a binary switch, with negligible signaling in the absence of an activating photon (Palczewski, 2006). However, many other GPCRs, like the cannabinoid receptor CB1, exhibit high level of signaling even in the absence of the activating ligand (Bouaboula et al., 1997; Coutts et al., 2001; Landsman et al., 1997; MacLennan et al., 1998; Nie and Lewis, 2001a, b). The protein CRIP1a is known to inhibit the constitutive activity of CB1 receptor. In order to begin characterizing the structural aspects of CRIP1a function, as described in Appendix A2, we employed a purification strategy based on the affinity between the prodomain of subtilisin and the mature subtilisin catalytic domain. We report a yield of 2-2.5mg of CRIP1a per liter of *E. coli* culture, and our analysis of the protein by CD spectroscopy finds CRIP1a to have ~42% β-sheet content and display stability in upto 3.5M urea. The cysteines of CRIP1a are likely not involved in inter or intramolecular disulfide bonds, but are surface accessible as assessed by their reactivity to thiol-modifying fluorophores. Finally, we have found some preliminary conditions that show promising results for the crystallization of CRIP1a and the refinement of conditions to obtain crystals of CRIP1a will help obtain a crystal structure of the protein and get further insight to its function.

4.6. Future directions

While our results provide two sites of direct contact between arrestin and the receptor, more sets of interactions will need to be discovered to come with a more complete model of the complex. Also, we have identified arrestin-opsin complexes that are quite stable, thus opening up the avenue for crystallization of the complex using these mutants.

Further, there are many parallels between G_t, arrestin and RK in terms of binding rhodopsin: (i) they all bind activated rhodopsin, (ii) they engage at least one common site on activated rhodopsin, and (iii) they all bind monomeric receptor in nanodisc. Now, both G_t and arrestin binding to rhodopsin is sensitive to the mutation of hydrophobic residues in the cytosolic face of TM5. It will be interesting to see if the mutation of these sites also affects RK-mediated phosphorylation of activated receptor. Also, the N-terminal helix of RK has been proposed to have an important role in binding rhodopsin. One could test the site of interaction of this helix with rhodopsin, using the TrIQ approach as well.

Finally, with respect to CRIP1a, more conditions need to be screened for the crystallization of the protein. Also, the binding of the purified protein with full-length CB1 and the CB1 tail needs to be tested in the presence of different ligands to confirm the role of the tail in CRIP1a binding and to find other possible functional roles played by the protein, which could be manipulated for pharmaceutical uses.

References

Abdulaev, N.G., Zhang, C., Dinh, A., Ngo, T., Bryan, P.N., Brabazon, D.M., Marino, J.P., and Ridge, K.D. (2005). Bacterial expression and one-step purification of an isotope-labeled heterotrimeric G-protein alpha-subunit. J Biomol NMR *32*, 31-40.

Abel, R.L., Haigis, M.C., Park, C., and Raines, R.T. (2002). Fluorescence assay for the binding of ribonuclease A to the ribonuclease inhibitor protein. Anal Biochem *306*, 100-107.

Abood, M.E., Rizvi, G., Sallapudi, N., and McAllister, S.D. (2001). Activation of the CB1 cannabinoid receptor protects cultured mouse spinal neurons against excitotoxicity. Neurosci Lett *309*, 197-201.

Ames, J.B., Levay, K., Wingard, J.N., Lusin, J.D., and Slepak, V.Z. (2006). Structural basis for calcium-induced inhibition of rhodopsin kinase by recoverin. J Biol Chem *281*, 37237-37245.

Aton, B.R., Litman, B.J., and Jackson, M.L. (1984). Isolation and identification of the phosphorylated species of rhodopsin. Biochemistry *23*, 1737-1741.

Attramadal, H., Arriza, J.L., Aoki, C., Dawson, T.M., Codina, J., Kwatra, M.M., Snyder, S.H., Caron, M.G., and Lefkowitz, R.J. (1992). Beta-arrestin2, a novel member of the arrestin/beta-arrestin gene family. J Biol Chem *267*, 17882-17890.

Banerjee, S., Huber, T., and Sakmar, T.P. (2008). Rapid incorporation of functional rhodopsin into nanoscale apolipoprotein bound bilayer (NABB) particles. J Mol Biol *377*, 1067-1081.

Bayburt, T.H., Leitz, A.J., Xie, G., Oprian, D.D., and Sligar, S.G. (2007). Transducin activation by nanoscale lipid bilayers containing one and two rhodopsins. J Biol Chem *282*, 14875-14881.

Bayburt, T.H., and Sligar, S.G. (2010). Membrane protein assembly into Nanodiscs. FEBS Lett *584*, 1721-1727.

Bayburt, T.H., Vishnivetskiy, S.A., McLean, M.A., Morizumi, T., Huang, C.C., Tesmer, J.J., Ernst, O.P., Sligar, S.G., and Gurevich, V.V. (2011). Monomeric rhodopsin is sufficient for normal rhodopsin kinase (GRK1) phosphorylation and arrestin-1 binding. J Biol Chem *286*, 1420-1428.

Bennion, B.J., and Daggett, V. (2003). The molecular basis for the chemical denaturation of proteins by urea. Proc Natl Acad Sci U S A *100*, 5142-5147.

Boguth, C.A., Singh, P., Huang, C.C., and Tesmer, J.J. (2010). Molecular basis for activation of G protein-coupled receptor kinases. EMBO J *29*, 3249-3259.

Bohn, L.M., Gainetdinov, R.R., Lin, F.T., Lefkowitz, R.J., and Caron, M.G. (2000). Mu-opioid receptor desensitization by beta-arrestin-2 determines morphine tolerance but not dependence. Nature *408*, 720-723.

Booker, T.K., Smith, K.W., Dodrill, C., and Collins, A.C. (1998). Calcium modulation of activation and desensitization of nicotinic receptors from mouse brain. J Neurochem *71*, 1490-1500.

Bouaboula, M., Bourrie, B., Rinaldi-Carmona, M., Shire, D., Le Fur, G., and Casellas, P. (1995). Stimulation of cannabinoid receptor CB1 induces krox-24 expression in human astrocytoma cells. J Biol Chem *270*, 13973-13980.

Bouaboula, M., Perrachon, S., Milligan, L., Canat, X., Rinaldi-Carmona, M., Portier, M., Barth, F., Calandra, B., Pecceu, F., Lupker, J., *et al.* (1997). A selective inverse agonist for central cannabinoid receptor inhibits mitogen-activated protein kinase activation stimulated by

insulin or insulin-like growth factor 1. Evidence for a new model of receptor/ligand interactions. J Biol Chem *272*, 22330-22339.

Brabazon, D.M., Abdulaev, N.G., Marino, J.P., and Ridge, K.D. (2003). Evidence for structural changes in carboxyl-terminal peptides of transducin alpha-subunit upon binding a soluble mimic of light-activated rhodopsin. Biochemistry *42*, 302-311.

Brown, A.J. (2007). Novel cannabinoid receptors. Br J Pharmacol *152*, 567-575.

Bruel, C., Cha, K., Reeves, P.J., Getmanova, E., and Khorana, H.G. (2000). Rhodopsin kinase: expression in mammalian cells and a two-step purification. Proc Natl Acad Sci U S A *97*, 3004-3009.

Buczylko, J., Gutmann, C., and Palczewski, K. (1991). Regulation of rhodopsin kinase by autophosphorylation. Proc Natl Acad Sci U S A *88*, 2568-2572.

Burke, C.L., and Stern, D.F. (1998). Activation of Neu (ErbB-2) mediated by disulfide bond-induced dimerization reveals a receptor tyrosine kinase dimer interface. Mol Cell Biol *18*, 5371-5379.

Carter, A.A., and Hill, S.J. (2005). Characterization of isoprenaline- and salmeterol-stimulated interactions between beta2-adrenoceptors and beta-arrestin 2 using beta-galactosidase complementation in C2C12 cells. J Pharmacol Exp Ther *315*, 839-848.

Cerione, R.A., and Ross, E.M. (1991). Reconstitution of receptors and G proteins in phospholipid vesicles. Methods Enzymol *195*, 329-342.

Cha, K., Bruel, C., Inglese, J., and Khorana, H.G. (1997). Rhodopsin kinase: expression in baculovirus-infected insect cells, and characterization of post-translational modifications. Proc Natl Acad Sci U S A *94*, 10577-10582.

Chen, J., Shi, G., Concepcion, F.A., Xie, G., and Oprian, D. (2006). Stable rhodopsin/arrestin complex leads to retinal degeneration in a transgenic mouse model of autosomal dominant retinitis pigmentosa. J Neurosci *26*, 11929-11937.

Choe, H.W., Kim, Y.J., Park, J.H., Morizumi, T., Pai, E.F., Krauss, N., Hofmann, K.P., Scheerer, P., and Ernst, O.P. (2011). Crystal structure of metarhodopsin II. Nature *471*, 651-655.

Coutts, A.A., Anavi-Goffer, S., Ross, R.A., MacEwan, D.J., Mackie, K., Pertwee, R.G., and Irving, A.J. (2001). Agonist-induced internalization and trafficking of cannabinoid CB1 receptors in hippocampal neurons. J Neurosci *21*, 2425-2433.

Demuth, D.G., and Molleman, A. (2006). Cannabinoid signalling. Life Sci *78*, 549-563.

Denisov, I.G., Grinkova, Y.V., Lazarides, A.A., and Sligar, S.G. (2004). Directed self-assembly of monodisperse phospholipid bilayer Nanodiscs with controlled size. J Am Chem Soc *126*, 3477-3487.

Deupi, X., Edwards, P., Singhal, A., Nickle, B., Oprian, D., Schertler, G., and Standfuss, J. (2012). Stabilized G protein binding site in the structure of constitutively active metarhodopsin-II. Proc Natl Acad Sci U S A *109*, 119-124.

DeWire, S.M., Ahn, S., Lefkowitz, R.J., and Shenoy, S.K. (2007). Beta-arrestins and cell signaling. Annu Rev Physiol *69*, 483-510.

Diaz-Laviada, I., and Ruiz-Llorente, L. (2005). Signal transduction activated by cannabinoid receptors. Mini Rev Med Chem *5*, 619-630.

Dinculescu, A., McDowell, J.H., Amici, S.A., Dugger, D.R., Richards, N., Hargrave, P.A., and Smith, W.C. (2002). Insertional mutagenesis and immunochemical analysis of visual arrestin interaction with rhodopsin. J Biol Chem *277*, 11703-11708.

Doan, T., Azevedo, A.W., Hurley, J.B., and Rieke, F. (2009). Arrestin competition influences the kinetics and variability of the single-photon responses of mammalian rod photoreceptors. J Neurosci *29*, 11867-11879.

Drake, M.T., Shenoy, S.K., and Lefkowitz, R.J. (2006). Trafficking of G protein-coupled receptors. Circ Res *99*, 570-582.

Dunham, T.D., and Farrens, D.L. (1999). Conformational changes in rhodopsin. Movement of helix f detected by site-specific chemical labeling and fluorescence spectroscopy. J Biol Chem *274*, 1683-1690.

Ebrey, T.G. (1971). Energy transfer in rhodopsin, N-retinyl-opsin, and rod outer segments. Proc Natl Acad Sci U S A *68*, 713-716.

Emeis, D., and Hofmann, K.P. (1981). Shift in the relation between flash-induced metarhodopsin I and metarhodpsin II within the first 10% rhodopsin bleaching in bovine disc membranes. FEBS Lett *136*, 201-207.

Emeis, D., Kuhn, H., Reichert, J., and Hofmann, K.P. (1982). Complex formation between metarhodopsin II and GTP-binding protein in bovine photoreceptor membranes leads to a shift of the photoproduct equilibrium. FEBS Lett *143*, 29-34.

Ernst, O.P., and Bartl, F.J. (2002). Active states of rhodopsin. Chembiochem *3*, 968-974.

Farrens, D.L., Altenbach, C., Yang, K., Hubbell, W.L., and Khorana, H.G. (1996). Requirement of rigid-body motion of transmembrane helices for light activation of rhodopsin. Science *274*, 768-770.

Farrens, D.L., and Khorana, H.G. (1995). Structure and function in rhodopsin. Measurement of the rate of metarhodopsin II decay by fluorescence spectroscopy. J Biol Chem *270*, 5073-5076.

Ferre, S., Baler, R., Bouvier, M., Caron, M.G., Devi, L.A., Durroux, T., Fuxe, K., George, S.R., Javitch, J.A., Lohse, M.J., *et al.* (2009). Building a new conceptual framework for receptor heteromers. Nat Chem Biol *5*, 131-134.

Feuerstein, S.E., Pulvermuller, A., Hartmann, R., Granzin, J., Stoldt, M., Henklein, P., Ernst, O.P., Heck, M., Willbold, D., and Koenig, B.W. (2009). Helix formation in arrestin accompanies recognition of photoactivated rhodopsin. Biochemistry *48*, 10733-10742.

Fotiadis, D., Liang, Y., Filipek, S., Saperstein, D.A., Engel, A., and Palczewski, K. (2003). Atomic-force microscopy: Rhodopsin dimers in native disc membranes. Nature *421*, 127-128.

Fotiadis, D., Liang, Y., Filipek, S., Saperstein, D.A., Engel, A., and Palczewski, K. (2004). The G protein-coupled receptor rhodopsin in the native membrane. FEBS Lett *564*, 281-288.

Fung, J.J., Deupi, X., Pardo, L., Yao, X.J., Velez-Ruiz, G.A., Devree, B.T., Sunahara, R.K., and Kobilka, B.K. (2009). Ligand-regulated oligomerization of beta(2)-adrenoceptors in a model lipid bilayer. EMBO J *28*, 3315-3328.

Gainetdinov, R.R., Premont, R.T., Bohn, L.M., Lefkowitz, R.J., and Caron, M.G. (2004). Desensitization of G protein-coupled receptors and neuronal functions. Annu Rev Neurosci *27*, 107-144.

Gavarini, S., Becamel, C., Chanrion, B., Bockaert, J., and Marin, P. (2004). Molecular and functional characterization of proteins interacting with the C-terminal domains of 5-HT2 receptors: emergence of 5-HT2 "receptosomes". Biol Cell *96*, 373-381.

Gibson, S.K., Parkes, J.H., and Liebman, P.A. (2000). Phosphorylation modulates the affinity of light-activated rhodopsin for G protein and arrestin. Biochemistry *39*, 5738-5749.

Goc, A., Angel, T.E., Jastrzebska, B., Wang, B., Wintrode, P.L., and Palczewski, K. (2008). Different properties of the native and reconstituted heterotrimeric G protein transducin. Biochemistry *47*, 12409-12419.

Gonsiorek, W., Lunn, C., Fan, X., Narula, S., Lundell, D., and Hipkin, R.W. (2000). Endocannabinoid 2-arachidonyl glycerol is a full agonist through human type 2 cannabinoid receptor: antagonism by anandamide. Mol Pharmacol *57*, 1045-1050.

Granzin, J., Wilden, U., Choe, H.W., Labahn, J., Krafft, B., and Buldt, G. (1998). X-ray crystal structure of arrestin from bovine rod outer segments. Nature *391*, 918-921.

Gray-Keller, M.P., Detwiler, P.B., Benovic, J.L., and Gurevich, V.V. (1997). Arrestin with a single amino acid substitution quenches light-activated rhodopsin in a phosphorylation-independent fashion. Biochemistry *36*, 7058-7063.

Greenfield, N.J. (2006). Using circular dichroism spectra to estimate protein secondary structure. Nat Protoc *1*, 2876-2890.

Grote, A., Hiller, K., Scheer, M., Munch, R., Nortemann, B., Hempel, D.C., and Jahn, D. (2005). JCat: a novel tool to adapt codon usage of a target gene to its potential expression host. Nucleic Acids Res *33*, W526-531.

Guo, W., Urizar, E., Kralikova, M., Mobarec, J.C., Shi, L., Filizola, M., and Javitch, J.A. (2008). Dopamine D2 receptors form higher order oligomers at physiological expression levels. EMBO J *27*, 2293-2304.

Gurevich, V.V., and Benovic, J.L. (1993). Visual arrestin interaction with rhodopsin. Sequential multisite binding ensures strict selectivity toward light-activated phosphorylated rhodopsin. J Biol Chem *268*, 11628-11638.

Gurevich, V.V., and Benovic, J.L. (1995). Visual arrestin binding to rhodopsin. Diverse functional roles of positively charged residues within the phosphorylation-recognition region of arrestin. J Biol Chem *270*, 6010-6016.

Gurevich, V.V., and Benovic, J.L. (1997). Mechanism of phosphorylation-recognition by visual arrestin and the transition of arrestin into a high affinity binding state. Mol Pharmacol *51*, 161-169.

Gurevich, V.V., Dion, S.B., Onorato, J.J., Ptasienski, J., Kim, C.M., Sterne-Marr, R., Hosey, M.M., and Benovic, J.L. (1995). Arrestin interactions with G protein-coupled receptors. Direct binding studies of wild type and mutant arrestins with rhodopsin, beta 2-adrenergic, and m2 muscarinic cholinergic receptors. J Biol Chem *270*, 720-731.

Gurevich, V.V., and Gurevich, E.V. (2006). The structural basis of arrestin-mediated regulation of G-protein-coupled receptors. Pharmacol Ther *110*, 465-502.

Gurevich, V.V., and Gurevich, E.V. (2008). GPCR monomers and oligomers: it takes all kinds. Trends Neurosci *31*, 74-81.

Han, M., Gurevich, V.V., Vishnivetskiy, S.A., Sigler, P.B., and Schubert, C. (2001). Crystal structure of beta-arrestin at 1.9 A: possible mechanism of receptor binding and membrane Translocation. Structure *9*, 869-880.

Han, M., Smith, S.O., and Sakmar, T.P. (1998). Constitutive activation of opsin by mutation of methionine 257 on transmembrane helix 6. Biochemistry *37*, 8253-8261.

Han, Y., Moreira, I.S., Urizar, E., Weinstein, H., and Javitch, J.A. (2009). Allosteric communication between protomers of dopamine class A GPCR dimers modulates activation. Nat Chem Biol *5*, 688-695.

Hansen, H.S., Moesgaard, B., Petersen, G., and Hansen, H.H. (2002). Putative neuroprotective actions of N-acyl-ethanolamines. Pharmacol Ther *95*, 119-126.

Hanson, S.M., Francis, D.J., Vishnivetskiy, S.A., Kolobova, E.A., Hubbell, W.L., Klug, C.S., and Gurevich, V.V. (2006). Differential interaction of spin-labeled arrestin with inactive and active phosphorhodopsin. Proc Natl Acad Sci U S A *103*, 4900-4905.

Hanson, S.M., Gurevich, E.V., Vishnivetskiy, S.A., Ahmed, M.R., Song, X., and Gurevich, V.V. (2007a). Each rhodopsin molecule binds its own arrestin. Proc Natl Acad Sci U S A *104*, 3125-3128.

Hanson, S.M., Van Eps, N., Francis, D.J., Altenbach, C., Vishnivetskiy, S.A., Arshavsky, V.Y., Klug, C.S., Hubbell, W.L., and Gurevich, V.V. (2007b). Structure and function of the visual arrestin oligomer. EMBO J *26*, 1726-1736.

Herkenham, M., Groen, B.G., Lynn, A.B., De Costa, B.R., and Richfield, E.K. (1991). Neuronal localization of cannabinoid receptors and second messengers in mutant mouse cerebellum. Brain Res *552*, 301-310.

Higgins, M.K., Oprian, D.D., and Schertler, G.F. (2006). Recoverin binds exclusively to an amphipathic peptide at the N terminus of rhodopsin kinase, inhibiting rhodopsin phosphorylation without affecting catalytic activity of the kinase. J Biol Chem *281*, 19426-19432.

Hirsch, J.A., Schubert, C., Gurevich, V.V., and Sigler, P.B. (1999). The 2.8 A crystal structure of visual arrestin: a model for arrestin's regulation. Cell *97*, 257-269.

Ho, B.Y., Uezono, Y., Takada, S., Takase, I., and Izumi, F. (1999). Coupling of the expressed cannabinoid CB1 and CB2 receptors to phospholipase C and G protein-coupled inwardly rectifying K+ channels. Receptors Channels *6*, 363-374.

Hofmann, K.P., Emeis, D., and Schnetkamp, P.P. (1983). Interplay between hydroxylamine, metarhodopsin II and GTP-binding protein in bovine photoreceptor membranes. Biochim Biophys Acta *725*, 60-70.

Hogg, P.J. (2003). Disulfide bonds as switches for protein function. Trends Biochem Sci *28*, 210-214.

Holinstat, M., Oldham, W.M., and Hamm, H.E. (2006). G-protein-coupled receptors: evolving views on physiological signalling: symposium on G-protein-coupled receptors: evolving concepts and new techniques. EMBO Rep *7*, 866-869.

Holm, L., Kaariainen, S., Wilton, C., and Plewczynski, D. (2006). Using Dali for structural comparison of proteins. Curr Protoc Bioinformatics *Chapter 5*, Unit 5 5.

Hopkins, A.L., and Groom, C.R. (2002). The druggable genome. Nat Rev Drug Discov *1*, 727-730.

Horn, F., Bettler, E., Oliveira, L., Campagne, F., Cohen, F.E., and Vriend, G. (2003). GPCRDB information system for G protein-coupled receptors. Nucleic Acids Res *31*, 294-297.

Hsieh, C., Brown, S., Derleth, C., and Mackie, K. (1999). Internalization and recycling of the CB1 cannabinoid receptor. J Neurochem *73*, 493-501.

Hu, S.S., Arnold, A., Hutchens, J.M., Radicke, J., Cravatt, B.F., Wager-Miller, J., Mackie, K., and Straiker, A. (2010). Architecture of cannabinoid signaling in mouse retina. J Comp Neurol *518*, 3848-3866.

Hua, L., Zhou, R., Thirumalai, D., and Berne, B.J. (2008). Urea denaturation by stronger dispersion interactions with proteins than water implies a 2-stage unfolding. Proc Natl Acad Sci U S A *105*, 16928-16933.

Huang, C.C., Orban, T., Jastrzebska, B., Palczewski, K., and Tesmer, J.J. (2011). Activation of G protein-coupled receptor kinase 1 involves interactions between its N-terminal region and its kinase domain. Biochemistry *50*, 1940-1949.

Huang, C.C., and Tesmer, J.J. (2011). Recognition in the face of diversity: interactions of heterotrimeric G proteins and G protein-coupled receptor (GPCR) kinases with activated GPCRs. J Biol Chem *286*, 7715-7721.

Huang, C.C., Yoshino-Koh, K., and Tesmer, J.J. (2009). A surface of the kinase domain critical for the allosteric activation of G protein-coupled receptor kinases. J Biol Chem *284*, 17206-17215.

Huang, L., Mao, X., Abdulaev, N.G., Ngo, T., Liu, W., and Ridge, K.D. (2012). One-step purification of a functional, constitutively activated form of visual arrestin. Protein Expr Purif *82*, 55-60.

Imamoto, Y., Tamura, C., Kamikubo, H., and Kataoka, M. (2003). Concentration-dependent tetramerization of bovine visual arrestin. Biophys J *85*, 1186-1195.

Islas, L.D., and Zagotta, W.N. (2006). Short-range molecular rearrangements in ion channels detected by tryptophan quenching of bimane fluorescence. J Gen Physiol *128*, 337-346.

Janz, J.M., and Farrens, D.L. (2004). Rhodopsin activation exposes a key hydrophobic binding site for the transducin alpha-subunit C terminus. J Biol Chem *279*, 29767-29773.

Kaur, K., Kehrl, J.M., Charbeneau, R.A., and Neubig, R.R. (2011). RGS-insensitive Galpha subunits: probes of Galpha subtype-selective signaling and physiological functions of RGS proteins. Methods Mol Biol *756*, 75-98.

Kaya, A.I., Thaker, T.M., Preininger, A.M., Iverson, T.M., and Hamm, H.E. (2011). Coupling efficiency of rhodopsin and transducin in bicelles. Biochemistry *50*, 3193-3203.

Keller, A., Nesvizhskii, A.I., Kolker, E., and Aebersold, R. (2002). Empirical statistical model to estimate the accuracy of peptide identifications made by MS/MS and database search. Anal Chem *74*, 5383-5392.

Kelly, E., Bailey, C.P., and Henderson, G. (2008). Agonist-selective mechanisms of GPCR desensitization. Br J Pharmacol *153 Suppl 1*, S379-388.

Kenakin, T. (2004). Principles: receptor theory in pharmacology. Trends Pharmacol Sci *25*, 186-192.

Keren, O., and Sarne, Y. (2003). Multiple mechanisms of CB1 cannabinoid receptors regulation. Brain Res *980*, 197-205.

Kieselbach, T., Irrgang, K.D., and Ruppel, H. (1994). A segment corresponding to amino acids Val170-Arg182 of bovine arrestin is capable of binding to phosphorylated rhodopsin. Eur J Biochem *226*, 87-97.

Kirchberg, K., Kim, T.Y., Moller, M., Skegro, D., Dasara Raju, G., Granzin, J., Buldt, G., Schlesinger, R., and Alexiev, U. (2011). Conformational dynamics of helix 8 in the GPCR rhodopsin controls arrestin activation in the desensitization process. Proc Natl Acad Sci U S A *108*, 18690-18695.

Kisselev, O.G., Kao, J., Ponder, J.W., Fann, Y.C., Gautam, N., and Marshall, G.R. (1998). Light-activated rhodopsin induces structural binding motif in G protein alpha subunit. Proc Natl Acad Sci U S A *95*, 4270-4275.

Klomsiri, C., Karplus, P.A., and Poole, L.B. (2011). Cysteine-based redox switches in enzymes. Antioxid Redox Signal *14*, 1065-1077.

Knepp, A.M., Periole, X., Marrink, S.J., Sakmar, T.P., and Huber, T. (2012). Rhodopsin forms a dimer with cytoplasmic helix 8 contacts in native membranes. Biochemistry *51*, 1819-1821.

Kobilka, B.K. (2007). G protein coupled receptor structure and activation. Biochim Biophys Acta *1768*, 794-807.

Kohout, T.A., and Lefkowitz, R.J. (2003). Regulation of G protein-coupled receptor kinases and arrestins during receptor desensitization. Mol Pharmacol *63*, 9-18.

Kosower, E.M., Kanety, H., Dodiuk, H., Hermolin, J. (1982). Bimanes. 9. Solvent and substituent effects on intramolecular charge-transfer quenching of the fluorescence of syn-1,5-diazabicyclo[3.3.0]octadienediones (syn-9,10-dioxabimanes). J Phys Chem *86*, 1270-1277.

Kota, P., Reeves, P.J., Rajbhandary, U.L., and Khorana, H.G. (2006). Opsin is present as dimers in COS1 cells: identification of amino acids at the dimeric interface. Proc Natl Acad Sci U S A *103*, 3054-3059.

Kovoor, A., Celver, J., Abdryashitov, R.I., Chavkin, C., and Gurevich, V.V. (1999). Targeted construction of phosphorylation-independent beta-arrestin mutants with constitutive activity in cells. J Biol Chem *274*, 6831-6834.

Kovoor, A., Nappey, V., Kieffer, B.L., and Chavkin, C. (1997). Mu and delta opioid receptors are differentially desensitized by the coexpression of beta-adrenergic receptor kinase 2 and beta-arrestin 2 in xenopus oocytes. J Biol Chem *272*, 27605-27611.

Krupnick, J.G., and Benovic, J.L. (1998). The role of receptor kinases and arrestins in G protein-coupled receptor regulation. Annu Rev Pharmacol Toxicol *38*, 289-319.

Krupnick, J.G., Gurevich, V.V., and Benovic, J.L. (1997). Mechanism of quenching of phototransduction. Binding competition between arrestin and transducin for phosphorhodopsin. J Biol Chem *272*, 18125-18131.

Krupnick, J.G., Gurevich, V.V., Schepers, T., Hamm, H.E., and Benovic, J.L. (1994). Arrestin-rhodopsin interaction. Multi-site binding delineated by peptide inhibition. J Biol Chem *269*, 3226-3232.

Kuhn, H., Hall, S.W., and Wilden, U. (1984). Light-induced binding of 48-kDa protein to photoreceptor membranes is highly enhanced by phosphorylation of rhodopsin. FEBS Lett *176*, 473-478.

Kuhn, H., and Wilden, U. (1982). Assay of phosphorylation of rhodopsin in vitro and in vivo. Methods Enzymol *81*, 489-496.

Kuhn, H., and Wilden, U. (1987). Deactivation of photoactivated rhodopsin by rhodopsin-kinase and arrestin. J Recept Res *7*, 283-298.

Kuszak, A.J., Pitchiaya, S., Anand, J.P., Mosberg, H.I., Walter, N.G., and Sunahara, R.K. (2009). Purification and functional reconstitution of monomeric mu-opioid receptors: allosteric modulation of agonist binding by Gi2. J Biol Chem *284*, 26732-26741.

Lagerstrom, M.C., and Schioth, H.B. (2008). Structural diversity of G protein-coupled receptors and significance for drug discovery. Nat Rev Drug Discov *7*, 339-357.

Lakowicz, J.R. (2006). Principles of Fluorescence Spectroscopy, Third edn (Springer).

Landsman, R.S., Burkey, T.H., Consroe, P., Roeske, W.R., and Yamamura, H.I. (1997). SR141716A is an inverse agonist at the human cannabinoid CB1 receptor. Eur J Pharmacol *334*, R1-2.

Leterrier, C., Bonnard, D., Carrel, D., Rossier, J., and Lenkei, Z. (2004). Constitutive endocytic cycle of the CB1 cannabinoid receptor. J Biol Chem *279*, 36013-36021.

Liang, Y., Fotiadis, D., Filipek, S., Saperstein, D.A., Palczewski, K., and Engel, A. (2003). Organization of the G protein-coupled receptors rhodopsin and opsin in native membranes. J Biol Chem *278*, 21655-21662.

Lohse, M.J., Benovic, J.L., Codina, J., Caron, M.G., and Lefkowitz, R.J. (1990). beta-Arrestin: a protein that regulates beta-adrenergic receptor function. Science *248*, 1547-1550.

Ludanyi, A., Eross, L., Czirjak, S., Vajda, J., Halasz, P., Watanabe, M., Palkovits, M., Magloczky, Z., Freund, T.F., and Katona, I. (2008). Downregulation of the CB1 cannabinoid receptor and related molecular elements of the endocannabinoid system in epileptic human hippocampus. J Neurosci *28*, 2976-2990.

Mackie, K. (2008). Cannabinoid receptors: where they are and what they do. J Neuroendocrinol *20 Suppl 1*, 10-14.

Mackie, K., Lai, Y., Westenbroek, R., and Mitchell, R. (1995). Cannabinoids activate an inwardly rectifying potassium conductance and inhibit Q-type calcium currents in AtT20 cells transfected with rat brain cannabinoid receptor. J Neurosci *15*, 6552-6561.

MacLennan, S.J., Reynen, P.H., Kwan, J., and Bonhaus, D.W. (1998). Evidence for inverse agonism of SR141716A at human recombinant cannabinoid CB1 and CB2 receptors. Br J Pharmacol *124*, 619-622.

Maeda, T., Imanishi, Y., and Palczewski, K. (2003). Rhodopsin phosphorylation: 30 years later. Prog Retin Eye Res *22*, 417-434.

Mansoor, S.E., Dewitt, M.A., and Farrens, D.L. (2010). Distance mapping in proteins using fluorescence spectroscopy: the tryptophan-induced quenching (TrIQ) method. Biochemistry *49*, 9722-9731.

Mansoor, S.E., and Farrens, D.L. (2004). High-throughput protein structural analysis using site-directed fluorescence labeling and the bimane derivative (2-pyridyl)dithiobimane. Biochemistry *43*, 9426-9438.

Mansoor, S.E., McHaourab, H.S., and Farrens, D.L. (1999). Determination of protein secondary structure and solvent accessibility using site-directed fluorescence labeling. Studies of T4 lysozyme using the fluorescent probe monobromobimane. Biochemistry *38*, 16383-16393.

Mansoor, S.E., McHaourab, H.S., and Farrens, D.L. (2002). Mapping proximity within proteins using fluorescence spectroscopy. A study of T4 lysozyme showing that tryptophan residues quench bimane fluorescence. Biochemistry *41*, 2475-2484.

Mansoor, S.E., Palczewski, K., and Farrens, D.L. (2006). Rhodopsin self-associates in asolectin liposomes. Proc Natl Acad Sci U S A *103*, 3060-3065.

Martini, L., Waldhoer, M., Pusch, M., Kharazia, V., Fong, J., Lee, J.H., Freissmuth, C., and Whistler, J.L. (2007). Ligand-induced down-regulation of the cannabinoid 1 receptor is mediated by the G-protein-coupled receptor-associated sorting protein GASP1. FASEB J *21*, 802-811.

Matsuda, T., and Fukada, Y. (2000). Functional analysis of farnesylation and methylation of transducin. Methods Enzymol *316*, 465-481.

Maurice, P., Guillaume, J.L., Benleulmi-Chaachoua, A., Daulat, A.M., Kamal, M., and Jockers, R. (2011). GPCR-interacting proteins, major players of GPCR function. Adv Pharmacol *62*, 349-380.

Milligan, G., MacEwan, D.J., Mercouris, M., and Mullaney, I. (1997). Inverse agonism at adrenergic and opioid receptors: studies with wild type and constitutively active mutant receptors. Receptors Channels *5*, 209-213.

Milligan, G., Ramsay, D., Pascal, G., and Carrillo, J.J. (2003). GPCR dimerisation. Life Sci *74*, 181-188.

Minor, D.L., Jr., and Kim, P.S. (1996). Context-dependent secondary structure formation of a designed protein sequence. Nature *380*, 730-734.

Molday, R.S., and MacKenzie, D. (1983). Monoclonal antibodies to rhodopsin: characterization, cross-reactivity, and application as structural probes. Biochemistry *22*, 653-660.

Molday, R.S., and MacKenzie, D. (1985). Inhibition of monoclonal antibody binding and proteolysis by light-induced phosphorylation of rhodopsin. Biochemistry *24*, 776-781.

Moore, C.A., Milano, S.K., and Benovic, J.L. (2007). Regulation of receptor trafficking by GRKs and arrestins. Annu Rev Physiol *69*, 451-482.

Mukhopadhyay, S., Shim, J.Y., Assi, A.A., Norford, D., and Howlett, A.C. (2002). CB(1) cannabinoid receptor-G protein association: a possible mechanism for differential signaling. Chem Phys Lipids *121*, 91-109.

Nemoto, T.K., Fukuma, Y., Itoh, H., Takagi, T., and Ono, T. (2006). A disulfide bridge mediated by cysteine 574 is formed in the dimer of the 70-kDa heat shock protein. J Biochem *139*, 677-687.

Neo, B.H., Kandhi, S., and Wolin, M.S. (2010). Roles for soluble guanylate cyclase and a thiol oxidation-elicited subunit dimerization of protein kinase G in pulmonary artery relaxation to hydrogen peroxide. Am J Physiol Heart Circ Physiol *299*, H1235-1241.

Nesvizhskii, A.I., Keller, A., Kolker, E., and Aebersold, R. (2003). A statistical model for identifying proteins by tandem mass spectrometry. Anal Chem *75*, 4646-4658.

Nie, J., and Lewis, D.L. (2001a). The proximal and distal C-terminal tail domains of the CB1 cannabinoid receptor mediate G protein coupling. Neuroscience *107*, 161-167.

Nie, J., and Lewis, D.L. (2001b). Structural domains of the CB1 cannabinoid receptor that contribute to constitutive activity and G-protein sequestration. J Neurosci *21*, 8758-8764.

Niehaus, J.L., Liu, Y., Wallis, K.T., Egertova, M., Bhartur, S.G., Mukhopadhyay, S., Shi, S., He, H., Selley, D.E., Howlett, A.C., *et al.* (2007). CB1 cannabinoid receptor activity is modulated by the cannabinoid receptor interacting protein CRIP 1a. Mol Pharmacol *72*, 1557-1566.

Niu, L., Kim, J.M., and Khorana, H.G. (2002). Structure and function in rhodopsin: asymmetric reconstitution of rhodopsin in liposomes. Proc Natl Acad Sci U S A *99*, 13409-13412.

Nyiri, G., Cserep, C., Szabadits, E., Mackie, K., and Freund, T.F. (2005). CB1 cannabinoid receptors are enriched in the perisynaptic annulus and on preterminal segments of hippocampal GABAergic axons. Neuroscience *136*, 811-822.

Ohguro, H., Palczewski, K., Walsh, K.A., and Johnson, R.S. (1994). Topographic study of arrestin using differential chemical modifications and hydrogen/deuterium exchange. Protein Sci *3*, 2428-2434.

Oldham, W.M., and Hamm, H.E. (2006). Structural basis of function in heterotrimeric G proteins. Q Rev Biophys *39*, 117-166.

Overington, J.P., Al-Lazikani, B., and Hopkins, A.L. (2006). How many drug targets are there? Nat Rev Drug Discov *5*, 993-996.

Palczewski, K. (2006). G protein-coupled receptor rhodopsin. Annu Rev Biochem *75*, 743-767.

Palczewski, K., Buczylko, J., Kaplan, M.W., Polans, A.S., and Crabb, J.W. (1991). Mechanism of rhodopsin kinase activation. J Biol Chem *266*, 12949-12955.

Palczewski, K., Buczylko, J., Lebioda, L., Crabb, J.W., and Polans, A.S. (1993). Identification of the N-terminal region in rhodopsin kinase involved in its interaction with rhodopsin. J Biol Chem *268*, 6004-6013.

Palczewski, K., Buczylko, J., Van Hooser, P., Carr, S.A., Huddleston, M.J., and Crabb, J.W. (1992a). Identification of the autophosphorylation sites in rhodopsin kinase. J Biol Chem *267*, 18991-18998.

Palczewski, K., Hofmann, K.P., and Baehr, W. (2006). Rhodopsin--advances and perspectives. Vision Res *46*, 4425-4426.

Palczewski, K., McDowell, J.H., and Hargrave, P.A. (1988a). Purification and characterization of rhodopsin kinase. J Biol Chem *263*, 14067-14073.

Palczewski, K., McDowell, J.H., and Hargrave, P.A. (1988b). Rhodopsin kinase: substrate specificity and factors that influence activity. Biochemistry *27*, 2306-2313.

Palczewski, K., Ohguro, H., Premont, R.T., and Inglese, J. (1995). Rhodopsin kinase autophosphorylation. Characterization of site-specific mutations. J Biol Chem *270*, 15294-15298.

Palczewski, K., Riazance-Lawrence, J.H., and Johnson, W.C., Jr. (1992b). Structural properties of arrestin studied by chemical modification and circular dichroism. Biochemistry *31*, 3902-3906.

Papermaster, D.S. (1982). Preparation of retinal rod outer segments. Methods Enzymol *81*, 48-52.

Paquette, J.J., Wang, H.Y., Bakshi, K., and Olmstead, M.C. (2007). Cannabinoid-induced tolerance is associated with a CB1 receptor G protein coupling switch that is prevented by ultra-low dose rimonabant. Behav Pharmacol *18*, 767-776.

Park, P.S., Filipek, S., Wells, J.W., and Palczewski, K. (2004). Oligomerization of G protein-coupled receptors: past, present, and future. Biochemistry *43*, 15643-15656.

Park, P.S., Lodowski, D.T., and Palczewski, K. (2008). Activation of G protein-coupled receptors: beyond two-state models and tertiary conformational changes. Annu Rev Pharmacol Toxicol *48*, 107-141.

Pin, J.P., Comps-Agrar, L., Maurel, D., Monnier, C., Rives, M.L., Trinquet, E., Kniazeff, J., Rondard, P., and Prezeau, L. (2009). G-protein-coupled receptor oligomers: two or more for what? Lessons from mGlu and GABAB receptors. J Physiol *587*, 5337-5344.

Premont, R.T., and Gainetdinov, R.R. (2007). Physiological roles of G protein-coupled receptor kinases and arrestins. Annu Rev Physiol *69*, 511-534.

Pulvermuller, A., Schroder, K., Fischer, T., and Hofmann, K.P. (2000). Interactions of metarhodopsin II. Arrestin peptides compete with arrestin and transducin. J Biol Chem *275*, 37679-37685.

Raman, D., Osawa, S., and Weiss, E.R. (1999). Binding of arrestin to cytoplasmic loop mutants of bovine rhodopsin. Biochemistry *38*, 5117-5123.

Rasmussen, S.G., DeVree, B.T., Zou, Y., Kruse, A.C., Chung, K.Y., Kobilka, T.S., Thian, F.S., Chae, P.S., Pardon, E., Calinski, D., *et al.* (2011). Crystal structure of the beta2 adrenergic receptor-Gs protein complex. Nature *477*, 549-555.

Resek, J.F., Farahbakhsh, Z.T., Hubbell, W.L., and Khorana, H.G. (1993). Formation of the meta II photointermediate is accompanied by conformational changes in the cytoplasmic surface of rhodopsin. Biochemistry *32*, 12025-12032.

Resek, J.F., Farrens, D., and Khorana, H.G. (1994). Structure and function in rhodopsin: covalent crosslinking of the rhodopsin (metarhodopsin II)-transducin complex--the rhodopsin

cytoplasmic face links to the transducin alpha subunit. Proc Natl Acad Sci U S A *91*, 7643-7647.

Richardson, S.M., Wheelan, S.J., Yarrington, R.M., and Boeke, J.D. (2006). GeneDesign: rapid, automated design of multikilobase synthetic genes. Genome Res *16*, 550-556.

Ridge, K.D., Abdulaev, N.G., Sousa, M., and Palczewski, K. (2003). Phototransduction: crystal clear. Trends Biochem Sci *28*, 479-487.

Rim, J., and Oprian, D.D. (1995). Constitutive activation of opsin: interaction of mutants with rhodopsin kinase and arrestin. Biochemistry *34*, 11938-11945.

Rosenbaum, D.M., Rasmussen, S.G., and Kobilka, B.K. (2009). The structure and function of G-protein-coupled receptors. Nature *459*, 356-363.

Ruan, B., Fisher, K.E., Alexander, P.A., Doroshko, V., and Bryan, P.N. (2004). Engineering subtilisin into a fluoride-triggered processing protease useful for one-step protein purification. Biochemistry *43*, 14539-14546.

Scheerer, P., Park, J.H., Hildebrand, P.W., Kim, Y.J., Krauss, N., Choe, H.W., Hofmann, K.P., and Ernst, O.P. (2008). Crystal structure of opsin in its G-protein-interacting conformation. Nature *455*, 497-502.

Schleicher, A., Kuhn, H., and Hofmann, K.P. (1989). Kinetics, binding constant, and activation energy of the 48-kDa protein-rhodopsin complex by extra-metarhodopsin II. Biochemistry *28*, 1770-1775.

Schneidman-Duhovny, D., Inbar, Y., Nussinov, R., and Wolfson, H.J. (2005). PatchDock and SymmDock: servers for rigid and symmetric docking. Nucleic Acids Res *33*, W363-367.

Schoneberg, T., Schulz, A., Biebermann, H., Hermsdorf, T., Rompler, H., and Sangkuhl, K. (2004). Mutant G-protein-coupled receptors as a cause of human diseases. Pharmacol Ther *104*, 173-206.

Schroder, K., Pulvermuller, A., and Hofmann, K.P. (2002). Arrestin and its splice variant Arr1-370A (p44). Mechanism and biological role of their interaction with rhodopsin. J Biol Chem *277*, 43987-43996.

Seifert, R., and Wenzel-Seifert, K. (2002). Constitutive activity of G-protein-coupled receptors: cause of disease and common property of wild-type receptors. Naunyn Schmiedebergs Arch Pharmacol *366*, 381-416.

Sheikh, S.P., Zvyaga, T.A., Lichtarge, O., Sakmar, T.P., and Bourne, H.R. (1996). Rhodopsin activation blocked by metal-ion-binding sites linking transmembrane helices C and F. Nature *383*, 347-350.

Shi, W., Sports, C.D., Raman, D., Shirakawa, S., Osawa, S., and Weiss, E.R. (1998). Rhodopsin arginine-135 mutants are phosphorylated by rhodopsin kinase and bind arrestin in the absence of 11-cis-retinal. Biochemistry *37*, 4869-4874.

Shichi, H., and Somers, R.L. (1978). Light-dependent phosphorylation of rhodopsin. Purification and properties of rhodopsin kinase. J Biol Chem *253*, 7040-7046.

Shilton, B.H., McDowell, J.H., Smith, W.C., and Hargrave, P.A. (2002). The solution structure and activation of visual arrestin studied by small-angle X-ray scattering. Eur J Biochem *269*, 3801-3809.

Singh, P., Wang, B., Maeda, T., Palczewski, K., and Tesmer, J.J. (2008). Structures of rhodopsin kinase in different ligand states reveal key elements involved in G protein-coupled receptor kinase activation. J Biol Chem *283*, 14053-14062.

Smith, T.H., Sim-Selley, L.J., and Selley, D.E. (2010). Cannabinoid CB1 receptor-interacting proteins: novel targets for central nervous system drug discovery? Br J Pharmacol *160*, 454-466.

Smith, W.C., Bolch, S., Dugger, D.R., Li, J., Esquenazi, I., Arendt, A., Benzenhafer, D., and McDowell, J.H. (2011). Interaction of arrestin with enolase1 in photoreceptors. Invest Ophthalmol Vis Sci *52*, 1832-1840.

Smith, W.C., Dinculescu, A., Peterson, J.J., and McDowell, J.H. (2004). The surface of visual arrestin that binds to rhodopsin. Mol Vis *10*, 392-398.

Smith, W.C., McDowell, J.H., Dugger, D.R., Miller, R., Arendt, A., Popp, M.P., and Hargrave, P.A. (1999). Identification of regions of arrestin that bind to rhodopsin. Biochemistry *38*, 2752-2761.

Sokal, I., Pulvermuller, A., Buczylko, J., Hofmann, K.P., and Palczewski, K. (2002). Rhodopsin and its kinase. Methods Enzymol *343*, 578-600.

Sommer, M.E., and Farrens, D.L. (2006). Arrestin can act as a regulator of rhodopsin photochemistry. Vision Res *46*, 4532-4546.

Sommer, M.E., Farrens, D.L., McDowell, J.H., Weber, L.A., and Smith, W.C. (2007). Dynamics of arrestin-rhodopsin interactions: loop movement is involved in arrestin activation and receptor binding. J Biol Chem *282*, 25560-25568.

Sommer, M.E., Hofmann, K.P., and Heck, M. (2011). Arrestin-rhodopsin binding stoichiometry in isolated rod outer segment membranes depends on the percentage of activated receptors. J Biol Chem *286*, 7359-7369.

Sommer, M.E., Smith, W.C., and Farrens, D.L. (2005). Dynamics of arrestin-rhodopsin interactions: arrestin and retinal release are directly linked events. J Biol Chem *280*, 6861-6871.

Sommer, M.E., Smith, W.C., and Farrens, D.L. (2006). Dynamics of arrestin-rhodopsin interactions: acidic phospholipids enable binding of arrestin to purified rhodopsin in detergent. J Biol Chem *281*, 9407-9417.

Standfuss, J., Xie, G., Edwards, P.C., Burghammer, M., Oprian, D.D., and Schertler, G.F. (2007). Crystal structure of a thermally stable rhodopsin mutant. J Mol Biol *372*, 1179-1188.

Stauffer, B., Wallis, K.T., Wilson, S.P., Egertova, M., Elphick, M.R., Lewis, D.L., and Hardy, L.R. (2011). CRIP1a switches cannabinoid receptor agonist/antagonist-mediated protection from glutamate excitotoxicity. Neurosci Lett *503*, 224-228.

Sutton, R.B., Vishnivetskiy, S.A., Robert, J., Hanson, S.M., Raman, D., Knox, B.E., Kono, M., Navarro, J., and Gurevich, V.V. (2005). Crystal structure of cone arrestin at 2.3A: evolution of receptor specificity. J Mol Biol *354*, 1069-1080.

Tan, S., and Richmond, T.J. (1998). Crystal structure of the yeast MATalpha2/MCM1/DNA ternary complex. Nature *391*, 660-666.

Tappe-Theodor, A., Agarwal, N., Katona, I., Rubino, T., Martini, L., Swiercz, J., Mackie, K., Monyer, H., Parolaro, D., Whistler, J., *et al.* (2007). A molecular basis of analgesic tolerance to cannabinoids. J Neurosci *27*, 4165-4177.

Tesmer, J.J. (2010). The quest to understand heterotrimeric G protein signaling. Nat Struct Mol Biol *17*, 650-652.

Thompson, M.D., Percy, M.E., McIntyre Burnham, W., and Cole, D.E. (2008). G protein-coupled receptors disrupted in human genetic disease. Methods Mol Biol *448*, 109-137.

Thornton, J.M. (1981). Disulphide bridges in globular proteins. J Mol Biol *151*, 261-287.

Tsukamoto, H., Sinha, A., DeWitt, M., and Farrens, D.L. (2010). Monomeric rhodopsin is the minimal functional unit required for arrestin binding. J Mol Biol *399*, 501-511.

Turu, G., and Hunyady, L. (2010). Signal transduction of the CB1 cannabinoid receptor. J Mol Endocrinol *44*, 75-85.

Vishnivetskiy, S.A., Francis, D., Van Eps, N., Kim, M., Hanson, S.M., Klug, C.S., Hubbell, W.L., and Gurevich, V.V. (2010). The role of arrestin alpha-helix I in receptor binding. J Mol Biol *395*, 42-54.

Vishnivetskiy, S.A., Gimenez, L.E., Francis, D.J., Hanson, S.M., Hubbell, W.L., Klug, C.S., and Gurevich, V.V. (2011). Few residues within an extensive binding interface drive receptor interaction and determine the specificity of arrestin proteins. J Biol Chem *286*, 24288-24299.

Vishnivetskiy, S.A., Hosey, M.M., Benovic, J.L., and Gurevich, V.V. (2004). Mapping the arrestin-receptor interface. Structural elements responsible for receptor specificity of arrestin proteins. J Biol Chem *279*, 1262-1268.

Wald, G. (1951). The photochemical basis of rod vision. J Opt Soc Am *41*, 949-956.

Weitz, C.J., and Nathans, J. (1993). Rhodopsin activation: effects on the metarhodopsin I-metarhodopsin II equilibrium of neutralization or introduction of charged amino acids within putative transmembrane segments. Biochemistry *32*, 14176-14182.

Wensel, T.G. (2008). Signal transducing membrane complexes of photoreceptor outer segments. Vision Res *48*, 2052-2061.

Whistler, J.L., and von Zastrow, M. (1998). Morphine activated opioid receptors elude desensitization by beta-arrestin. Proc Natl Acad Sci USA *95*, 9914–9919.

Whitmore, L., and Wallace, B.A. (2004). DICHROWEB, an online server for protein secondary structure analyses from circular dichroism spectroscopic data. Nucleic Acids Res *32*, W668-673.

Whorton, M.R., Bokoch, M.P., Rasmussen, S.G., Huang, B., Zare, R.N., Kobilka, B., and Sunahara, R.K. (2007). A monomeric G protein-coupled receptor isolated in a high-density lipoprotein particle efficiently activates its G protein. Proc Natl Acad Sci U S A *104*, 7682-7687.

Whorton, M.R., Jastrzebska, B., Park, P.S., Fotiadis, D., Engel, A., Palczewski, K., and Sunahara, R.K. (2008). Efficient coupling of transducin to monomeric rhodopsin in a phospholipid bilayer. J Biol Chem *283*, 4387-4394.

Wilden, U., Hall, S.W., and Kuhn, H. (1986). Phosphodiesterase activation by photoexcited rhodopsin is quenched when rhodopsin is phosphorylated and binds the intrinsic 48-kDa protein of rod outer segments. Proc Natl Acad Sci U S A *83*, 1174-1178.

Wilden, U., and Kuhn, H. (1982). Light-dependent phosphorylation of rhodopsin: number of phosphorylation sites. Biochemistry *21*, 3014-3022.

Wu, D.F., Yang, L.Q., Goschke, A., Stumm, R., Brandenburg, L.O., Liang, Y.J., Hollt, V., and Koch, T. (2008). Role of receptor internalization in the agonist-induced desensitization of cannabinoid type 1 receptors. J Neurochem *104*, 1132-1143.

Xie, G., Gross, A.K., and Oprian, D.D. (2003). An opsin mutant with increased thermal stability. Biochemistry *42*, 1995-2001.

Yang, K., Farrens, D.L., Hubbell, W.L., and Khorana, H.G. (1996). Structure and function in rhodopsin. Single cysteine substitution mutants in the cytoplasmic interhelical E-F loop region show position-specific effects in transducin activation. Biochemistry *35*, 12464-12469.

Zhan, X., Gimenez, L.E., Gurevich, V.V., and Spiller, B.W. (2011). Crystal structure of arrestin-3 reveals the basis of the difference in receptor binding between two non-visual subtypes. J Mol Biol *406*, 467-478.

Zhang, L., Sports, C.D., Osawa, S., and Weiss, E.R. (1997). Rhodopsin phosphorylation sites and their role in arrestin binding. J Biol Chem *272*, 14762-14768.

Appendix 1

Monomeric Rhodopsin Is the Minimal Functional Unit Required for Arrestin Binding

A1.1. Summary

We have tested whether arrestin binding requires the G protein-coupled receptor be a dimer or a multimer. To do this, we encapsulated single rhodopsin molecules into nanoscale phospholipid particles (so-called nanodiscs) and measured their ability to bind arrestin. Our data clearly show that both visual arrestin and β-arrestin 1 can bind to monomeric rhodopsin and stabilize the active metarhodopsin II form. Interestingly, we find that the monomeric rhodopsin in nanodiscs has a higher affinity for wild-type arrestin binding than does oligomeric rhodopsin in liposomes or nanodiscs, as assessed by stabilization of metarhodopsin II. Together, these results establish that rhodopsin self-association is not required to enable arrestin binding.

All the rhodopsin and phosphorylated rhodopsin were prepared by the author of this dissertation. Also, all the different arrestin forms – wild-type, R175E and β-arrestin 1 were purified by the author. The author also helped with the extra-meta II assays and the preparation of the manuscript. Mark DeWitt prepared the MSP proteins. Dr. Hisao Tsukamoto reconstituted rhodopsin in nanodiscs, performed the characterization experiments and prepared the manuscript. Portion of this work has been published (Tsukamoto, H., Sinha, A., DeWitt, M., and Farrens, D.L. (2010). J Mol Biol *399*, 501-511.) and was presented (poster at the 54th Annual Biophysical Society Meeting, San Francisco, CA, 2010).

A1.2. Introduction

G protein-coupled receptors (GPCRs) are widely used by cells to transmit extracellular signals to intracellular signaling cascades (Kobilka, 2007; Rosenbaum et al., 2009). The ability of GPCRs to couple with and to activate G proteins is blocked when the receptors are phosphorylated and bound by a protein called arrestin. Increasingly, the importance of GPCR–arrestin interactions is becoming apparent as studies discover their role in receptor internalization, (Gurevich and Gurevich, 2006; Moore et al., 2007) susceptibility to drug tolerance, (Bohn et al., 2000; Whistler and von Zastrow, 1998) retinal disease states, (Chen et al., 2006) and G protein independent signaling (DeWire et al., 2007).

At present, it is still not clear exactly how arrestin interacts with the cytoplasmic face of a GPCR. In fact, even the stoichiometry of the arrestin–GPCR interaction is not established, and a number of different and conflicting models have been proposed (Gurevich and Gurevich, 2008; Park et al., 2004) (some possible arrangements are shown in Fig. A1.1a). One report has provided evidence that the overall stoichiometry of arrestin/rhodopsin binding is 1:1, (Hanson et al., 2007a) although that study could not determine if the actual stoichiometry of the complex was 1:1 versus 2:2, 4:4, or even higher ratios of arrestin/rhodopsin (Gurevich and Gurevich, 2008)

Questions about the minimal stoichiometry required for arrestin–GPCR interaction are compelling, given the known ability of GPCRs to self-associate into dimers and/or even higher-order species. For example, rhodopsin, a light-sensitive GPCR, has been found under in vivo conditions to form dimers and higher-order species in rod outer segments (ROS) (Fotiadis et al., 2003). Moreover, opsin has been shown to self-associate when expressed in COS cells, (Kota et al., 2006) and our laboratory has found that purified rhodopsin self-associates when it is

reconstituted into lipid vesicles (liposomes) (Mansoor et al., 2006) Other rhodopsin-like (family A) GPCRs are also reported to form oligomers in a lipid environment (Ferre et al., 2009; Fung et al., 2009; Guo et al., 2008; Gurevich and Gurevich, 2008). In the case of family C GPCRs, it is well known that dimerization or oligomerization of the receptors plays important functional roles (Pin et al., 2009). Together, these observations raise the possibility that a multimeric form of (Park et al., 2004) rhodopsin (and other family A GPCRs) is a requirement for interaction with arrestin, but this possibility has never been directly tested previously.

Thus, in the present work, we set out to directly test if a dimeric or oligomeric GPCR is required for arrestin binding. To do this, we reconstituted single phosphorylated rhodopsin into small lipid particles, called nanodiscs (Fig. A1.1b), and measured their ability to bind and interact with visual arrestin and β-arrestin 1. Nanodiscs consist of lipids and membrane scaffold proteins (MSPs), which are derivatives of apolipoprotein A-1 (apo A-1) (Bayburt and Sligar, 2010). Recently, several laboratories have used nanodiscs in a similar approach to unequivocally demonstrate that a monomeric GPCR is the minimal unit required for activating a G protein, at least for the GPCR rhodopsin, (Banerjee et al., 2008; Bayburt et al., 2007; Whorton et al., 2008) the β-adrenergic receptor, (Whorton et al., 2007) and the μ-opioid receptor (Kuszak et al., 2009). To enable a comparison of our monomeric rhodopsin results with oligomeric rhodopsin results, we also reconstituted rhodopsin molecules into liposomes (Fig. A1.1c) and nanodiscs containing multiple-rhodopsin molecules.

Our data clearly show that monomeric light-activated phosphorylated rhodopsin in nanodiscs can interact with both visual arrestin and β-arrestin 1, resulting in stabilization of the active rhodopsin form called metarhodopsin II (meta-II). Interestingly, we find that monomeric rhodopsin in nanodiscs shows a higher affinity for wild-type (WT) visual arrestin than does

oligomeric rhodopsin in liposomes as assessed by meta-II stabilization. Our data also show that phospholipids with acidic head groups enhance the interaction of monomeric rhodopsin with visual arrestin, in agreement with our previous studies of arrestin/rhodopsin interaction in detergent (Sommer et al., 2006). Together, our data provide the first direct evidence of an interaction between a monomeric GPCR and arrestins, and they indicate that a monomeric rhodopsin is the minimal functional unit needed for arrestin binding.

A1.3. Materials and Methods

Materials

POPC and POPG were obtained from Avanti Polar Lipids, whereas octyl glucoside and sodium cholate were obtained from Anatrace. Cy3-maleimide and Cy5-maleimide were purchased from GE Healthcare. Frozen bovine retinas were purchased from Lawson and Lawson, Inc. All other chemicals and reagents were purchased from Sigma.

Preparation of ROS and purification of rhodopsin

ROS and highly phosphorylated ROS were prepared from bovine retinas as described previously (Sommer et al., 2005). Rhodopsin was purified from ROS as described previously (Mansoor et al., 2006).

Labeling of rhodopsin with Cy3-maleimide and Cy5-maleimide

Solubilized rhodopsin in buffer A [20 mM HEPES, 140 mM NaCl, 2 mM CaCl2, 2 mM MgCl2, and 1 mM MnCl2 (pH 7.0)] containing 4% octyl glucoside was mixed with ConA-Sepharose (GE Healthcare) for 3–4 h at 4 °C. The mixture was washed using 20 mL of buffer A

containing 1.46% octyl glucoside and then mixed with a 7-fold excess of the Cy3-maleimide or Cy5-maleimide label. The slurry was then nutated for 16 h at 4 °C, and the mixture was then washed extensively using buffer A containing 1.46% octyl glucoside. Finally, rhodopsin was eluted with buffer A containing 1.46% octyl glucoside and 0.3 M methyl-α-D-mannopyranoside. Labeling efficiency was calculated from the absorbance spectra and the known extinction coefficients of rhodopsin and the labels as previously described (Mansoor et al., 2006).

Construction, expression, and purification of MSP

We designed a synthetic gene for the MSP based on the published work of Denisov et al. (Denisov et al., 2004). Essentially, their MSP, which they call MSPE3D1, is an optimized derivative of human apo A-1. MSPE3D1 contains additional helices introduced into the middle of apo A-1 in order to increase the length of the MSP "belt" around the phospholipids bilayer, and it also includes a His-tag and a TEV protease cleavage site at the N-terminus to facilitate purification (Denisov et al., 2004). In addition to those features, in our gene, we mutated three tryptophan residues at positions 41, 77, and 143 in MSP1E3D1 with phenylalanine residues in order to decrease intrinsic protein fluorescence. The molecular coefficient of MSPE3D1 is reported to be 29,910 (Bayburt et al., 2007), and that of our tryptophan-substituted mutant MSPE3D1-F1 is calculated to be 13,410. We also optimized the codons to increase expression levels and to simplify cloning strategies. This optimized "Trp-less" MSP gene, which we call MSPE3D1-F1, was expressed and purified in accordance with Denisov et al. (Denisov et al., 2004). Briefly, MSP1E3D1-F1 was expressed in Escherichia coli BL21 and purified using Ni-NTASepharose (Qiagen). The 6× His tag at the N-terminus was cleaved using TEV protease, and the cleaved MSP was obtained as flow-through from the nickel column.

Preparation and purification of nanodiscs

Phosphorylated or unphosphorylated rhodopsin (solubilized in 1.46% octyl glucoside), MSP, and lipid (solubilized in 0.5Msodium cholate) were mixedwith~2/3 volume of Bio-Beads SM-2 (Bio-Rad) overnight at 4 °C. The Rh/MSP/lipid molar ratio was set to 0.1:1:75. In order to make nanodiscs containing predominantly dimeric (or oligomeric) rhodopsins (see Fig. A1.5), the molar ratio was changed to 1:1:41.25 in accordance with Banerjee et al.(Banerjee et al., 2008). The Bio-Beads were removed by centrifugation (1000g, 1 min). Liposome samples were prepared without MSP using the same methods described above. After reconstitution of the rhodopsin into nanodiscs or liposomes, the samples were injected onto a Superdex 200 column (GE Healthcare; column volume, 23.55 mL) run at 0.5mL/min. For the nanodisc samples, a fraction corresponding to a diameter of ~12 nm was collected (see Fig. A1.2a). The diameter of nanodiscs was estimated by comparison to a Gel Filtration Calibration Kit HMW (GE Healthcare) (see Fig. A1.2a). The collected sample was concentrated by Amicon Ultra 0.5-mL - Centrifugal Filters (10,000 molecular weight cut-off; Millipore).

Electron microscopy of nanodiscs

Nanodiscs (~1mg/mL) were lifted onto ultrathin carbon film/holey carbon 400-mesh copper grids (Ted Pella 01824) for 3min,wicked, rinsed in water for 1 min, stained for 45 s in filtered 1.33% uranyl acetate, wicked, stained again, and air dried. Samples were imaged at 100 kV on a Philips CM120 TEM transmission electron microscope. Images were collected as 1024×1024-pixel 14-bit gray-scale Gatan Digital Micrograph 3 (DM3) files on a Gatan 794CCD multiscan camera and converted into 8-bit gray-scale TIF images using the program Digital micrograph 3.4.

Expression and purification of arrestins

Both the bovine visual arrestin cDNA containing a single glycine inserted at position 2 (a generous gift from Dr.Vsevolod Gurevich) and the bovine β-arrestin 1 cDNA (a generous gift from Dr. Robert Lefkowitz) were cloned in the pET15b vector (Invitrogen). Both of these proteins were expressed in *E. coli* BL21(DE3) and purified using two-step ion-exchange chromatography as described previously (Sommer et al., 2006). The constitutively active visual arrestin mutant R175E was cloned at the C-terminal of a modified 77-amino-acid prodomain region of subtilisin BPN′ (proR8FKAM) in a pG58 expression vector (a generous gift from Dr. Kevin Ridge) (Abdulaev et al., 2005; Ruan et al., 2004). The R175E arrestin fused with the prodomain was expressed in BL21(DE3)-RP cells (Stratagene). The cells were grown in 1 L of LB media in the presence of 100 μg/mL ampicillin at room temperature to an A550 of 0.3, and then induced with 30 μM IPTG for 12–14 h at room temperature. The cell pellet was resuspended in 50 mM Tris–HCl (pH 8.0) containing 50 mM NaCl, 5 mM β-mercaptoethanol, 0.1 mM PMSF, and a protease inhibitor tablet (Roche), and then disrupted by sonication. The supernatant, obtained after centrifuging the cell lysate at 100,000g for 45 min, was loaded onto a 5-mL Profinity eXact column (Bio-Rad). The column was washed with 20 column volumes of 100mMsodium phosphate (pH 7.2) and 10 column volumes of 100mMsodium phosphate and 300 mM sodium acetate (pH 7.2). The cleavage of arrestin from the prosubtilisin tag was initiated by passing 1 column volume of 100 mM sodium phosphate (pH 7.2) containing 100 mM sodium fluoride (elution buffer). The fluoride-mediated cleavage reaction was allowed to occur for 1 h at room temperature. Tag-free arrestin was eluted off the column by passing 5 column volumes of the elution buffer and was further purified by cation-exchange chromatography using a 1-mL HiTrap Heparin column.

FRET measurements to test for the presence of oligomeric rhodopsin

Fluorescence excitation and emission spectra were recorded using a PTI steady-state fluorescence spectrophotometer. Emission spectra were measured by exciting the donor (Cy3) at 520 nm (0.5-nm bandpass) while scanning the fluorescence intensity of the acceptor (Cy5) (10-nm bandpass) at 10 °C. Excitation spectra were measured by collecting emission from the acceptor (Cy5) at 670 nm (10-nm bandpass) while scanning the excitation spectrum of the donor (Cy3) (0.5-nm bandpass). All measurements were performed in the dark state, immediately after light activation (with N500 nm light) at 10 °C. The total sample volume was 250 μL in a 4 mm×4 mm cuvette. Further details about measuring and calculating FRET are provided by Mansoor et al (Mansoor et al., 2006).

Measurement of absorption spectra

Absorption spectra were recorded using a UV-1601 spectrophotometer (Shimadzu). All measurements were performed in the dark state, immediately after 15 s of light activation (with N 500-nm light) at 10 °C using a T-Q/FOI-1 150-W fiber optic illuminator (Techni-Quip).

Orientation of rhodopsin in liposomes as determined by proteolysis

The orientation of rhodopsin in liposomes was assessed using the endoprotease Asp-N as described previously (Mansoor et al., 2006; Niu et al., 2002). Asp-N specifically cleaves between Gly329 and Asp330 at the C-terminus of rhodopsin (Palczewski et al., 1991). Briefly, the liposome samples were incubated with Asp-N at an Asp-N/rhodopsin molar ratio of 1:20 in the dark at room temperature for 4 h. The reaction was terminated by the addition of SDS-PAGE

loading buffer. The samples were then subjected to SDS-PAGE, and the amount of cleavage was determined by densitometry**.**

A1.4. Results

We prepared rhodopsin in nanodiscs by mixing purified phosphorylated rhodopsin and solubilized lipids [a mixture of 1-palmitoyl-2-oleoyl phosphatidylcholine (POPC) and 1-palmitoyl-2-oleoyl phosphatidylglycerol (POPG) at a 3:2 ratio] with MSP (Fig. A1.1b). Separately, we also prepared rhodopsin in liposomes by mixing purified phosphorylated rhodopsin and the solubilized lipid mixture in the absence of MSP (Fig. A1.1c). We chose this lipid mixture because it has been used for previous nanodisc studies using rhodopsin and other GPCRs, and because it mimics the zwitterionic environment of a cell membrane and is suited for retaining functional activity for GPCRs (Cerione and Ross, 1991; Whorton et al., 2007; Whorton et al., 2008). After removal of detergents using Bio-Beads, the samples were injected onto a size-exclusion column. In the presence of MSP, the majority of the sample eluted with a Stokes diameter of ~12 nm (as determined by protein standards), a value typical of nanodiscs containing monomeric rhodopsin (Fig. A1.2a) (Bayburt et al., 2007; Denisov et al., 2004). Our images of the nanodiscs, using electron microscopy, were consistent with this size (Fig. A1.2b). We collected this fraction and concentrated it using centrifugal filter devices (see Materials and Methods). In the absence of MSP, the samples formed lipid vesicles (liposomes) and eluted at the void volume (Fig. A1.2a).

Analysis by SDS-PAGE shows that the nanodisc samples contain phosphorylated rhodopsin and MSP, and the liposome samples contain only rhodopsin (Fig. A1.2c). The absorption spectra of the nanodisc samples indicate that the phosphorylated rhodopsin was successfully reconstituted into nanodiscs and retained spectral functionality. In the dark, the absorption maximum was at 500 nm; upon irradiation, this value shifted to a mixture of ~380 nm and ~480 nm, values typical of the light activated form of rhodopsin (meta-II) and its precursor [metarhodopsin I (meta-I)], respectively (Fig. A1.2d). The absorption spectra of nanodiscs showed very little light scattering (Fig. A1.2d), in contrast to the liposome spectra (Fig. A1.2e). These facts are again consistent with the nanodiscs having a much smaller size than the liposomes. Furthermore, we observed no loss in the absorbance of nanodisc samples even upon centrifugation at 100,000g for 30 min (data not shown), demonstrating that our rhodopsin nanodisc samples are fully soluble even in the absence of detergent.

We confirmed that the rhodopsin was monomeric in the nanodiscs by carrying out fluorescence energy transfer (FRET) experiments. We have previously shown that FRET can be used to measure rhodopsin self-association in liposomes (Mansoor et al., 2006). Briefly, these FRET experiments involved mixing equivalent molar amounts of Cy3-labeled and Cy5-labeled phosphorylated rhodopsin samples together, and then reconstituting them into either nanodiscs or liposomes. The results from these experiments clearly showed that the FRET efficiency between Cy3-labeled and Cy5-labeled rhodopsins was significantly higher in liposomes (26%) than in nanodiscs (9%) (Fig. A1.3a and b), indicating that rhodopsin was predominantly dimeric (or oligomeric) in liposomes and predominantly monomeric in nanodiscs. The higher FRET efficiency in liposomes and the lower FRET efficiency in nanodiscs are consistent with previous

studies using Cy3-labeled and Cy5-labeled rhodopsin17 and β-adrenergic receptor (Whorton et al., 2007).

Using an approach described in two previous reports of monomeric rhodopsin in nanodiscs, we also confirmed that our nanodisc preparations contained monomeric rhodopsin (Bayburt et al., 2007; Whorton et al., 2008). In this approach, we repurified the rhodopsin-containing nanodiscs using concanavalin A (ConA)-Sepharose, measured the absorption spectra (Fig. A1.3c), and then calculated the rhodopsin–MSP stoichiometry by comparing the extinction coefficients for rhodopsin (at 280 nm and 500 nm) with those for MSP (at 280 nm) (Bayburt et al., 2007; Whorton et al., 2008). This analysis showed a rhodopsin/MSP molar ratio of ~1:2.3. Since each nanodisc is formed by two MSP molecules (see figure legend to Fig. A1.3c), this result confirms that there was one rhodopsin per nanodisc, consistent with previous studies of monomeric rhodopsin in nanodiscs (Bayburt et al., 2007; Whorton et al., 2008). In summary, both our FRET data and absorption spectral analyses indicate that our nanodisc samples contained monomeric rhodopsin.

We next measured the ability of monomeric rhodopsin in nanodiscs and the ability of multimeric rhodopsin in liposomes to bind arrestin by measuring the amount of “extra meta-II” formation. Extra meta-II formation is a well-defined process that occurs when the binding of arrestin or G protein to photoactivated rhodopsin causes a shift of equilibrium between meta-II and its precursor meta-I toward meta-II (Emeis et al., 1982; Gibson et al., 2000; Schleicher et al., 1989). Extra meta-II can be easily quantified from difference spectra, which are obtained by simply subtracting the spectra of the rhodopsin in the dark from the spectra obtained after photoactivation. Typically, these difference spectra will show negative absorbance at ~500 nm

(from the loss of dark-state rhodopsin absorbance) and an increase in absorbance at 380 nm (due to the formation of active meta-II species). Since meta-II absorbs at 380 nm and meta-I absorbs at 480 nm, when arrestin binding to and stabilization of meta-II shifts the meta-I/meta-II equilibrium towards the formation of more meta-II, one observes an increase in absorbance at 380 nm, or extra meta-II.

Our results show that addition of WT visual arrestin to nanodiscs clearly increases the amount of meta-II in the difference spectra (note the increase in ~380-nm species in Fig. A1.4a). Importantly, the increase in meta-II was dependent on arrestin concentration, and the difference spectra in the presence of various concentrations of arrestin showed an isosbestic point at ~420 nm (Fig. A1.4a), with both spectral properties typical of extra meta-II formation induced by arrestin binding (Schleicher et al., 1989; Schroder et al., 2002).

Interestingly, we observed a much less increase in meta-II formation when we added WT visual arrestin to our multimeric rhodopsin samples in liposomes (Fig. A1.4b), in which ~85% of the rhodopsin was oriented with its cytoplasmic faces outside of the liposomes (Fig. A1.S1). This intriguing result could indicate that visual arrestin prefers binding to monomeric rhodopsin over binding to multimeric rhodopsin. However, the assay that we used to obtain this result formally cannot rule out the possibility of arrestin binding to multimeric rhodopsin, merely that if it does so, it does not produce extra meta-II. Either way, this is a curious result: Previous studies of rhodopsin in ROS membranes have demonstrated that significant extra meta-II formation occurs upon arrestin binding (Gibson et al., 2000; Schleicher et al., 1989; Schroder et al., 2002).Thus, our results may suggest that the extra meta-II signal observed in ROS

membranes is due to arrestin binding to monomeric rhodopsin formed transiently in the ROS membranes, and very few of these transient monomers exist in our reconstituted liposomes.

In addition, we measured extra meta-II formation induced by a constitutively active R175E mutant of visual arrestin, which can bind to both unphosphorylated rhodopsin and phosphorylated rhodopsin (Gurevich and Benovic, 1997; Gurevich and Gurevich, 2006). The R175E mutant induced significant extra meta-II formation both in nanodiscs and in liposomes to an extent much greater than WT arrestin (Fig. A1.4c and d). This result is not surprising, since another constitutively active form of arrestin, named p44 (Arr1–370A), is reported to induce larger extra meta-II formation than WT arrestin (Schroder et al., 2002). We also find that arrestin mutant R175E can induce extra meta-II formation of unphosphorylated rhodopsin in nanodiscs (Fig. A1.S2). Taken together, our data show that WT visual arrestin and the constitutively active arrestin mutant R175E possess typical abilities for forming a complex with rhodopsin in nanodiscs.

The concentration dependence of arrestin binding is shown in Fig. A1.4e and f. The plot shows that the amount of extra meta-II formation (difference absorbance between 390 nm and 426 nm) in nanodiscs and liposomes is dependent on arrestin concentration. In both nanodisc and liposomes, the R175E arrestin mutant showed a higher affinity (a lower EC_{50} value) than WT arrestin. Interestingly, the R175E mutant appears to have a similar affinity for rhodopsin in either nanodiscs or liposomes (EC_{50}=~0.6 μM), although WT arrestin appears to show a higher affinity for rhodopsin in nanodiscs (EC_{50}=~1.4 μM) than for rhodopsin in liposomes (EC_{50}=~7.9 μM). Based on these results, it is tempting to speculate that WT visual arrestin prefers binding to

monomeric rhodopsin over binding to oligomeric rhodopsin, but the R175E mutation destroys this discrimination.

To enable a better comparison between our various results, we estimated the amount of meta-II induced by arrestin binding to nanodiscs in accordance with the methods described by Weitz and Nathans (Weitz and Nathans, 1993). In the absence of arrestin (Fig. A1.4a, black line), meta-II formation in nanodiscs containing predominantly monomeric rhodopsin was calculated to be 18% ([meta-II]/([meta-I]+[meta-II])=0.18). In the presence of 4 μM arrestin WT (Fig. A1.4a, purple line) and R175E mutant (Fig. A1.4c, purple line), meta-II formation was 50% and 76%, respectively. Thus, the amount of meta-II increased by 32% upon the binding of WT arrestin, and by 58% upon binding of the mutant, R175E.

We used these values to assess whether the extra meta-II formation we see (Fig. A1.4a and c) might be due to arrestin binding to a small amount of dimeric (or oligomeric) rhodopsin present as "contamination" in our monomeric rhodopsin nanodisc samples. We tested this possibility by preparing nanodiscs containing predominantly dimeric (or oligomeric) rhodopsins, which we obtained by changing the rhodopsin/MSP/lipid ratio (rhodopsin/MSP/lipid = 1:1:41.25), as described in previous studies (Banerjee et al., 2008; Bayburt et al., 2007) These nanodisc samples exhibited a very high FRET efficiency (33%) between Cy3-labeled and Cy5-labeled rhodopsins, indicating that each of these nanodiscs predominantly contained two or more rhodopsin molecules (Fig. A1.5a and b). The 33% FRET efficiency for these samples is much higher than the 9% efficiency for the monomeric rhodopsin/nanodiscs (Fig. A1.3a). It is even higher than the 26% efficiency for the labeled rhodopsin reconstituted into liposome (Fig. A1.3a). These dimeric/oligomeric rhodopsin nanodisc samples showed a shift in the meta-

I/meta-II equilibrium towards more meta-I (Fig. A1.5c), consistent with a previous report (Bayburt et al., 2007). Addition of WT arrestin to these oligomeric rhodopsin nanodisc samples induced very little extra meta-II formation, and addition of arrestin mutant R175E produced a small amount of extra meta-II (Fig. A1.5c).

However, we must be cautious about inferring too much from these results because we do not know for sure the orientation of the dimeric/multimeric rhodopsin in the nanodiscs. However, these results make one thing clear. The arrestin-induced extra meta-II signal we see in our monomeric rhodopsin nanodiscs (Fig. A1.4a and c) is clearly larger than that seen in the multimeric rhodopsin samples (Figs. A1.4b and d and A1.5c). Thus, even if one postulates that there could be some multimeric rhodopsin "contaminating" monomeric rhodopsin nanodisc preparations, our data show that the extra meta-II signal we see for the monomeric rhodopsin samples cannot be due to arrestin binding only to a hypothetical multimeric rhodopsin "contaminant" because multimeric rhodopsin produces less (or no) extra meta-II in the presence of arrestin, compared to the monomeric rhodopsin nanodisc samples. Thus, based on our experiments, we can safely conclude that the extra meta-II formation we observed for monomeric rhodopsin samples (Fig. A1.4a and c) has to be due to arrestin binding to at least some monomeric rhodopsin, thus demonstrating that monomeric rhodopsin can bind arrestin.

We also tested the effect of lipid composition on the interaction between arrestin and rhodopsin in nanodiscs. We have found previously that phospholipids with acidic head groups enhance the interaction of rhodopsin in detergent micelles, resulting in a stabilized meta-II (Sommer et al., 2006; Wensel, 2008). Of the lipids used in our present study, POPC has a basic head group, and POPG has an acidic head group. To test the effect of lipid head-group charge,

we measured the ability of arrestin to bind to rhodopsin in nanodiscs containing only POPC. As shown in Fig. A1.6, rhodopsin in nanodiscs containing only POPC showed much less extra meta-II formation induced by WT arrestin and the R175E mutant compared to nanodiscs containing POPC and POPG. This result suggests that POPG can enhance arrestin/rhodopsin interaction and stabilize meta-II. These results are consistent with our abovementioned study showing a role for negatively charged lipid head groups in arrestin binding in detergent micelles (Sommer et al., 2006).

Finally, to test if the ability to bind to a monomeric receptor is unique to visual arrestin, we tested the ability of β-arrestin 1 (arrestin 2) to bind rhodopsin in nanodiscs. Although it is well established that β-arrestin can bind to phosphorylated rhodopsin (Gurevich et al., 1995; Kovoor et al., 1999), it has not previously been established whether β-arrestin can bind to a monomeric GPCR. Our results in Fig. A1.7 show that addition of β-arrestin 1 also induces significant extra meta-II formation for phosphorylated rhodopsin (Fig. A1.7a and c), but not for unphosphorylated rhodopsin in nanodiscs (Fig. A1.7b and d). Thus, these results show that, as with visual arrestin, β-arrestin can bind to a monomeric rhodopsin.

A1.5. Discussion

In this study, we found that arrestin shows robust binding to a monomeric rhodopsin in nanodiscs (Figs. A1.4 and A1.7). This result directly demonstrates that an oligomeric GPCR is not required for arrestin binding. Below, we discuss our results in relation to the stoichiometry of arrestin/rhodopsin complex and possible functional roles for GPCR oligomerization. It is known that rhodopsin and other rhodopsin-like (family A) GPCRs can form dimers (or oligomers) in the lipid membrane (Ferre et al., 2009; Gurevich and Gurevich, 2008; Kota et al., 2006; Liang et al.,

2003; Mansoor et al., 2006) Visual arrestin can also form dimers and tetramers in a concentration dependent manner (Hanson et al., 2007b; Hirsch et al., 1999; Imamoto et al., 2003; Shilton et al., 2002). Thus, various stoichiometries of the arrestin/rhodopsin complex can be imagined (see Fig. A1.1a). However, our data provide the first clear indication that monomeric rhodopsin is the minimal unit required for arrestin binding (Figs. A1.4 and A1.7). Our results, combined with recent spin labeling studies of arrestin showing that only monomeric arrestin binds to rhodopsin (Hanson et al., 2007b), strongly suggested that the stoichiometry of the arrestin/rhodopsin complex is 1:1.

This conclusion is completely consistent with our experimental work using purified rhodopsin in detergent (M. E. Sommer and D.L.F., unpublished data). It is also consistent with the results of a recent study that investigated the stoichiometry of rhodopsin and arrestin based on in vivo studies and pull-down assay using ROS membranes (Hanson et al., 2007a). In the latter study, the authors concluded an overall stoichiometry of 1:1; unfortunately, their experimental methods could not determine if monomeric rhodopsin binds one arrestin molecule or if their data were due to higher-order stoichiometries (such as 2:2 or 4:4 arrestin/rhodopsin, etc.) (Gurevich and Gurevich, 2008). In light of our results presented here, it is clear that one rhodopsin molecule can bind one arrestin molecule, consistent with the fact that the maximal amount of arrestin in ROS is close to the amount of rhodopsin (Hanson et al., 2007a). However, it is important to note several caveats about our results. They do not rule out a role for arrestin binding to dimeric/multimeric rhodopsin under some conditions, and they do not prove that WT arrestin is incapable of binding to dimeric or multimeric rhodopsin, only that if it does bind, it produces and stabilizes less extra meta-II.

We also find that monomeric rhodopsin in nanodiscs can interact with a β-arrestin, β-arrestin 1 (Fig. A1.7a and c). This finding suggests a general possibility that monomeric forms of family A GPCRs are sufficient to interact with all of the arrestins, and that multimeric receptors are not required for arrestin binding as a general rule. However, as noted above, our results do not rule out other possible roles for GPCR oligomerization in arrestin function (discussed below).

Previously, studies of rhodopsin, the β-adrenergic receptor, and the μ-opioid receptor in nanodiscs have all shown that monomeric GPCRs can activate G proteins efficiently (Banerjee et al., 2008; Bayburt et al., 2007; Kuszak et al., 2009; Whorton et al., 2007; Whorton et al., 2008). Those results, along with the results reported here, strongly suggest that dimerization (or oligomerization) is not necessary for the interaction of a GPCR with a G protein, or with arrestin, at least for family A GPCRs. Thus, the question remains: What are the functional roles of dimerization/multimerization for family A GPCRs? Our data in Fig. A1.4 may provide a tantalizing hint. The data show that WT arrestin has a higher affinity for monomeric rhodopsin in nanodiscs than for oligomeric rhodopsin in liposomes (Fig. A1.4e and f). Thus, it is tempting to speculate that the arrestin/rhodopsin interaction may, in fact, be regulated by a dynamic transition of the receptor between monomeric and oligomeric states. This type of regulation would be consistent with a recent study of the dopamine receptor, which found that agonist-induced G protein activation of the receptor is negatively regulated within its dimer (Han et al., 2009). Another possibility is that the interaction of GPCRs with other GPCR affiliated proteins may require dimerization of GPCRs (Park et al., 2008). Clearly, further biochemical and biophysical studies are required to elucidate these myriad possible functional roles for GPCR dimerization.

Fig. A1.1. Cartoon scheme outlining the strategy behind this study.

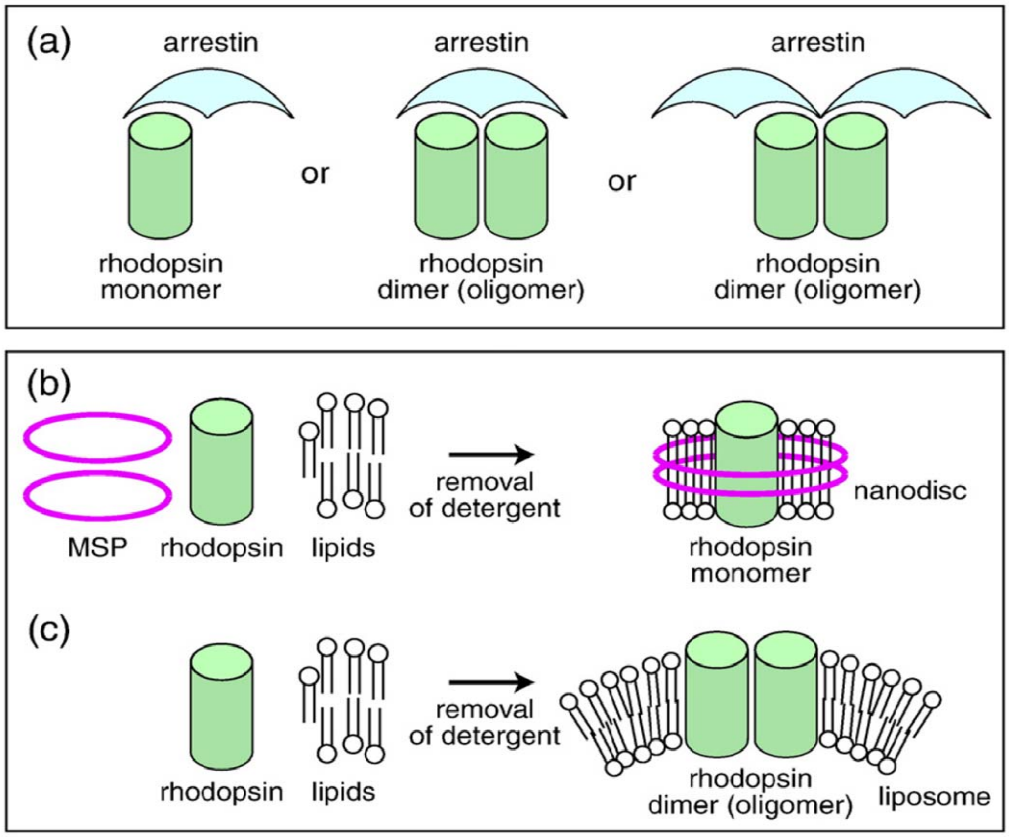

Fig. A1.1. Cartoon scheme outlining the strategy behind this study.

(a) Models showing some possible stoichiometries of the arrestin/rhodopsin complex. Other stoichiometries can also be imagined. (b) In the presence of MSP (purple circles), nanodiscs containing monomeric rhodopsin and lipids are formed. (c) In the absence of MSP, liposomes containing dimeric (or oligomeric) rhodopsin and lipids are formed.

Fig. A1.2. Characterization of phosphorylated rhodopsin reconstituted into nanodiscs by size-exclusion chromatography, absorption spectroscopy, and electron microscopy.

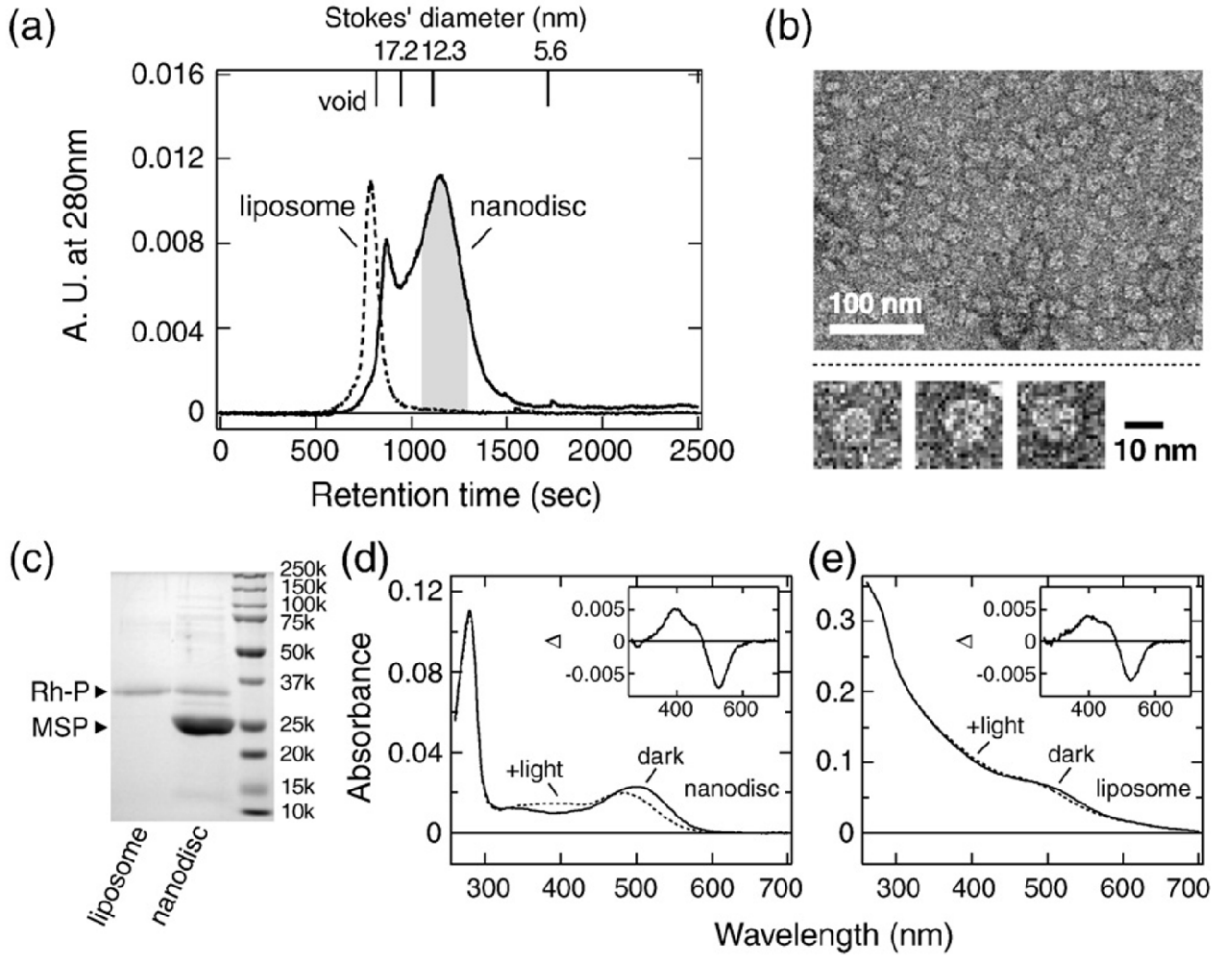

Fig. A1.2. Characterization of phosphorylated rhodopsin reconstituted into nanodiscs by size-exclusion chromatography, absorption spectroscopy, and electron microscopy.

(a) Purified phosphorylated rhodopsin reconstituted into nanodiscs was resolved on a Superdex 200 size-exclusion column (continuous line; “nanodisc”). In separate experiments, liposome samples were also resolved (broken line; “liposome”). For the preparation of monomeric rhodopsin in nanodiscs, the fraction eluting from 1050 s to 1290 s (shaded area) was collected and concentrated. The calibrated Stokes diameter scale and void volume (“void”) for this column are shown at the top. (b) Electron micrograph of nanodiscs. Expanded images are shown at the bottom of this panel. Scale bars are also shown. (c) SDS-PAGE analysis of a peak collected in (a) shows both phosphorylated rhodopsin (“Rh-P”) and MSP proteins (center lane; “nanodisc”). The nanodisc sample contains Rh-P and MSP at a molar ratio of 1:10 (see Materials and Methods). A liposome sample (without MSP) was also loaded as control and shows only phosphorylated rhodopsin (left lane; “liposome”). Molecular sizes of standard proteins are also indicated (right lane). Proteins were visualized using Coomassie staining. (d) Absorption spectra of phosphorylated rhodopsin in nanodiscs collected from size-exclusion chromatography indicate that the rhodopsin in nanodiscs retains its light-sensitive properties. Continuous (“dark”) and broken (“+light”) lines indicate spectra before and after irradiation, respectively. (e) Absorption spectra of phosphorylated rhodopsin in liposomes. Continuous (“dark”) and broken (“+light”) lines indicate spectra before and after irradiation, respectively. The insets in (d) and (e) show the difference spectra of the samples (after irradiation−before irradiation). The spectra in (d) and (e) were recorded at 10 °C and pH 7.4. The lipid composition in nanodiscs and liposomes is POPC/POPG at a ratio of 3:2.

Fig.A1.3. FRET and absorption spectral analyses indicating that rhodopsin is monomeric in these nanodiscs.

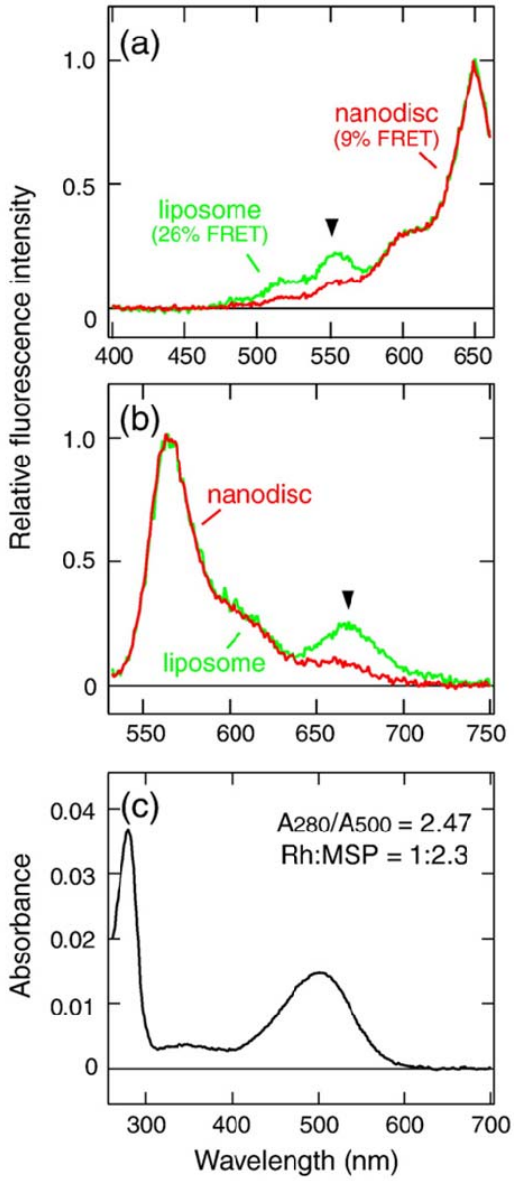

Fig.A1.3. FRET and absorption spectral analyses indicating that rhodopsin is monomeric in these nanodiscs.

(a) FRET studies showing strong and weak Rh–Rh energy transfer in liposomes and nanodiscs, respectively. Fluorescence excitation spectra of nanodiscs (red line) and liposomes (green line) containing Cy3-labeled and Cy5-labeled rhodopsin. The calculated FRET efficiencies (Mansoor et al., 2006) are 26% (in liposomes) and 9% (in nanodiscs). The spectra are normalized to a maximal fluorescence intensity of 1.0. (b) Fluorescence emission spectra of nanodiscs (red line) and liposomes (green line) containing Cy3-labeled and Cy5- labeled rhodopsin. The arrowheads in (a) and (b) indicate the strong FRET signal observed in liposomes. Spectra were recorded at 10 °C and pH 7.4. The lipid composition in nanodiscs is POPC/POPG at a ratio of 3:2. The spectra are normalized to a maximal fluorescence intensity of 1.0. (c) Absorption spectrum of rhodopsin in nanodiscs, purified from excess MSP using ConA-Sepharose. The extinction coefficient of rhodopsin at 500 nm is 40,000, and purified rhodopsin should have an A_{280}/A_{500} ratio of 1.7 (Whorton et al., 2008). The molecular coefficient of our tryptophan-substituted mutant MSPE3D1-F1 is 13,410. In the present example, the A_{280}/A_{500} ratio of purified nanodiscs was 2.47, indicating a rhodopsin/MSP molar ratio of about 1:2.3, consistent with one rhodopsin per two MSP proteins required to assemble a nanodisc.

Fig.A1.4. Arrestin can bind to monomeric rhodopsin as indicated by extra meta-II formation induced by the presence of WT arrestin and the constitutively active arrestin mutant R175E.

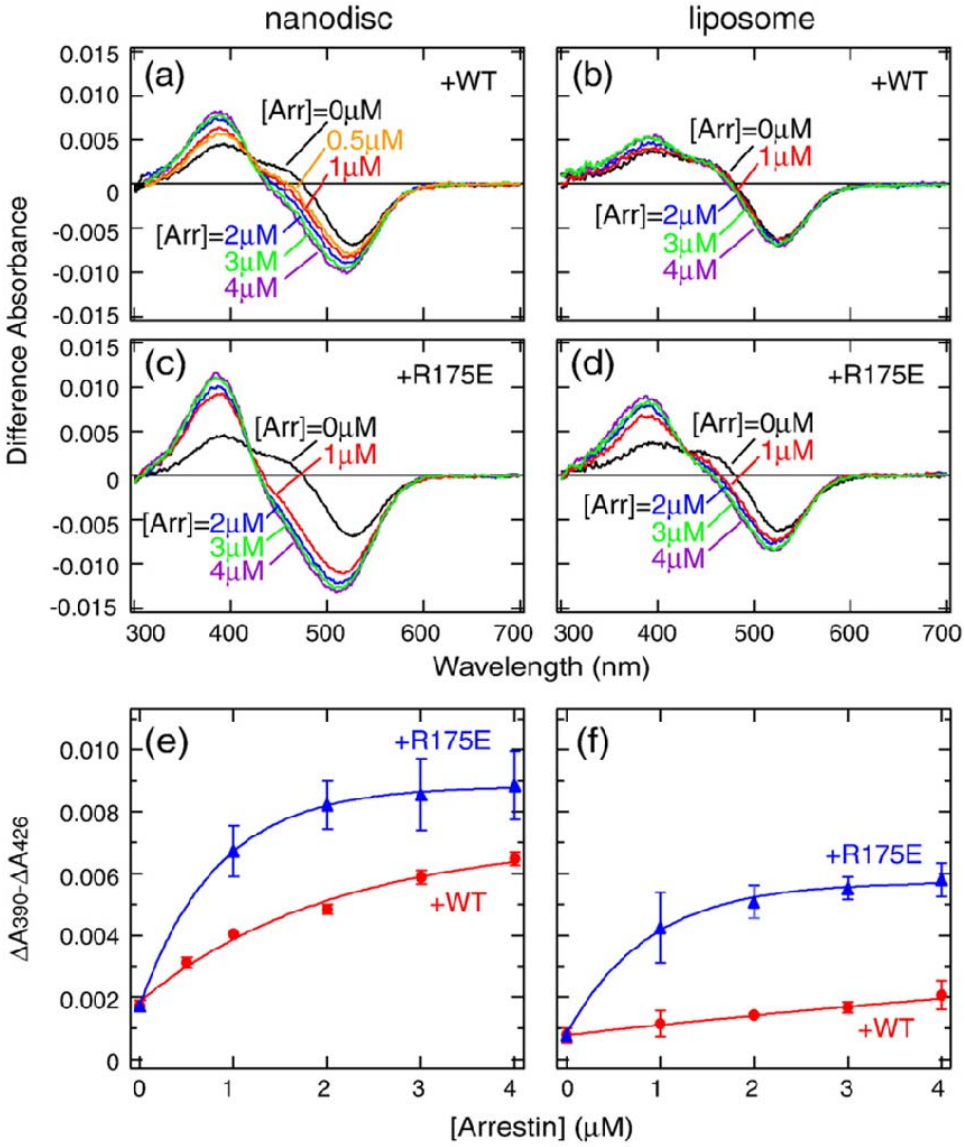

Fig.A1.4. Arrestin can bind to monomeric rhodopsin as indicated by extra meta-II formation induced by the presence of WT arrestin and the constitutively active arrestin mutant R175E.

(a–d) Difference absorption spectra, obtained by subtracting the spectra before irradiation from the spectra after irradiation in the presence or in the absence of visual arrestin. (a) Phosphorylated rhodopsin (625 nM) in nanodiscs with visual arrestin WT. (b) Phosphorylated rhodopsin (625 nM) in liposomes with visual arrestin WT. (c) Phosphorylated rhodopsin (625 nM) in nanodiscs with visual arrestin R175E mutant. (d) Phosphorylated rhodopsin (625 nM) in liposomes with visual arrestin R175E mutant. Arrestin concentration is indicated. Surprisingly, more extra meta-II formation was observed for arrestin binding to monomeric rhodopsin in nanodiscs than for arrestin binding to oligomeric rhodopsin in liposomes. (e and f) Plots of the difference absorbance between 390 nm and 426 nm (from the difference spectra) as a function of arrestin concentration. Red circles and blue triangles indicate values in the presence of visual arrestin WT and R175E mutant, respectively. (e) Nanodisc samples. (f) Liposome samples. The rhodopsin concentration was 625 nM. Spectra were recorded at 10 °C and pH 7.4. The lipid composition in nanodiscs is POPC/POPG at a ratio of 3:2. Error bars reflect SE for two separate experiments.

Fig.A1.5. Fluorescence and absorption spectroscopic properties of nanodiscs containing predominantly multiple rhodopsin molecules per nanodisc.

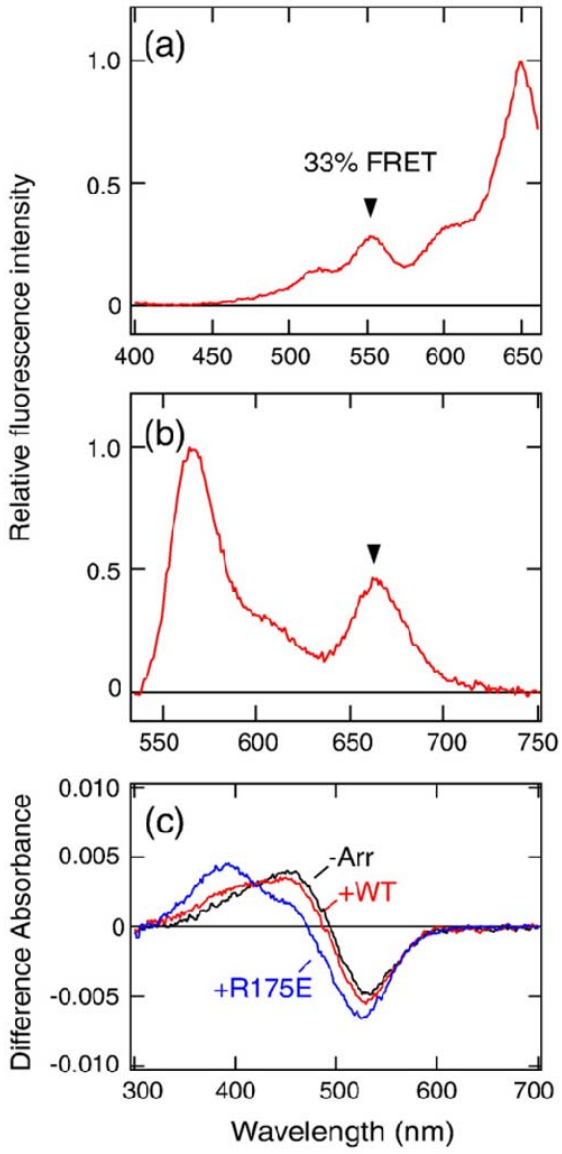

Fig.A1.5. Fluorescence and absorption spectroscopic properties of nanodiscs containing predominantly multiple rhodopsin molecules per nanodisc.

(a) Fluorescence excitation spectrum. The calculated FRET efficiency is 33%. For comparison, the spectra are normalized to a maximal fluorescence intensity of 1.0. (b) Fluorescence emission spectrum. The arrowheads in (a) and (b) indicate strong FRET signal. The spectra are normalized to a maximal fluorescence intensity of 1.0. (c) Difference absorption spectra (obtained by subtracting the spectra before irradiation from the spectra after irradiation) in the presence of visual arrestin WT (red line; "+WT"), in the presence of R175E mutant (blue line; "+R175E"), or in the absence of visual arrestin (black line; "−Arr") are shown. Rhodopsin and arrestin concentrations were 625 nM and 4 μM, respectively. Spectra were recorded at 10 °C and pH 7.4. The lipid composition in nanodiscs is POPC/POPG at a ratio of 3:2.

Fig.A1.6. A lipid with an acidic head group (POPG) enhances arrestin binding to monomeric rhodopsin in nanodiscs.

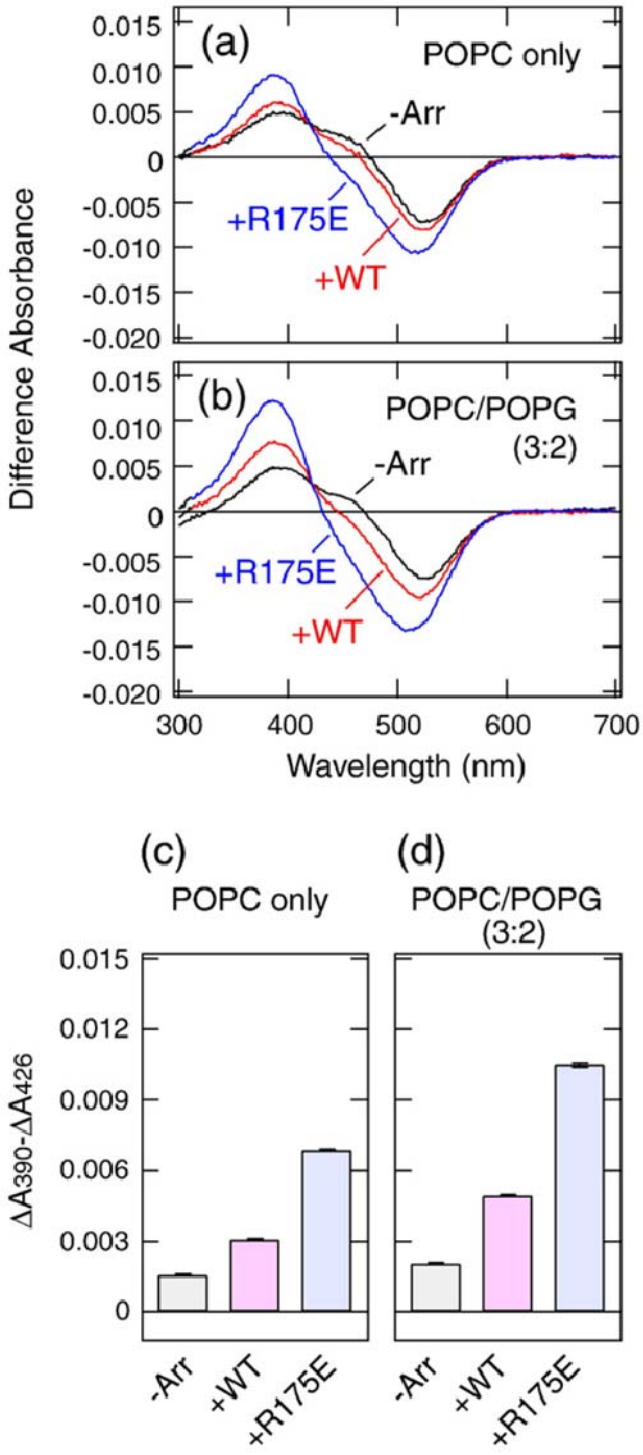

Fig.A1.6. A lipid with an acidic head group (POPG) enhances arrestin binding to monomeric rhodopsin in nanodiscs.

(a and b) Difference absorption spectra after irradiation minus difference absorption spectra before irradiation in the presence of visual arrestin WT (red line; "+WT"), in the presence of R175E mutant (blue line; "+R175E"), or in the absence of visual arrestin (black line; "−Arr") are shown. The relative amount of POPC/POPG is indicated. The rhodopsin and arrestin concentrations were 625 nM and 2 μM, respectively. Spectra were recorded at 10 °C and pH 7.4. (c and d) Difference absorbance between 390 nm and 426 nm in the difference spectra under the same conditions as in (a) and (b). The relative amount of POPC/POPG is indicated. Black, red, and blue bars indicate values in the absence of arrestin, in the presence of arrestin WT, and in the presence of R175E mutant, respectively. Error bars reflect SE for two separate experiments.

Fig.A1.7. β-Arrestin can also bind to monomeric rhodopsin in nanodiscs, as indicated by extra meta-II formation in the absorption spectra.

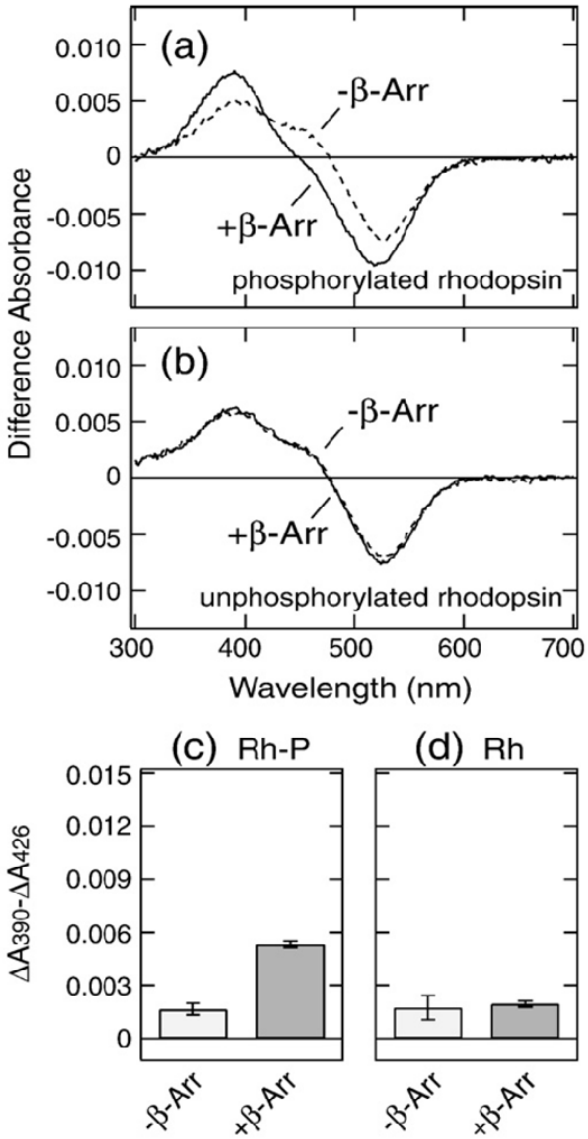

Fig.A1.7. β-Arrestin can also bind to monomeric rhodopsin in nanodiscs, as indicated by extra meta-II formation in the absorption spectra.

(a) Difference absorption spectra of phosphorylated rhodopsin (625 nM) in nanodiscs with (continuous line; "+β-Arr") or without (broken line; "−β-Arr") β-arrestin (2 μM). (b) Difference absorption spectra of unphosphorylated rhodopsin (625 nM) in nanodiscs with (continuous line; "+β-Arr") or without (broken line; "−β-Arr") β-arrestin (2 μM). Spectra were recorded at 10 °C and pH 7.4. The lipid composition in nanodiscs is POPC/POPG at a ratio of 3:2. (c and d) Difference absorbance between 390 nm and 426 nm in the difference spectra of phosphorylated (c; Rh-P) and unphosphorylated (d; Rh) rhodopsin under the same conditions as in (a) and (b). Light and dark gray bars indicate values in the absence of β-arrestin and in the presence of β-arrestin, respectively. Error bars reflect SE for two separate experiments.

Fig.A1.S1. Asp-N proteolysis indicates that most of the phosphorylated rhodopsin in liposomes is oriented with its cytoplasmic face on the outside.

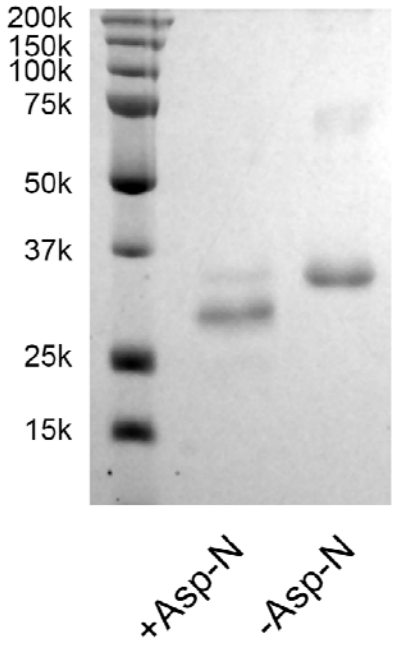

Fig.A1.S1. Asp-N proteolysis indicates that most of the phosphorylated rhodopsin in liposomes is oriented with its cytoplasmic face on the outside.

To determine the orientation of the rhodopsin in liposomes, we tested the liposome-bound rhodopsin samples for their susceptibility to proteolysis by Asp-N protease. Asp-N only cleaves rhodopsin at the C-terminus. Thus, for digestion to occur, the rhodopsin cytoplasmic face must be on the outside of the vesicles. SDS-PAGE analysis shows that liposome samples incubated with Asp-N protease ("+ Asp-N") show a shift in protein mobility compared with samples without incubation ("− Asp-N"), indicating that at least ~ 85% of the samples are oriented with the cytoplasmic faces exposed to the outside of the vesicles, and are accessible to the protease. This result is consistent with previous reports (Mansoor et al., 2006; Niu et al., 2002) using a similar approach. Proteins were visualized using Coomassie staining.

Fig.A1.S2. Constitutively active arrestin mutant R175E can bind to unphosphorylated monomeric rhodopsin in nanodiscs.

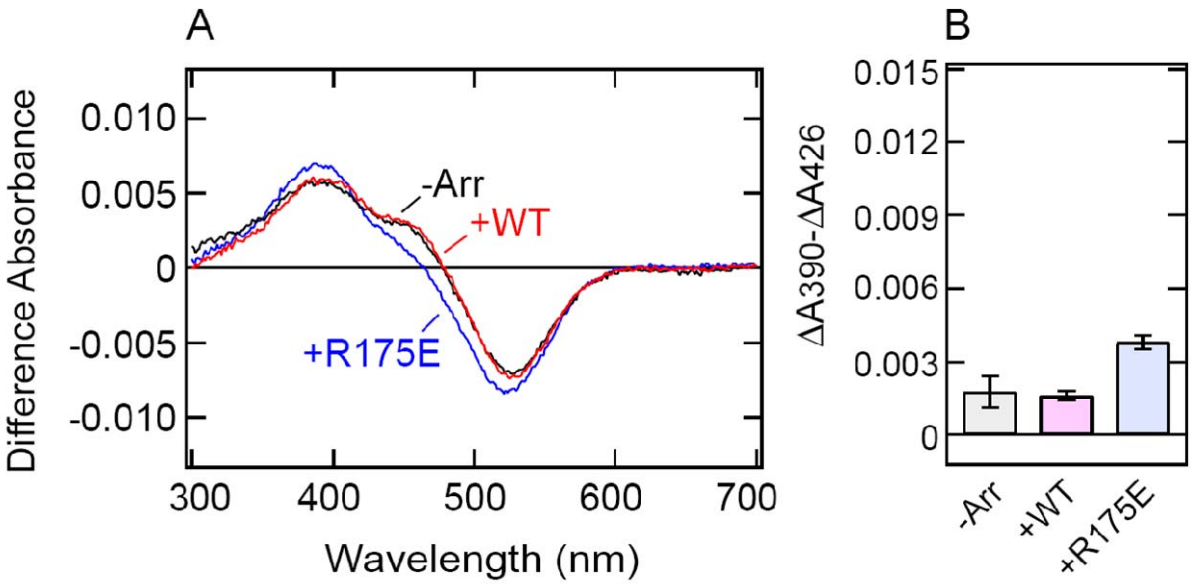

Fig.A1.S2. Constitutively active arrestin mutant R175E can bind to unphosphorylated monomeric rhodopsin in nanodiscs.

(a) Difference absorption spectra of unphosphorylated rhodopsin (625 nM) in nanodiscs with 2 μM visual arrestin WT (red line; "+ WT"), with 2 μM R175E mutant (blue line; "+ R175E"), or without arrestin (black line; "− Arr"). Spectra were recorded at 10 °C and pH 7.4. The lipid composition in nanodiscs is POPC/POPG at a ratio of 3:2. (b) Difference absorbance between 390 nm and 426 nm in difference spectra under the same conditions as in (a). Black, red, and blue bars indicate values in the absence of arrestin, in the presence of arrestin WT, and in the presence of R175E mutant, respectively. Error bars reflect SE for two separate experiments.

Appendix 2

Purification and Biochemical Analysis of CRIP1a, a Novel Inhibitor of CB1 Receptor Signaling

A2.1. Summary

In summary, we have described the expression and purification of CRIP1a, a novel inhibitor of the constitutive activity of CB1 receptor. Circular dichroism studies show that CRIP1a is a well-structured protein, with ~42% β-sheet content, and is quite stable in urea. Size exclusion chromatography indicates that the protein exists as a monomer in solution. The native cysteines of CRIP1a appear to surface accessible, but do not appear to form inter- or intra-molecular disulfides. Finally, we have found some preliminary conditions that show promising results for the crystallization of CRIP1a and the refinement of the conditions to obtain crystals of CRIP1a will help obtain crystal structure of the protein and get further insight to its function.

All the samples preparation and experimental analysis reported in this chapter were performed by the author of this dissertation, except for the Western blot which was done by Emily Lorenzen and the mass spectrometry which was done by Dr. Larry David at the Proteomics Core of OHSU.

A2.2. Introduction

The major psychoactive ingredient in marijuana, Δ^9-tetrahydrocannabinol (THC) belongs to a family of lipophilic molecules called cannabinoids. These compounds bind to and activate specific cell surface receptors, termed cannabinoid receptors, which are members of the G Protein-Coupled Receptor (GPCR) superfamily (Mukhopadhyay et al., 2002; Turu and Hunyady, 2010). Two types of cannabinoid receptors have been identified so far: CB1, which is present in the central nervous system, and CB2, which is predominantly present in immune cells and tissues (Demuth and Molleman, 2006; Diaz-Laviada and Ruiz-Llorente, 2005; Mackie, 2008). In addition, some "orphan" GPCRs have also been proposed to interact with endocannabinoids (Brown, 2007). The CB1 receptor is one of the most abundant GPCRs in the central nervous system and is present in high levels in the cortex, amygdala, cerebellum, basal ganglia and brainstem emetic centers – regions of the brain that are implicated in mediating the actions of cannabis, thus providing functional correlation with its localization (Herkenham et al., 1991). CB1 receptors show a predominant presynaptic localization in axons and axon terminals (Nyiri et al., 2005). These receptors signal via inhibitory G proteins G_i/G_o and lead to inhibition of adenylyl cyclase, N- and P/Q-type Ca^{2+} channels, inwardly rectifying potassium channels and various MAP kinases (Mukhopadhyay et al., 2002).

The CB1 receptor has been shown to exhibit a high level of basal signaling, even in the absence of an agonist, in both heterologous expression as well as in the case of endogenous receptors in neuronal cells (Bouaboula et al., 1997; Coutts et al., 2001; Landsman et al., 1997; MacLennan et al., 1998; Nie and Lewis, 2001a, b). Such basal signaling is indicated by the reduction in signaling in the presence of an inverse agonist. While the phenomenon of constitutive activity and any inverse agonism is generally observed under high receptor levels,

which is mostly seen in over-expression systems, the high levels of CB1 receptor expression in the brain might indicate the relevance of this phenomenon *in vivo*. An important effect of the constitutive activity of the receptor is constitutive endocytosis and recycling of the receptor, which leads to a predominantly intracellular localization (as much as 85%) of the receptor at steady state (Leterrier et al., 2004). As such, constitutive activity significantly affects cellular response to an agonist by limiting the number of receptors on the cell surface. However, much less is known about the regulation of the constitutive activity compared to traditional activation paradigms.

One insight into such regulation came from truncation studies on the CB1 receptor where it was found that truncation of the distal C-terminal tail at position 417 of CB1 receptor enhanced the constitutive activity of the receptors heterologously expressed in superior cervical ganglion (SCG) cells (Nie and Lewis, 2001a). This presented the possibility that either the distal tail adopted a conformation that inhibited receptor constitutive activity or that the region was bound by some protein, which then caused this inhibition. A yeast two-hybrid screen using the receptor tail as the bait discovered two new proteins that bound to this region (Niehaus et al., 2007). The two proteins were termed Cannabinoid Receptor Interacting Protein 1a and 1b (CRIP1a and 1b), and were alternative splice forms coded by the *cnrip1* gene. CRIP1a was shown to cause significant attenuation of CB1-mediated tonic inhibition of Ca^{2+} channels, while CRIP1b did not. CRIP1a did not show any effect on agonist binding or on agonist mediated inhibition of Ca^{2+} channels (Niehaus et al., 2007).

Being a relatively recently discovered protein, there is not a lot of information about the functional role of CRIP1a. However, one study report CRIP1a disrupted agonist-induced neuroprotection and conferred antagonist-induced neuroprotection, the mechanism of which is

unclear, but hypothesized to be linked to the PDZ ligand in CRIP1a (Stauffer et al., 2011). Also, in patients with sclerotic epilepsy, the mRNA levels of both CB1 and CRIP1a decreased, indicating a possible role for CRIP1a mediated modulation of CB1 receptor function in the pathogenesis of or in response to epilepsy (Ludanyi et al., 2008). While evidence for the functional role of CRIP1a is beginning to appear, there is as yet no biochemical or biophysical information about the protein.

We set out to explore CRIP1a structure-function parameters. Our first focus was developing a simple way to purify large amounts of protein in a tag-free form to also enable the generation of specific antibodies that can be used to make affinity columns and fish out potential interacting partners.

We report here the purification of CRIP1a from a recombinant bacterial expression system, using a recent approach based on the picomolar affinity of subtilisin for its prodomain (Ruan et al., 2004), which has been previously used to purify G_{α} and arrestin, among other proteins (Abdulaev et al., 2005; Huang et al., 2012; Ruan et al., 2004; Tsukamoto et al., 2010). The expression/purification system utilizes the interaction between a mutant prodomain (ProR8FKAM) of subtilisin BPN' and the mature subtilisin BPN' S189 enzyme. Circular dichroism spectroscopy of the purified CRIP1a shows the protein to be well-structured with high beta sheet content and high stability to urea. We analyzed the behavior of the protein on a size exclusion column and found it to be mostly monomeric, and cysteine labeling studies indicate that the two native cysteines in the protein are solvent accessible and do not appear to be involved in inter- or intra-molecular disulfide formation. Finally, preliminary crystallization screens provide starting conditions which need further optimization to obtain CRIP1a crystals for structure determination.

A2.3. Materials and Methods

Materials

All restriction enzymes, ligase and DNA polymerase were from New England Biolabs. Tissue culture media was purchased from HyClone, while polyethyleneimine was from Polysciences, Inc. n-Dodecyl-β-D-maltoside (DM) was purchased from Anatrace. The fluorophores monobromobimane (mBBr) and Alexa 594 were purchased from Invitrogen, while Cy3 maleimide was from GE Healthcare. BL21-CodonPlus(DE3)-RP strain of *E. coli* was purchased from Agilent Technologies. Yeast extract and BactoTryptone were from BD Biosciences. Protease Inhibitor Cocktail (EDTA Free) was purchased from Roche Diagnostics. Profinity eXact^{TM} and HiTrap Heparin^{TM} columns were from Bio-Rad and GE Healthcare Life Sciences respectively. Amicon Ultra protein concentrators (3kD cut-off) and nitrocellulose filters (0.45um) were from Millipore. Size exclusion molecular weight standards blue dextran, bovine serum albumin and carbonic anhydrase were from Sigma-Aldrich, while ovalbumin and myoglobin were from Bio-Rad. Cuvettes were purchased from Uvonics (Plainview, NY). Superdex 200 media was obtained from GE Healthcare. CRIP1a polyclonal antibody was from Abcore USA. Goat anti-rabbit secondary antibody coupled with Alexa Fluor 680 was purchased from Invitrogen. All other chemicals and reagents were obtained from Sigma-Aldrich.

Cloning, expression and purification of CRIP1a

The coding sequence of human CRIP1a was optimized for bacterial expression using the online tool JCat (www.jcat.de/*)* (Grote et al., 2005). A codon for alanine, GCC, was attached before the initiator methionine codon ATG, to introduce an NcoI site (CCATGG) at the 5'- end of the gene and an XhoI site (CTCGAG) was inserted after the terminator codon TGA. The

restrictions sites EcoRI, SacI, SpeI, NdeI, PsiI were introduced for cloning purposes through silent mutations in the coding sequence, using the online Gene Design tool from Johns Hopkins University (http://genedesign.thruhere.net/gd/) (Richardson et al., 2006). The DNA sequence was synthesized by Celtek Genes, Nashville, TN. For purification purposes, the gene was expressed as a fusion construct with the subtilisin prodomain at its N-terminus (Abdulaev et al., 2005; Huang et al., 2012; Ruan et al., 2004; Tsukamoto et al., 2010). The synthetic gene was sub-cloned into a modified pG58 vector, termed pG58ABS, which was modified to introduce an NcoI site after the subtilisin prodomain sequence. The CRIP1a gene was sub-cloned into the pG58ABS vector within NcoI and XhoI restriction sites.

The protein was expressed in BL21-CodonPlus(DE3)-RP strain of *E. coli* after induction tests at 16^{o}C, 25^{o}C and 37^{o}C to find conditions for obtaining soluble CRIP1a. BL21(DE3)-RP cells harboring the pG58 expression vector containing the prodomain/CRIP1a fusion were grown in 1L of LB media in the presence of 100 μg/ml ampicillin at room temperature to A_{550} of 0.6, and then induced with 100 μM IPTG for 16hr at 25^{o}C. The cell pellet was resuspended in 50 mM Tris–phosphate, pH 7.2, containing 50 mM NaCl, 5 mM β-mercaptoethanol, 0.1 mM PMSF and 1X protease inhibitor cocktail and then disrupted by French press. The supernatant obtained by centrifugation of the cell lysate at 100,000 x g for 45 min was loaded onto a 5mL Profinity eXact column. The column was washed with 20 column volumes of 100 mM sodium phosphate, pH 7.2 and 20 column volumes of 100 mM sodium phosphate, 300 mM sodium acetate, pH 7.2. The column was briefly washed with 3 column volumes of 100 mM sodium phosphate, pH 7.2 and the cleavage of CRIP1a from the prosubtilisin tag was initiated by passing one column volume of 100 mM sodium phosphate, pH7.2 containing 100 mM sodium fluoride (elution buffer). The fluoride-mediated cleavage reaction was allowed to occur for 2hr on ice. Tag-free CRIP1a was

eluted off the column by passing 5 column volumes of the elution buffer and was further purified by cation exchange chromatography using a 1ml HiTrap Heparin column. The resulting protein was >95% pure, as assessed by SDS-PAGE.

Confirmation of CRIP1a identity by western blot and mass spectrometry

The purified CRIP1a was subjected to western blot analysis using a rabbit polyclonal antibody. The blot was incubated with the primary antibody at 1:3000 dilution for overnight at 4^{o}C and then probed with a goat anti-rabbit secondary antibody coupled with Alexa Fluor 680 at 1:5000 dilution for 1 hour at room temperature. The blot was visualized using the Odyssey LiCOR system.

For mass spectrometry, the gel band corresponding to CRIPa was excised from a Coomassie stained SDS-PAGE gel, reduced with 10mM DTT and then alkylated with 55mM iodoacetamide. The gel spots were then trypsinized with 10mg/ml proteomics grade trypsin (Sigma-Aldrich). After overnight digestion at 37^{o}C, the excess trypsin solution was removed and peptides extracted from the gel, vacuum dried and rehydrated in 40 ml of 5% formic acid in preparation for mass spectrometric analysis. Protein digests were analyzed by LC-MS/MS using an Agilent 1100 series capillary LC system (Agilent Technologies Inc, Santa Clara, CA) and an LTQ Velos linear ion trap mass spectrometer (Thermo Scientific, San Jose, CA). Peptides were identified from collected MS/MS spectra using the program Sequest (Thermo Scientific) using a human Uniprot database supplemented with the CRIPa sequence. Thresholds for peptide and protein probabilities were set at 95 and 99%, respectively, as specified using the Peptide Prophet algorithm (Keller et al., 2002) and the Protein Prophet algorithm (Nesvizhskii et al., 2003) respectively, and required a minimum of 2 peptides matched to each protein entry.

Circular dichroism spectroscopy

Purified CRIP1a was diluted to 0.2mg/ml in 10mM Tri-HCl, 100mM NaCl, 2mM EDTA, pH 7. The CD measurements were taken using AVIV 215 spectrophotometer. A 1mm path length quartz cuvette was used to measure the spectra. The spectra were recorded at 4^{o}C from 260nm to 195nm in 0.5nm steps with 3s averaging. The reported spectrum represents the average of three independent scans and was buffer subtracted.

For the urea stability assay, the molar ellipticity was recorded at 225nm, while urea at 8M (made in 10mM Tris-HCl, 100mM NaCl, 2mM EDTA, pH7) was added to CRIP1a in a stepwise manner to increase the urea concentration from 0M to 6M in 40 steps at 4^{o}C. The sample was continuously mixed with a magnetic stirrer for 300s after each urea addition, to allow for complete mixing of urea and equilibration of the protein under the conditions.

Size exclusion chromatography

150ul of CRIP1a at 40μM was injected onto a 22.5ml bed volume of Superose 200 column at 20^{o}C. The buffer flow rate was 0.5ml/min. The elution off the column was monitored by an in-line UV-vis absorbance spectrophotometer. CRIP1a was applied to the column either in the absence of DTT or after incubation with 1mM DTT for 1 hour on ice. The samples were brought to 20^{o}C before loading on the column. The molecular weight corresponding to the elution peaks was determined based on the calibration of the column with five molecular weight standards: blue dextran (2000kDa, void volume), bovine serum albumin (BSA, 66kDa), ovalbumin (44kDa), carbonic anhydrase (29kDa) and myoglobin (17kDa).

Labeling of native cysteines

The accessibility and oxidation oxidation state of the two native cysteines of CRIP1a were assessed by incubating the protein with three different thiol-reactive fluorophores – monobromobimane (mBBr), Alexa 594 maleimide and Cy3 maleimide. For labeling with mBBr, 80-100μM CRIP1a in 20mM HEPES, 140mM NaCl, pH7.2 was incubated with 10X excess of mBBr overnight at 4^{o}C. For labeling with the fluorophores with maleimide reactive group (Alexa 594 and Cy3), 50μM MOPS pH6.5 was added to lower the pH of the reaction mix to ~6.5 to avoid amine reactivity and maleimide ring opening (Mansoor et al., 2010), and the labeling reaction was carried out overnight with 5X excess fluorophore at 4^{o}C. The labeling reactions were quenched by adding 20mM L-cysteine and incubating the samples on ice for 30min. Free label was removed by passing the protein through two Bio-Spin 30 columns. The amount of free label was determined as described earlier (Mansoor and Farrens, 2004). Briefly, this assay involves precipitating the protein with 10% tricholoroacetic acid (TCA) on ice for 30 min and spinning down the precipitated protein by centrifugation, so that any fluorescence seen in the supernatant is from unattached free label. The percent labeling was calculated based on the extinction coefficients of CRIP1a and the fluorophores - CRIP1a: ε_{280} = 27,000 M $^{-1}$ cm^{-1}; mBBr: ε_{380} = 5,000 M $^{-1}$ cm^{-1}; Cy3: ε_{550} = 150,000 M $^{-1}$ cm^{-1}; Alexa594: ε_{594} = 90,000 M $^{-1}$ cm^{-1}. The contribution of the fluorophore to the absorbance at 280nm was subtracted to determine the protein concentration (Mansoor et al., 2010; Mansoor et al., 2002).

Crystallization screens

Crystallization screens were set up with freshly purified CRIP1a. Six different commercially available crystal screens (Crystal Screen and Crystal Screen 2 from Hampton

Research and Wizard I, Wizard II, Wizard III and Wizard IV from Emerald Biosystems) were set up with 20mg/ml CRIP1a using the mosquito® Crystal system (TTP Labtech) at two different temperatures (4°C and 25°C). A few of the conditions that seemed promising include 0.1 M HEPES sodium pH 7.5, 0.2 M sodium citrate tribasic dihydrate, 30% v/v (+/-)-2-Methyl-2,4-pentanediol; 0.1 M sodium acetate trihydrate pH 4.6, 0.01 M cobalt(II) chloride hexahydrate, 1.0 M 1,6-hexanediol, and 0.1M Tris-HCl pH 8.0, 40% (v/v) 2-methyl-2,4-pentanediol. A number of conditions containing diols like 1,6-hexanediol (1,6-HD) and (+/-)-2-methyl-2,4-pentanediol (MPD) or tertiary alcohols like t-butanol yielded promising microcrystals. These conditions can be used to further refine the crystallization conditions to get crystals of CRIP1a for structure determination. Some of the refinements include addition of different salts – NaCl, $MgCl_2$, NH_4Cl, $MgSO_4$, $CoCl_2$, $LiSO_4$, $(NH_4)_2SO_4$, CH_3COONH_4, CH_3COONa and $(CH_3COO)_2Mg$ – or polyethyleneglycol (PEG4000 or PEG8000), in combination with one of 1,6-HD, MPD or t-butanol as the precipitant in pH 5.5 – pH 8.5 range.

A2.4. Results and Discussion

Purification of CRIP1a

To enable biophysical and structural studies of CRIP1a, we report here a quick, two-step purification scheme. We used a modified pG58 expression vector containing the proR8FKAM fusion and immobilized S189 subtilisin BPN' for the expression and purification of tag-free CRIP1a (Ruan et al., 2004), which has earlier been used for the purification of G proteins and arrestin (Abdulaev et al., 2005; Huang et al., 2012; Tsukamoto et al., 2010) and is commercially available as the Profinity eXact system from Bio-Rad. The cloning of the CRIP1a coding sequence to the 3'-end of the prodomain was facilitated by the creation of an NcoI site, which

inserted an extra Ala residue between the prodomain and CRIP1a (Fig. A2.1a). However, this insertion is not expected to disrupt the recognition or cleavage of the prodomain by the mature subtilisin enzyme, based on the manufacturer's literature.

An induction test was carried out to determine conditions for the expression of CRIP1a in the soluble form (Fig. A2.1b). At 37^{o}C, while the expression is quite high, most of the CRIP1a fusion protein appears in the pellet after cell lysis, likely going into inclusion bodies. The best condition seems to be induction with 100μM IPTG at 25^{o}C, which yields the highest amount of soluble CRIP1a.

SDS-PAGE analysis of the purification fractions shows that a lot of the fusion protein is present in the flow through from the Profinity eXact column, suggesting that a lot of the fusion protein may not be in a conformation suitable for recognition and/or cleavage by the subtilisin enzyme on the immobilized on the column, since the amount of protein applied was below the column binding capacity. The wash steps removed most of the impurities and the tag-free protein (lower molecular weight than the fusion protein) eluted after triggering prodomain cleavage by the addition of fluoride ions. The protein was relatively pure, but had a high absorbance at 260nm (data not shown), indicating the presence of nucleotides or nucleotide-binding proteins. A subsequent heparin column chromatography step cleaned up the impurities and the protein, and also did not have a strong 260nm absorbance. Our final yield for the purification is 2-2.5mg CRIP1a per liter of culture.

Western blot analysis with a commercially available CRIP1a polyclonal antibody confirmed the identity of the purified protein as CRIP1a (Fig. A2.1d). The blot shows that the antibody can detect as little as 2ng of CRIP1a. Also, peptide mass fingerprinting further

confirmed the protein as CRIP1a and showed almost complete coverage of the amino acid sequence of CRIP1a in the mass spectrometric profile (Fig. A2.1e).

It is worth noting that we found CRIP1a to be quite "sticky". Simply pipetting the protein caused its absorbance to go down, indicating that the protein was sticking to the pipettes (Fig. A2.S2). We found that adding a small amount (0.01%) of detergent like n-dodecyl-β-D-maltoside prevented this problem of CRIP1a sticking.

Secondary structure and stability

Circular dichroism (CD) spectroscopy was used to estimate the secondary structure present in CRIP1a. The averaged spectrum shows a strong CD signal at ~218nm (Fig.A2.2a), qualitative indicator of high beta sheet content (Greenfield, 2006). The estimation of the secondary structure content using DichroWeb (Whitmore and Wallace, 2004) showed that CRIP1a has 9% α-helical content, 42% β-sheet content and 48% random coils. This shows the protein to be well structured. We then tested the stability of the protein by measuring using CD to measure the secondary structure of CRIP1a upon titration of urea as a denaturant. Urea likely causes protein denaturation by binding to hydrophobic surfaces of the protein, displacing water from the hydration shell (Hua et al., 2008) and/or by disrupting the hydration of hydrophilic parts of a protein, while preferentially binding to those regions itself via hydrogen bonds (Bennion and Daggett, 2003). CRIP1a is stable in up to ~3.5M urea and shows a single step denaturation with a transition mid-point of ~4.5M urea (Fig. A2.2b). These data indicate that the protein is quite tightly structured and relatively resistant to the disruption of hydrophobic interactions (and possibly hydrophilic interactions, too) in the protein by urea.

Oligomerization and cysteine oxidation status of CRIP1a

Cysteines act as redox sensors in many proteins and the oxidation status of cysteines can significantly affect the structure and function of proteins. Through their reactive sulphur, cysteines can form disulfide binds with other cysteine molecules and assist in protein folding by destabilizing the unfolded form (Hogg, 2003; Thornton, 1981). Disulfide bonds can also help in protein dimerization (Burke and Stern, 1998; Nemoto et al., 2006; Neo et al., 2010), thus affecting their structure and function. The reactive thiol in cysteine can be post-translationally modified by prenylation, glycosylation and palmitoylation, and affect protein structure, localization and function (Klomsiri et al., 2011). Given the importance of cysteines in protein structure and function, we tested the oxidation status of the native cysteines of CRIP1a.

We first tested if CRIP1a undergoes disulfide-mediated oligomerization. We performed size exclusion chromatography on purified CRIP1a and found that the protein runs predominantly at ~16kD, in either the absence or presence of a reducing agent (DTT) (Fig. A2.3a). This indicates that CRIP1a is a monomer in solution at least under the conditions tested. Similar result was obtained by SDS-PAGE analysis of CRIP1a (Fig. A2.3b). Both under reducing and non-reducing conditions, the protein migrated essentially as a monomer. In the absence of the reducing agent, though, a small fraction of the protein did run at ~42kD, likely as a dimer. These results indicate that the cysteines are likely not involved in intermolecular disulfide bonds.

We also studied the accessibility and oxidation status of the cysteines by testing their reactivity to thiol-reactive fluorophores like monobromobimane (mBBr), Alexa-594 maleimide and Cy3 maleimide. As shown by the in-gel fluorescence in Fig. A2.3c, the protein showed labeling with mBBr. Both the in-gel fluorescence data (Fig. A2.3c) and the fluorescence

emission spectra (Fig. A2.3d) show that even after TCA precipitation, there is no free, unattached label in solution – in other words, the label stays specifically attached to the protein. The labeling percentage was determined from the absorbance spectra of the labeled protein (Fig. A2.3e). All the three thiol-reactive fluorophores labeled CRIP1a to the same extent of ~200% or 2 labels per CRIP1a (Fig. A2.3f). Since CRIP1a has two native cysteines, it appears that both the cysteines get labeled, showing that they are quite reactive and are quite solvent accessible, too.

Binding of CRIP1a to the CB1 tail peptide

CRIP1a S-tag fusion protein was shown to bind immobilized GST-tagged CB1 C-terminal tail (Niehaus et al., 2007). We tried to measure CRIP1a binding to CB1 C-terminal tail by various methods but have not succeeded so far (data not shown). These methods have included: intrinsic Trp fluorescence of CRIP1a, fluorescence anisotropy of GFP-CB1 tail fusion, native gel retardation assay for CRIP1a binding to GFP-CB1 tail and the pulldown of CRIP1a by hexahistidine-tagged GFP-CB1 tail fusion protein attached to nickel beads. However, either due to low affinity or due to buffer conditions not being favourable for the binding, we have not been able to see binding of CRIP1a to the CB1 C-terminal tail so far.

Crystallization screens show formation of microcrystals

Our motivation behind the purification of milligram quantities of CRIP1a was to perform biophysical and structural studies. Crystal structure of CRIP1a will enable us to find domains and structural homologs by comparison of the crystal structure with those in protein structure databases using tools such as Dali (Holm et al., 2006). To this end, we set out to determine optimal conditions to crystallize CRIP1a for structure determination by X-ray crystallography. We first performed a coarse screening of conditions using commercially available random sparse

matrix screens - Crystal Screen and Crystal Screen 2 from Hampton Research and Wizard I, II, III and IV from Emerald Biosystems. We screened the crystallization conditions using 20mg/ml CRIP1a at two different temperatures (4^{o}C and 25^{o}C). A number of conditions came up as promising hits, showing the formation of microcrystals, which appeared after a long incubation (~3-4 weeks) (Fig. A2.4). Most of these promising conditions have alcohols like 1,6-hexanediol, (+/-)-2-methyl-2,4-pentanediol or t-butanol as the precipitant. The conditions need further refining to obtain bigger crystals of CRIP1a, which can be used for X-ray crystallography.

Fig. A2.1. CRIP1a expression and purification.

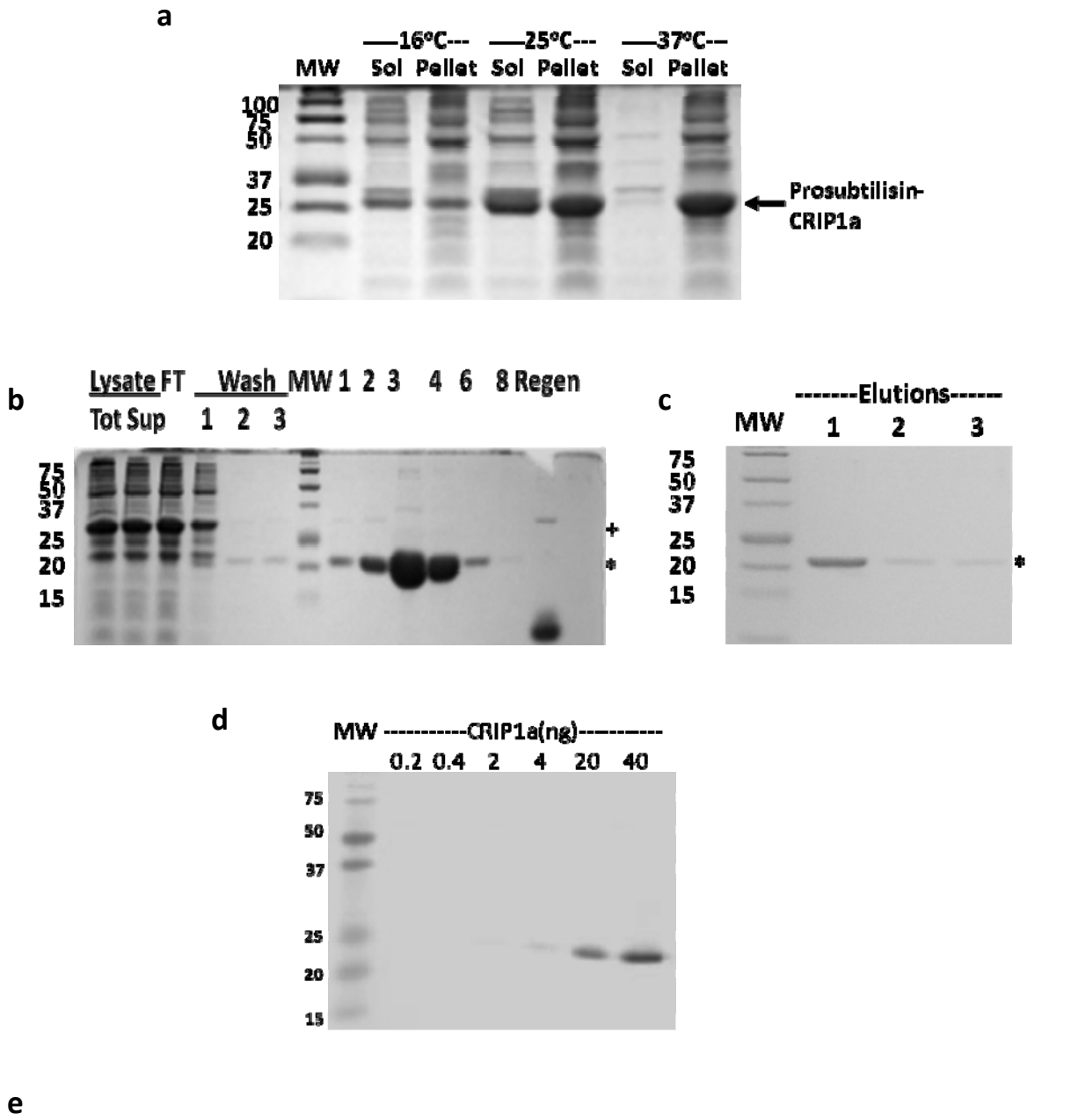

e

[CRIP1a.]
22 unique peptides, 36 unique spectra, 261 total spectra, 159/164 amino acids (97% coverage)

MGDLPGLVRL SIALRIQPND GPVFYKVDGQ RFGQNRTIKL LTGSSYKVEV
KIKPSTLQVE NISIGGVLVP LELKSKEPDG DRVVYTGTYD TEGVTPTKSG
ERQPIQITMP FTDIGTFETV WQVKFYNYHK RDHCQWGSPF SVIEYECKPN
ETRSLMWVNK ESFL

Fig. A2.1. CRIP1a expression and purification.

CRIP1a was expressed as a fusion protein with an N-terminal prosubtilisin tag and purified using an affinity column with immobilized mutant subtilisin mature enzyme (Profinity eXact from Bio-Rad) followed by cation exchange chromatography using a heparin column. (a) Induction of CRIP1a tested at three different temperatures: 16^{o}C, 25^{o}C and 37^{o}C to find conditions for the expression of soluble CRIP1a. Matched amounts of lysate of cultures induced with 100μM IPTG were run on a 15% tricine gel. The 16^{o}C and 25^{o}C cultures were harvested after 16 hr, while the 37^{o}C culture was harvested at 4.5 hour post induction. 25^{o}C expression yields the maximum amount of soluble prosubtilisin-CRIP1a fusion protein in the soluble fraction. (b) Purification of CRIP1a expressed in BL21(DE3)-RP cells at 25^{o}C with 100μM IPTG using Profinity eXact column. The load, flow through (FT), wash and elution fractions off the Profinity column were run on a 15% tricine gel. The "+" mark indicates the position of the fusion protein, while the "*" mark indicates the position of the tag-free CRIP1a protein eluted in the elution fractions 1-8. "Regen" lane contained the fraction collected during regeneration of the column, and shows the cleaved subtilisin prodomain at ~8kDa. (c) The elution fractions off the Profinity column were further purified using a cation exchange chromatography step, in which the pooled fractions were loaded on a heparin column and eluted with a short NaCl gradient. The elution fractions in Lanes 2-4 were >95% pure. (d) The purified CRIP1a was verified by western blot analysis using a CRIP1a polyclonal antibody with which we could detect 2ng CRIP1a. (e) Purified CRIP1a was subjected to a tryptic digestion and analyzed by peptide mass fingerprinting mass spectrometry. Coverage map made using the program Scaffold (Proteome Software, Inc., Portland, OR) shows the peptides that were identified highlighted in yellow. The modified C and M residues are indicated in green due to alkylation and oxidization, respectively. Residues that

were not represented in the mass spectra are not colored. The sequence coverage map indicates that almost all of CRIP1a peptides were recovered (94%), again confirming the identity of the purified protein as CRIP1a.

Fig. A2.2. Secondary structure and stability.

a.

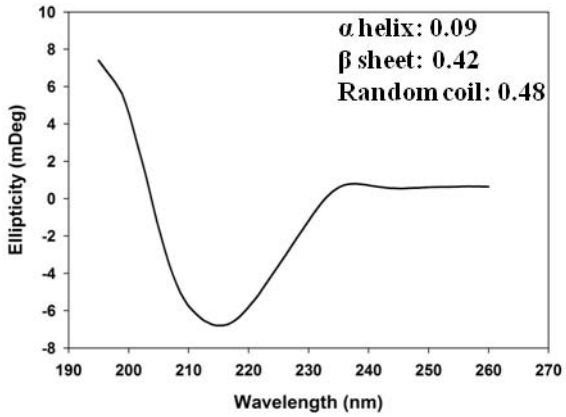

b.

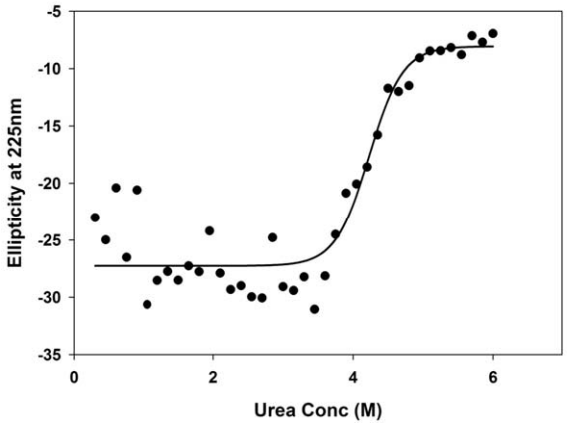

Fig. A2.2. Secondary structure and stability.

Circular dichroism spectroscopy was performed to determine the secondary structure content and stability of CRIP1a. (a) Far UV Circular Dichroism spectrum of 0.2mg/ml CRIP1a was measured from 260nm to 195nm at 4^{o}C. The spectrum is representative of three different scans. The fractional secondary structure content of CRIP1a from deconvolution of the data by the DichroWeb server was 9% α-helix, 42% β-sheet and 48% random coils (Whitmore and Wallace, 2004). (b) The measured change in ellipticity of CRIP1a at 225nm was plotted as a function of urea concentration, which was increased from 0 to 6M urea, by adding a precise volume of 8M urea in 40 steps at 4^{o}C. The data plotted were corrected for dilution due to urea addition. These results indicate CRIP1a is quite stable.

Fig. A2.3. Oligomerization and cysteine oxidation status of CRIP1a.

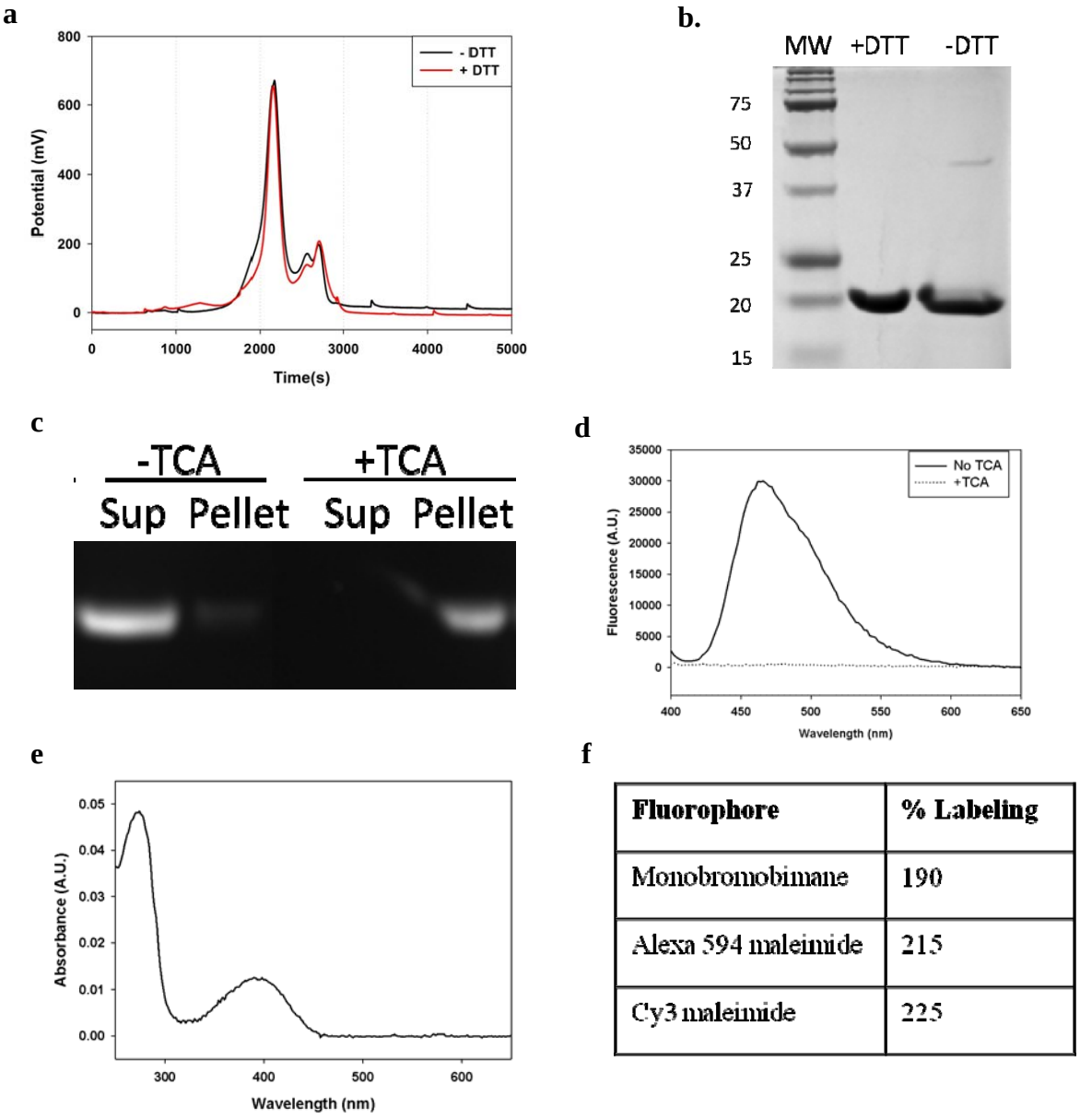

f

Fluorophore	% Labeling
Monobromobimane	190
Alexa 594 maleimide	215
Cy3 maleimide	225

Fig. A2.3. Oligomerization and cysteine oxidation status of CRIP1a.

The oligomeric status and oxidation status of the two native cysteines of CRIP1a was assessed by the effect of reducing agents on the mobility of the protein on a size exclusion column and SDS-PAGE, as well as by the reactivity of the protein to thiol-reactive fluorophores. (a) Purified CRIP1a was analyzed by size exclusion chromatography using a Superose 200 column. Comparison to molecular weight standards blue dextran (2000kDa, void volume), BSA (66kDa), ovalbumin (44kDa), carbonic anhydrase (29kDa) and myoglobin (17kDa), the molecular weight of CRIP1a was determined to be ~16kDa. The presence or absence of 1mM DTT did not considerably change the CRIP1a elution profile, suggesting the absence of any intermolecular disulfides. (b) CRIP1a was also tested for any intermolecular disulfide formation by SDS-PAGE analysis in the absence and presence of DTT. CRIP1a ran predominantly as a monomer under both reducing and non-reducing conditions. (c) In-gel fluorescence showing the labeling of CRIP1a with mBBr. Unreacted free label was removed by size exclusion chromatography and the labeled protein was centrifuged in the absence or presence of trichloroacetic acid as the precipitating agent. The supernatant and precipitate were run on a 15% tricine gel and in-gel fluorescence was monitored to visualize the labeled protein. (d) Quantitative assessment of the amount of free label was done by measuring the fluorescence emission of the labeled protein and that of the supernatant after TCA precipitation to estimate the % free label (Mansoor and Farrens, 2004). No free label was detected, as seen by the lack of a fluorescence emission at 465nm. (e) Absorbance spectrum of mBBr-labeled CRIP1a after the removal of free label. The peak at 390nm was used to determine the concentration of the label and the absorbance at 280nm (after subtracting the contribution of mBBr absorbance at 280nm) was used to determine the concentration of the protein. (f) The amount of label incorporated

expressed as percent of protein concentration. The table shows the percent labeling of CRIP1a by three different fluorophores – mBBr, Alexa 594 lameimide and Cy3 maleimide. All the three fluorophores showed ~200 % labeling, suggesting that both the cysteines of CRIP1a were labeled with the fluorophores.

Fig. A2.4. Screening of conditions for the crystallization of CRIP1a.

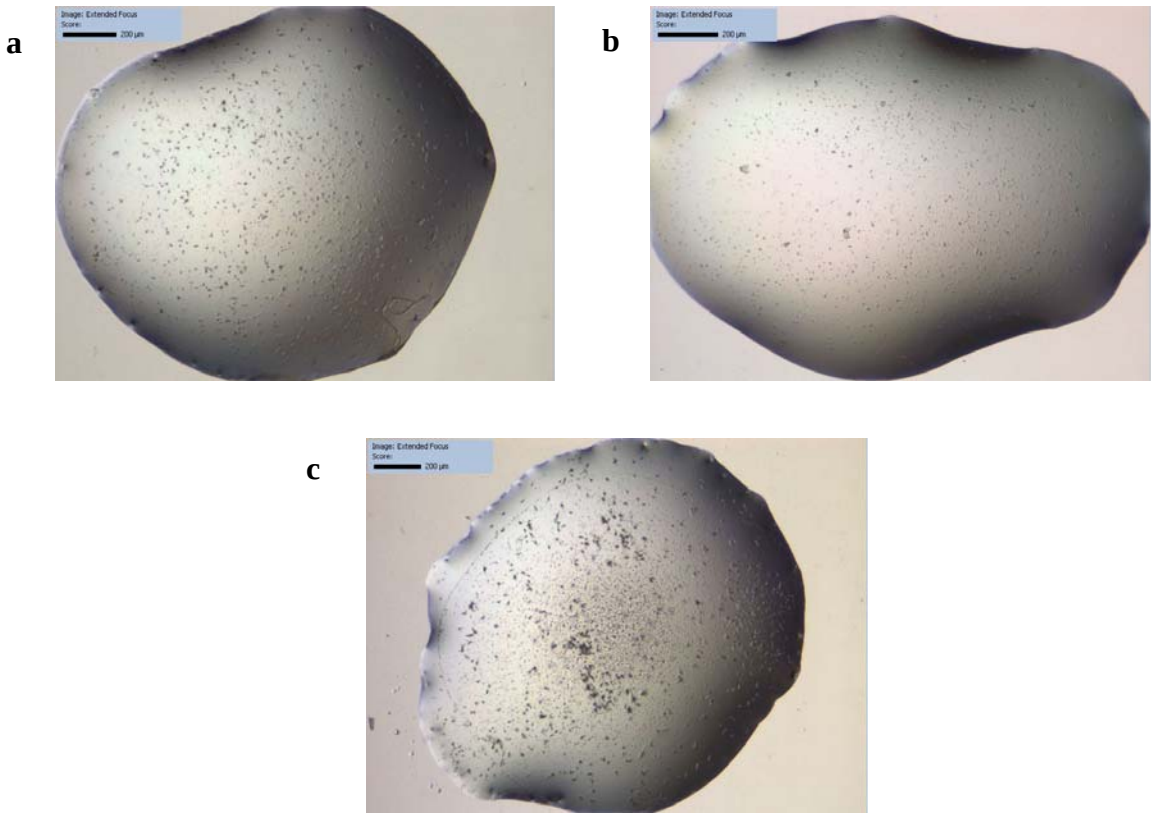

Fig. A2.4. Screening of conditions for the crystallization of CRIP1a.

Various commercially available crystallization screens (Crystal Screen and Crystal Screen 2 from Hampton Research and Wizard 1-4 from Emerald Biosystems) were tested for crystallization of CRIP1a for a preliminary coarse screening of crystallization conditions. 20mg/ml CRIP1a was used in this screens that were set up using the mosquito® Crystal system and incubated at 4^{o}C or 25^{o}C. A number of conditions at 4^{o}C yielded micro-crystals which have potential to yield bigger crystals upon further refinement of the conditions and/or constructs. Representative images are shown of the drops with microcrystals. The conditions in the wells in which these microcrystals formed are: (a) Crystal Screen: 0.1 M HEPES sodium pH 7.5, 0.2 M sodium citrate tribasic dihydrate, 30% v/v (+/-)-2-Methyl-2,4-pentanediol, (b) Crystal Screen 2: 0.1 M sodium acetate trihydrate pH 4.6, 0.01 M cobalt(II) chloride hexahydrate, 1.0 M 1,6-hexanediol, and (c) Wizard 4: 0.1M Tris-HCl pH 8.0, 40% (v/v) 2-methyl-2,4-pentanediol .

Fig. A2.S1. CRIP1a construct and purification scheme.

a

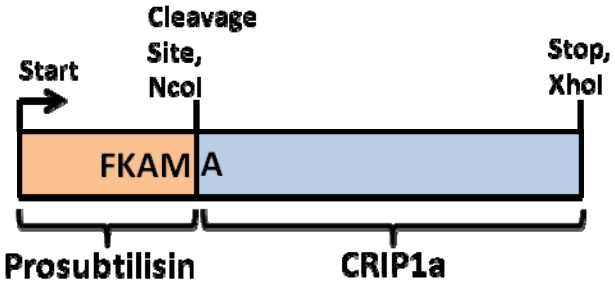

b

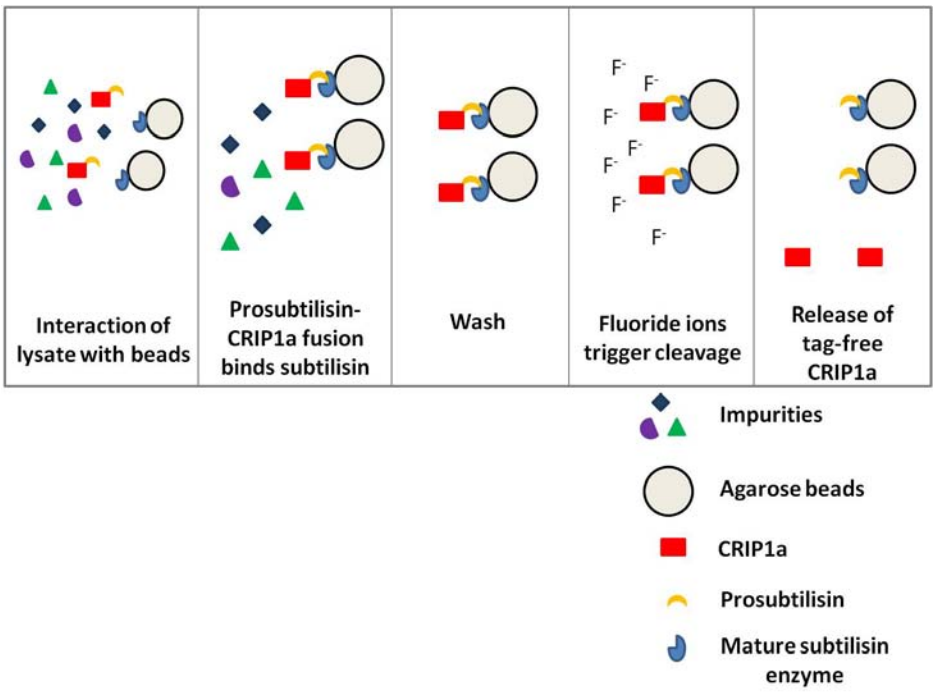

Fig. A2.S1. CRIP1a construct and purification scheme.

CRIP1a was purified making use of the affinity between the subtilisin prodomain (prosubtilisin) and the mature enzyme (Abdulaev et al., 2005; Ruan et al., 2004; Tsukamoto et al., 2010). (a) CRIP1a was expressed as a fusion construct with prosubtilisin fused to its N-terminus in pG58ABS vector, (a variant of pG58 vector with an NcoI site introduced at the junction of the prodomain and an alanine codon introduced in the middle to maintain the reading frame). The resultant construct has prosubtilisin ending with FKAM and the tag-free, cleaved CRIP1a starting with an extra Ala at the N-terminus. (b) Purification scheme using the Profinity eXact system. The fusion protein with N-terminal prosubtilisin and C-terminal protein of interest (CRIP1a) binds to mature subtilisin enzyme immobilized on agarose beads. The impurities do not bind to the mature enzyme and are washed away. After extensive washing, the activity of the mature subtilisin enzyme is triggered by fluoride ions (NaF) and the beads are incubated with NaF for 1 hour on ice and pure, tag-free CRIP1a is released. CRIP1a is cleaned up further using traditional cation exchange chromatography using heparin column.

Fig. A2.S2. CRIP1a sticks to pipette tips.

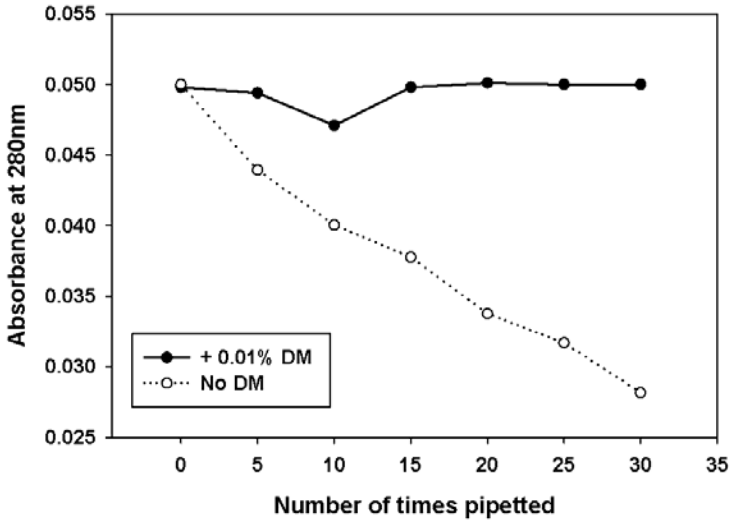

Fig. A2.S2. CRIP1a sticks to pipette tips.

Absorbance spectrum of 2μM CRIP1a in 20mM HEPES, 140mM NaCl, pH7.4 was measured in a 100uL sample volume quartz cuvette at 20^{o}C. The absorbance was measured from 600nm to 250nm. The sample was pipette up and down 5 times and the absorbance measured again. The process was repeated for a total of 30 times of pipetting. The peak absorbance at 280nm was plotted as a function of the number of times the sample was pipette. To the same amount of CRIP1a in the same buffer, 0.01% DM was added. The presence of the detergent prevented the reduction in 280nm absorbance, which was ostensibly due to the sticking of CRIP1a to the plastic pipette tips, and the addition of the detergent prevented the sticking issue, possibly by reducing the surface tension.